MECHANISM AND BEHAVIOR OF NUCLEATE BOILING HEAT TRANSFER TO THE ALKALI LIQUID METALS

Charles W. Deane, IV

Warren M. Rohsenow

Report No. DSR 76303-65

Contract No. AT-(30-1)-3357 A/3

Department of Mechanical Engineering
Engineering Projects Laboratory
Massachusetts Institute of Technology

October 1969

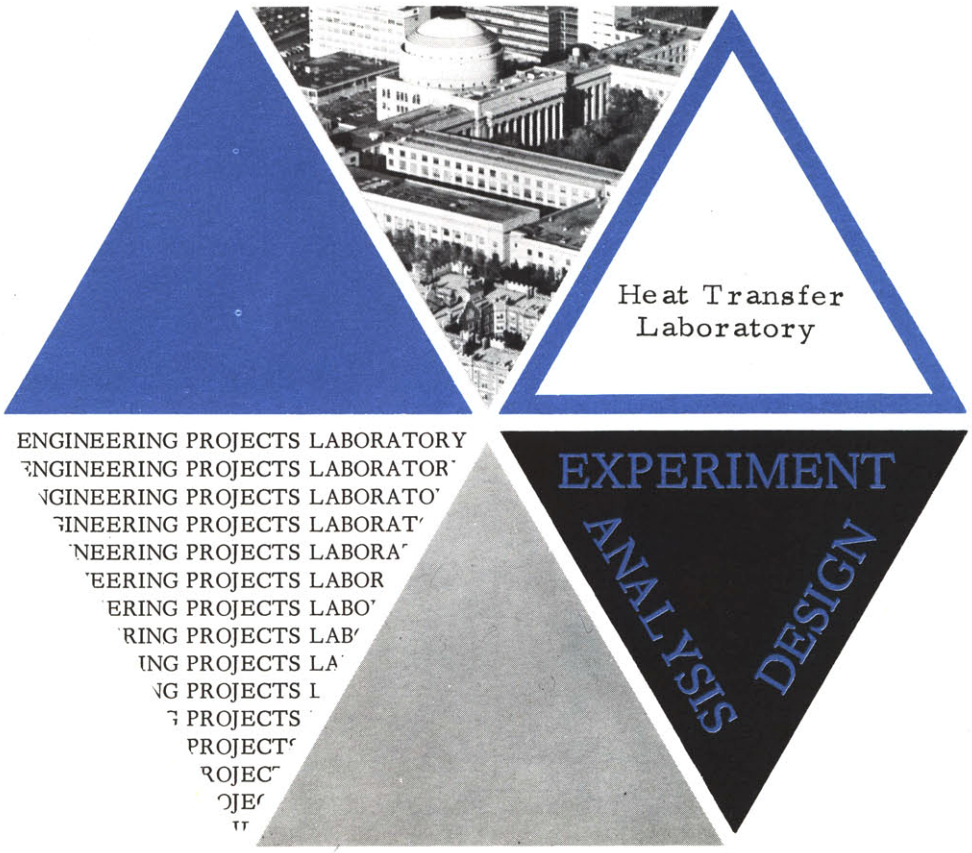

TECHNICAL REPORT NO. 76303-65

MECHANISM AND BEHAVIOR OF NUCLEATE BOILING HEAT TRANSFER TO THE ALKALI LIQUID METALS

by

Charles W. Deane, IV
Warren M. Rohsenow

Sponsored by

United States Atomic Energy Commission

Contract AT-(30-1)-3357 A/3

October 1969

Heat Transfer Laboratory
Mechanical Engineering Department
Massachusetts Institute of Technology
Cambridge, Massachusetts
02139

ABSTRACT

A model of boiling heat transfer to the alkali liquid metals is postulated from an examination of the events and phases of the nucleate boiling cycle. The model includes the important effect of microlayer evaporation which causes a wave of temperature depression to penetrate into the heating solids; calculated results predict the periodic boiling behavior in the heating solid as a function of the heat flux, the system pressure, the cavity size, and the thermophysical properties of the liquid and the solid.

An experimental program was designed to examine the microscale boiling behavior of sodium and to verify the calculated predictions of the boiling model. Artificial cylindrical cavities are used in most of the test sections; a thermocouple is placed close to the boiling surface and adjacent to the cavity wall, and microscale temperature measurements were obtained for stable boiling of sodium from artificial cavities and also from a natural cavity. Horizontal heating surfaces were made from nickel "A", stainless steel 316, and molybdenum-1/2%-titanium; the range of saturation pressure is from 20 to 780 mm Hg.

Favorable comparisons with the predictions of the boiling model are obtained with data for the bubble period and for the amplitude of temperature oscillation at a thermocouple close to the boiling surface; these results indicate the importance of the microlayer in a model for boiling sodium.

The effect of pressure-temperature history on incipient superheats for boiling was examined; the presence of inert gas in a cavity can lower the incipient superheat. Also, an analysis of unstable boiling indicates that outgassing from the heating solid at high temperatures can cause erratic temperature fluctuations by sporadically triggering nucleation at a previously inactive site.

ACKNOWLEDGEMENTS

The author cites Professor W.M. Rohsenow, his thesis supervisor, for definitive direction throughout this investigation.

The author is very appreciative of the time and interest that Professor P. Griffith has freely bestowed during the author's several years at M.I.T.

Professors A.E. Bergles and D.G. Wilson, as other thesis committee members, also contributed fruitful discussions.

Professor B.B. Mikic furthered progress with several valuable ideas.

Mr. S. P. Loutrel assisted in the early alleviation of several potentially troublesome conditions. Mr. F. Johnson was project mechanic. Miss D. Mountain typed the manuscript.

This investigation was sponsored in substantial part by the United States Atomic Energy Commission under Contract AT-(30-1)-3357 A/3. The author also held a National Science Foundation Traineeship during a portion of the investigation.

Machine calculations were done at the M.I.T. Department of Mechanical Engineering Computation Center.

TABLE OF CONTENTS

LIST OF TABLE AND FIGURES

NOMENCLATURE

a	patch radius
A	unit area
A	empirical constant
B	empirical constant
C	constant
c	gas concentration
c_a	ambient gas concentration
c_o	initial gas concentration
c_p	specific heat at constant pressure
D	diffusion coefficient
D_d	bubble departure diameter
d	diameter
g	gravitational acceleration
g_c	gravitational conversion coefficient 32.2 lbm-ft/lbf-sec^2
G_o	empirical constant
h	overall microlayer heat transfer coefficient
h_c	contact coefficient of heat transfer
h_{eq}	equivalent microlayer heat transfer coefficient, defined by Eq. (4)
h_{fg}	latent heat of vaporization
h_i	interphase heat transfer coefficient
k	thermal conductivity
L	penetration depth

M	molecular weight
M	dimensionless modulus, defined by Eq. (13)
N	dimensionless modulus, defined by Eq. (17)
N_{Eo}	dimensionless Eotvos number, defined by Eq. (23)
N^*_{Ja}	dimensionless modified Jakob number, defined by Eq. (24)
P	pressure
q	instantaneous heat flux
q_o	time average heat flux
R	universal gas constant
r	radial position
r_c	radius of cavity mouth
r_d	deactivation radius
T	temperature
$T_w)_{ext}$	extrapolated wall temperature at surface
$T_7)_{max}$	maximum temperature of thermocouple 7
t	time
t_c	bubble contact time
V	volume
w/A	mass flux
x	distance into solid
Y	dimensionless property group, defined by Eq. (25)
y	distance into liquid
α	thermal diffusivity
β	vapor liquid contact angle through the liquid
Δ	increment

δ	microlayer thickness
δ_o	initial thickness of microlayer
δ_r	delay angle, defined by Eq. (D4)
θ	$(T-T_{SAT})$
$\theta_w(0,0)$	surface superheat for nucleation
$\theta'_w(0,0)$	temperature gradient at surface immediately prior to nucleation
λ	integration variable, Eq. (11)
μ	dynamic viscosity
ρ	density
σ	surface tension
σ_e	accommodation coefficient of evaporation
τ	bubble period
ϕ	angle

Subscripts

g	gas
I	node index
L	condition at penetration depth, X=L
ℓ	liquid
max	maximum
min	minimum
SAT	saturation conditions at liquid pressure
v	vapor
w	heating solid

I. INTRODUCTION

I.1 Applications of Alkali Liquid Metals

Alkali liquid metals increasingly are being used in modern process equipment as a high-temperature working fluid; the high thermal conductivity of these fluids allows efficient heat transfer. Sodium, potassium, and their eutectic compounds are the most important alkali liquid metals; the others are cesium, lithium, and rubidium. However, examination of the boiling behavior of sodium permits a good understanding of the behavior of the other alkali liquid metals.

Two important areas of application of the alkali liquid metals are fast breeder reactors and space power plants. Liquid-metal fast breeder reactors will use sodium at atmospheric pressure as the heat-transfer agent from the nuclear reactor to the steam generator; normal operation of the reactor specifies single-phase heat transfer to the sodium for reasons of reactor stability, but the boiling behavior of sodium is required for prediction of reactor behavior during an accident. A reactor accident can be caused by loss of coolant, either by channel blockage or by loss of pumping power. Another application is to use boiling potassium as the working fluid in Rankine-cycle space power systems with a nuclear heat source.

I.2 Scope and Objectives of the Investigation

Several previous investigations of the boiling of alkali liquid

metals (reviewed by Collier and Kosky (1)*, for example) have been directed towards obtaining overall heat-transfer characteristics. Although this information is important for the purposes of equipment design, few investigations have undertaken to examine the microscale boiling behavior of the alkali liquid metals; detailed information on this behavior is necessary for the comprehensive prediction of the over-all heat transfer behavior.

Several previous investigators (2, 3, 4, and others) encountered the problem of unstable boiling of alkali liquid metals at low pressures; this unstable mode consists of random alternation between natural convection and stable boiling and is apparently caused by the erratic deactivation and reactivation of the nucleating cavities. Marto and Rohsenow (4) developed an approximate analysis which predicted that nucleation for sodium should be unstable.

Subsequently, Shai and Rohsenow (5) extended this work. In order to study the mechanism of boiling heat transfer to sodium, a thermocouple was placed in the heating solid near an artificial cavity that was nucleating; using information from this thermocouple, a simplified model of boiling behavior was postulated by neglecting bubble growth and microlayer evaporation.

Recently, Bobrovich et al. (6) took x-ray pictures of boiling potassium vapor bubbles; the pictures were synchronized with a thermocouple near the boiling surface in the heating solid. The presence of a potassium microlayer on the boiling surface during

*References are given on pp. 84-86.

bubble growth was inferred, but no theoretical work on the boiling behavior was presented.

Another problem is the prediction of the superheat required to initiate boiling subsequent to a period of pressurization and subcooling and during a reactor accident. During this period of time, potential nucleation sites can be deactivated if they become filled with liquid, and high superheats may be required to establish boiling. Two recent investigations by Holtz and Singer (7) and by Chen (8) have examined this problem, and varying effects due to the presence of inert gas were deduced.

In general, there are two major phases of the periodic boiling cycle. First, during bubble growth, a thin layer of liquid ("microlayer") remains on the boiling surface directly beneath the bubble as it grows; the microlayer causes high rates of heat transfer as it evaporates into the bubble. Second, after bubble departure, formation of a superheated region occurs near the surface of the heating solid as the liquid is heated back up to nucleation temperature.

In a previous investigation at M.I.T., Shai and Rohsenow (5) suggested that the formation of the superheated region is the most significant feature of the boiling cycle for alkali liquid metals. Then, omitting the effects of bubble growth and microlayer evaporation, Shai solved the transient conduction problem for a periodic process. However, an empirical additive correction which lacks a theoretical basis and is the same order of magnitude as the theoretical result

was required in order to correlate his experimental data for sodium boiling on nickel. Shai attributed this empirical correction to natural convection effects and neglected microlayer heat transfer.

The purpose of this work is to examine the microscale boiling behavior of the alkali liquid metals by means of an analytical and experimental investigation.

For the case of alkali liquid metals, even though microlayer evaporation occurs only during the very short time of bubble growth, the high rates of heat transfer cause a severe wave of temperature depression to penetrate into the heating solid. Hence, the microlayer is considered in the model of the boiling cycle presented in Chapter III.

An experimental program was designed to examine the boiling behavior of sodium and to verify the calculated predictions of the boiling model presented in Chapter III. In order to perform microscale temperature measurements of the boiling cycle, a thermocouple must be close to the actual site from which the bubbles nucleate. For this reason, an essential feature of the present investigation is to identify the exact location of the boiling site with the use of an artificial drilled cylindrical cavity of known geometry; a thermocouple is adjacent to the cavity wall and close to the boiling surface.

Cavity deactivation caused by pressure temperature history is examined in Chapter IV; additional experiments were run to investigate the effect of prior pressurization and subcooling on subsequent

incipient boiling superheats since earlier investigators had deduced varying effects due to the presence of inert gas. In addition, an analysis of unstable boiling is presented in Chapter V.

II. EXPERIMENTAL PROGRAM

Artificial cylindrical cavities of known geometry with a thermocouple close to the boiling surface and adjacent to the cavity wall were used in most of the test surfaces in order to examine the boiling behavior of sodium and to verify the boiling model presented in Chapter III.

The apparatus for this investigation was originally built and used by Marto (4); Shai (5) used the apparatus in his subsequent investigation. Fig. 1 shows a diagram of the whole apparatus, and Fig. 2 is a simplified diagram which emphasizes important characteristics of the test section. Sodium is boiled from a horizontal test surface, with the generated vapor condensing near the top of the vertical pipe and falling back into the boiler section. Heat is transferred to the test surface by radiation from tantalum-10%-tungsten corrugated filaments which operate in a vacuum to avoid oxidation embrittlement. Cylindrical guard heaters reduce radial temperature gradients. The helium cover gas is dried and filtered by a trap at liquid-nitrogen temperatures, and the sodium is filtered by a stainless-steel-wool strainer at 350°F before flowing into the test section. Further details of the various system components are given in Appendix A.

The general design of the test surfaces made of nickel "A" and of stainless steel 316 is shown in Fig. 3; the test surface is a disc of 2-9/16 in. diameter and 0.850 in. thickness. Six holes

of 0.067 in. diameter were drilled radially in the disc for the installation of removable thermocouples for measurement of the temperature gradient from which the heat flux is deduced. In addition, two holes of 0.041 in. diameter were drilled radially at a distance of 0.050 in. from the boiling surface for thermocouples to measure the steady-state temperature oscillations. The boiling surface was ground to a final finish. Then, the artificial cavity used in most of the test surfaces was also drilled as shown in Fig. 3. The disc was then welded on an external lip to a pipe of the same materials as shown in Fig. 3, and this pipe was welded to the condenser section of Fig. 54.

A special design for the test surface of molybdenum-1/2%-titanium alloy was used to avoid forming brittle intermetallic compounds which result when molybdenum is welded to nickel. Fig. 4 shows the geometry. A gold (82%)-nickel eutectic alloy with a brazing temperature of 1742°F was used to vacuum-braze the molybdenum test surface containing an artificial cavity to the nickel pipe which had been stress-relieved. The circumferential braze was then nickel-plated to protect the gold from corrosion by sodium; and the nickel was cured to release trapped hydrogen by bringing it slowly up to 800°F in a vacuum.

The three materials used as the heating solid were chosen in order to have a wide range of thermal conductivity and thermal diffusivity, and also to be compatible with sodium.

Specimen surfaces of nickel were prepared in the same way as the boiler surfaces and were then tested with the "bubble-meter" technique developed by Brown (9) and extended by Dina (10). This technique yields the density distribution of mouth radii of the cavities and also the mouth radius of the largest cavity present in the surface. Cavities in the mechanical joint at the junction of the boiler pipe and the boiler surface were determined to be of similar radius as those in the boiler surface. Hence, the joint area does not contribute cavities of sizes larger than those already present. The "bubble-meter" technique, however, does not determine whether the shape of the cavity is conical, cylindrical, or re-entrant.

Eight calibrated chromel-alumel thermocouples with magnesium-oxide insulation are used in the test surface for temperature measurement with a precision potentiometer. Six of these thermocouples have 0.067-in. diameter inconel sheaths with ungrounded tips; the other two thermocouples have 0.041-in. diameter sheaths with grounded tips and a time constant of 0.04 seconds. Two calibrated chromel-alumel thermocouples with 1/16-in. diameter sheaths are used inside the two vertical liquid and vapor temperature probes. Transient temperatures are measured with a recording oscillograph; the maximum sensitivity obtainable with the galvanometers is 30°F/in. Pressure in the helium line is measured with an open-end mercury manometer. Other instrumentation details are given in Appendix B.

Appendix C describes the lengthy experimental procedures of this investigation, which are preparation of system and method of operation.

III. NUCLEATE BOILING HEAT TRANSFER

A model of the boiling cycle is postulated from an examination of the events and phases of nucleate boiling of sodium. From these considerations, the boiling model is mathematically formulated, and the calculated results are compared with experimental data.

III.1 Model of Nucleate Boiling

Nucleate boiling is a steady-periodic process in which wall temperatures close to the bubble site cycle with period τ. There are two main events: bubble nucleation, and bubble departure, which separate the two major phases from each other: bubble at cavity, and liquid on surface, as shown in Fig. 5a. The qualitative behavior with time of the wall temperature at the boiling surface during these events and phases is depicted in Fig. 5b which is adapted from the work of Cooper and Lloyd (11) and modified for the case of sodium. The events and phases of nucleate boiling are described:

1. Bubble Nucleation

   At time zero, bubble nucleation occurs at the wall superheat required for nucleation, $T_w(0,0) - T_{SAT}$. An expression for the liquid superheat required for nucleation has been derived by several authors (for example, see (5)):

$$T_l(0,0) - T_{SAT} = \frac{T_{SAT}^2}{B} \log_{10}\left[1 + \frac{2\sigma}{r_c P_{SAT}}\right] \qquad (1)$$

where B is an empirical fluid constant in the saturation pressure-temperature relationship of the fluid (see Eq. (35)). The value of B is determined from thermodynamic properties as 9396.°R for sodium; 3890.°R for water; 2705.°R for Freon-113. For sodium, the liquid superheat near the wall is the same as the wall superheat due to the high liquid thermal conductivity; and this liquid superheat for sodium is considerably higher than that for other common fluids at the same pressure and cavity size as seen in Fig. 6.

2. Bubble at Cavity

During Phase I (see Fig. 5) while the bubble is at the cavity, the bubble rapidly grows (10 ft/sec and faster for sodium) and a thin layer of liquid (microlayer) is left on the solid heating surface directly beneath the growing bubble. This microlayer gradually evaporates into the bubble and causes high rates of locally cooling heat transfer to lower the temperature of the heating solid. The temperature will not begin to rise in the heating solid before bubble departure until the microlayer has been completely evaporated; calculations as

given in Section III.3.4 for the case of sodium indicate that the thickness of the microlayer hardly changes during this time.

3. Bubble Departure

   At time t_c, the bubble departs from the boiling surface, and relatively cold liquid at approximately saturation temperature rushes to the surface of the solid. Bubble contact times, t_c, for sodium as given in Fig. 18 are of the order of 0.017 seconds with bubble departure diameters of 3 in. at 40 mm Hg pressure absolute, while of the order of 0.003 seconds and 0.2 in, respectively, at atmospheric pressure.

4. Liquid on Surface

   During Phase II while liquid is on the surface, the surface temperature, which was previously depressed, now rises and the liquid near the wall becomes superheated. The formation of this superheated region continues until the wall superheat is sufficient to cause bubble nucleation at the cavity at time τ, the bubble period. The duration of Phase II is typically 1 second for sodium, which is an order of magnitude longer than for fluids of low thermal conductivity.

The inclusion of the evaporative cooling caused by the microlayer is shown to be important since this effect overshadows the subsequent quenching which occurs at the time of bubble departure

from its site.

The new model is not limited to the alkali liquid metals but is applicable with the thermophysical properties of the proposed liquid-solid combination to the general boiling problem, if assumptions appropriate to the fluid are made concerning bubble growth, the microlayer, and convection effects during Phase II.

III.2 Mathematical Formulation of the Boiling Model

Based on the discussion of the preceding section, the governing equations of the boiling model are stated along with the necessary boundary conditions, initial conditions, and cyclic condition.

The wall-temperature oscillation of steady-state boiling penetrates into the heating solid a distance L, beyond which the solid temperature is constant in time and linear in distance. Fig. 7 indicates the fundamental geometry of the problem. The temperature of the heating solid, $T_w(x,t)$ is a function of distance into the solid, x, and of time, t. Similarly, the temperature of the liquid, $T(y,t)$, is a function of distance into the liquid, y, and of time, t. The problem is treated one-dimensionally; this assumption is verified in Section III.2.2. At position L, heat is transferred into the oscillation zone at a fixed constant flux of q_o, which is also the time-average heat flux into the alkali liquid metal.

For convenience the following quantities are used:

$$\theta_w(x,t) \equiv T_w(x,t) - T_{SAT} \tag{2}$$

$$\theta_\ell(y,t) \equiv T_\ell(y,t) - T_{SAT} \tag{3}$$

III.2.1 Mathematical Formulation

The problem is mathematically formulated (see Fig. 8) as follows. During Phase I which is the time when the vapor bubble is at the cavity ($0 \leq t \leq t_c$), heat transfer at the solid-liquid interface occurs as:

$$q = k_w \frac{\partial \theta_w(0,t)}{\partial x} = h\left[T_w(0,t) - T_v\right] \equiv h_{eq}\left[T_w(0,t) - T_{SAT}\right] \tag{4}$$

where h is the total heat transfer coefficient over the liquid microlayer including interphase resistance, and where h_{eq} is an equivalent microlayer heat transfer coefficient discussed below.

During bubble growth, the temperature of the vapor in the bubble, T_v, is bounded in value by the temperature of the bubble wall in the case of inertia-controlled growth, and by the saturation temperature corresponding to the system pressure, T_{SAT}, in the case of conduction-controlled growth. The driving force for evaporation of the microlayer, $T_w(0,t) - T_v$, is directly multiplied by the total heat transfer coefficient over the microlayer, h. However, as discussed in Section III.3.4, there is no valid method at the present time to predict h with precision. Hence, lacking

this required information, this parameter h is lumped with the evaporative driving force in the term, $h_{eq}(T_w(0,t) - T_{SAT})$ of Eq. (4); h_{eq} is a parameter which contains effects of both micro-layer and vapor temperature and which is left to be determined by experimental data for the bubble period in Section III.5.3.

Heat conduction in the solid during Phase I is governed by the conduction equation:

$$\frac{\partial^2 \theta_w(x,t)}{\partial x^2} = \frac{1}{\alpha_w} \frac{\partial \theta_w(x,t)}{\partial t} \tag{5}$$

An initial temperature profile in the solid at t = 0 will also be required, and its choice is discussed in Section III.3.5.

During Phase II which is the time subsequent to bubble departure and when the thermal layer is being formed ($t_c \leq t \leq \tau$), continuity of temperature and of heat flux obtain at the solid-liquid interface:

$$\theta_w(0,t) = \theta_\ell(0,t) \tag{6}$$

$$k_w \frac{\partial \theta_w(0,t)}{\partial x} = -k_\ell \frac{\partial \theta_\ell(0,t)}{\partial y} \tag{7}$$

Heat transfer in the solid and in the liquid during Phase II is governed by the two conduction equations:

$$\frac{\partial^2 \theta_w(x,t)}{\partial x^2} = \frac{1}{\alpha_w} \frac{\partial \theta_w(x,t)}{\partial t} \tag{8}$$

$$\frac{\partial^2 \theta_\ell(y,t)}{\partial y^2} = \frac{1}{\alpha_\ell} \frac{\partial \theta_\ell(y,t)}{\partial t} \tag{9}$$

In using the conduction equation for the liquid during Phase II, the assumption is made that transient conduction is much larger than natural convection due to the high thermal conductivity of liquid metals.

The initial condition at time $t = t_c$ for Phase II is the solid temperature profile at time $t = t_c$ in Phase I, while the initial temperature profile in the liquid is $\theta_\ell(y,t_c) = 0$, uniform at saturation temperature. This initial condition for the profile of the liquid temperature at time $t = t_c$ assumes that the microlayer is swept off the surface of the heating solid and is replaced by relatively cold liquid at saturation temperature.

During Phase II, the formation of the thermal layer continues until the wall superheat is sufficient to cause bubble nucleation at the cavity; this event occurs at time $t = \tau$. Hence, the cyclic condition for the boiling cycle is:

$$\theta_w(0,\tau) = \theta_w(0,0) \tag{10}$$

These conduction equations along with the boundary conditions,

the initial conditions, and the cyclic condition fully specify the problem.

III.2.2 Validity of Assumption of One-Dimensional Model

A one-dimensional treatment of distance is used in the boiling model. The validity of this assumption is shown by examining the problem solution for the two-dimensional transient temperature depression in a semi-infinite solid due to a cold patch of constant heat flux q_o with disc radius a, and insulated elsewhere. The initial temperature is uniform. The geometry of the problem is shown in Fig. 9, and the solution to this problem is given by Carslaw and Jaeger (12):

$$T(r,x,t) = \frac{a q_o}{2k_w}\left[\int_0^\infty \frac{J_o(\lambda r) J_1(\lambda a)}{\lambda}\left\{e^{-\lambda x}\left(\operatorname{erfc}\left[\frac{x}{2\sqrt{\alpha_w t}} - \lambda\sqrt{\alpha_w t}\right]\right) - e^{\lambda x}\left(\operatorname{erfc}\left[\frac{x}{2\sqrt{\alpha_w t}} + \lambda\sqrt{\alpha_w t}\right]\right)\right\} d\lambda\right] \quad (11)$$

Assuming a patch size (or bubble radius) of a = 0.50 in. and a bubble contact time of 0.017 seconds which from Fig. 18 is a longer contact time, numerical integration of Eq. (11) is performed for values of x and r; the results are shown in Fig. 10 as are the results for an infinite patch. As described in Chapter II, the location of the 0.041-in. diameter thermocouple (TC 7) closest to the bubble site is at a centerline distance of 0.050 in. from the

boiling surface. As compared to an infinite patch, the effect of two-dimensional heat transfer in the vicinity of the thermocouple is small. With this rationale, the model is assumed to be one-dimensional.

III.3 Method of Solution

III.3.1 Method of Finite Differences

The method of finite differences in a marching-time solution is used to solve the governing equations of boiling behavior, Eqs. (4) - (10).

The physical locations of the nodes remain fixed throughout all the calculations.

The difference equation for nodes inside the oscillation zone can be shown to be:

$$\theta_I' = \frac{\theta_{I-1} + (M-2)\theta_I + \theta_{I+1}}{M} \tag{12}$$

where M is a dimensionless modulus,

$$M \equiv \frac{(\Delta X)^2}{\alpha_w (\Delta t)} \tag{13}$$

θ_I' is the future temperature at time $(t + \Delta t)$ in terms of its present temperature θ_I and the present temperature of the neighboring nodes θ_{I-1} and θ_{I+1} at time t, as shown in Fig. 11.

At position x=L where the heat flux q_0 is constant, an energy

balance in Fig. 12 yields:

$$q_o A - \frac{k_w A(\theta_L - \theta_{L-1})}{\Delta X} = A\Delta X \rho_w C_{p_w} \frac{(\theta'_L - \theta_L)}{\Delta t} \tag{14}$$

and the difference equation for this node becomes

$$\theta'_L = \frac{\frac{q_o \Delta X}{k_w} + (M-1)\theta_L + \theta_{L-1}}{M} \tag{15}$$

For Phase I ($0 \leq t \leq t_c$), the boundary condition at x = 0 is taken to be:

$$k_w \frac{\partial \theta_w(0,t)}{\partial X} = h_{eq} \theta_w(0,t) \tag{4}$$

The difference equation for this condition is:

$$\theta'_o = \frac{2\theta'_1 + [M - (2N+2)]\theta_o}{M} \tag{16}$$

where

$$N \equiv \frac{h_{eq}(\Delta X)}{k_w} \tag{17}$$

For Phase II ($t_c \leq t \leq \tau$), the boundary conditions are:

$$\theta_w(0,t) = \theta_\ell(0,t) \tag{6}$$

$$k_w \frac{\partial \theta_w(0,t)}{\partial x} = -k_\ell \frac{\partial \theta_\ell(0,t)}{\partial y} \tag{7}$$

and the difference equation for these conditions, as derived by an energy balance in Fig. 13, is:

$$k_w \frac{(\theta_1 - \theta_o)}{\Delta x} - k_\ell \frac{(\theta_o - \theta_{\ell 1})}{\Delta y} = \left[\frac{\rho_\ell C_{p\ell} \Delta y}{2} + \frac{\rho_w C_{pw} \Delta x}{2}\right]\left(\frac{\theta_o' - \theta_o}{\Delta t}\right) \tag{18}$$

Whence,

$$\theta_o' = \theta_o + \frac{(\theta_1 - \theta_o) - \frac{k_\ell \Delta x}{k_w \Delta y}(\theta_o - \theta_{\ell 1})}{\frac{M}{2}\left[1 + \frac{\alpha_w k_\ell \Delta y}{\alpha_\ell k_w \Delta x}\right]} \tag{19}$$

III.3.2 Definition of Penetration Depth, L

The penetration depth, L, is defined as:

$$L \equiv 2\sqrt{\pi \alpha_w T} \tag{20}$$

For a sinusoidal variation of surface temperature of unit amplitude, this distance represents (13) a depth where the amplitude of temperature oscillation is 0.002. This penetration depth, L, is

actually greater than the depth of penetration of temperature variation during boiling and designates the depth to which the finite-difference calculations are done in the boiling model.

III.3.3 Bubble Contact Time

The bubble contact time is the amount of time required for the bubble to grow to its departure diameter from nucleation. Microlayer heat transfer is considered in Section III.3.4 separately from bubble growth. Evaporation of the microlayer produces sodium vapor for bubble growth, in addition to possible vapor production from the other surface area of the bubble. In the pressure range of the bubble period data ($P_{SAT} \leq 100$ mm Hg), however, calculations with the model show that more vapor is produced from microlayer evaporation than is required for bubble growth. This excess vapor will condense on the upper sides of the bubble, and will delay the transition of bubble growth from inertia-controlled growth to conduction-controlled growth. In the pressure range of the data, sodium bubble growth will be primarily limited by inertia. This conclusion is based on a dimensionless growth criterion developed by Lien and Griffith (14) which was verified with data for water in an infinite medium, in both the inertia-controlled regime and the conduction-controlled regime; furthermore, the presence of added vapor from microlayer evaporation would lengthen the regime of inertia-controlled growth, since the reduced conduction restriction would not be encountered

until later in the bubble growth.

The limited amount of data on bubble departure diameter D_d in potassium taken by Bobrovich et al. (6) is shown in Fig. 14. The two correlations also shown are recommended by Cole and Rohsenow (15) for bubble departure diameters in water:

$$N_{Eo}^{1/2} = 1.5 \times 10^{-4} \left(N_{Ja}^{*}\right)^{5/4} \tag{21}$$

and in "other fluids" (mostly organic compounds):

$$N_{Eo}^{1/2} = 4.65 \times 10^{-4} \left(N_{Ja}^{*}\right)^{5/4} \tag{22}$$

where the dimensionless Eotvos number is:

$$N_{Eo} \equiv \frac{g(\rho_\ell - \rho_v) D_d^2}{g_c \sigma} \tag{23}$$

and the dimensionless modified Jakob number is:

$$N_{Ja}^{*} \equiv \frac{\rho_\ell C_{p_\ell} T_{SAT}}{\rho_v h_{fg}} \tag{24}$$

The limited amount of available potassium data show only a small variation of departure diameter with pressure, but these

diameters are in the range of 1-1/2 in. to 2-1/2 in. which is the order of magnitude of the chamber size (11 in. x 7 in. x 4 in.); this small chamber size increases the mass inertia of the liquid as seen by the vapor bubble and would artifically increase both the departure diameter of the bubble and its contact time on the surface.

Only this one set of limited data for bubble departure diameters in boiling potassium is existent in the literature, and its validity is open to question since it does not follow the trend of pressure as exhibited by all other fluids. This data is probably tainted by the restrictive size of the test chamber. The long time (0.06 sec.) required for bubble growth to departure size at a pressure of 8 psia substantiates the suspicion of apparatus effects on the data. In addition, the thermophysical properties which are represented by the modified Jakob number, N^*_{Ja}, for sodium very closely match those of water as seen in Fig. 15; potassium properties are distinctly different on this basis of comparison.

For these reasons, it is assumed here that the correlation of Eq. (21) is probably a better representation of bubble departure diameter and is used to predict D_d in the ensuing analysis. The results are shown in Fig. 16.

Then, using this departure diameter, the time for the bubble to grow to this size is calculated as a function of pressure and cavity size from the model of Wichner and Hoffman (16) for bubble-

growth rates in superheated liquid metals. Their model is a numerical integration of the Navier-Stokes equation for an inviscid incompressible fluid deforming with spherical symmetry in a uniformly superheated liquid; bubble growth is controlled by inertia. The results of their calculations for liquid metals yield the bubble size r as a function of time t and are shown in Fig. 17 as a function of a dimensionless property group Y which is defined as:

$$Y \equiv \frac{2g^2 \rho_\ell^{3/2} (\rho_\ell - \rho_v) r_c^3}{9\mu \left(\frac{2\sigma}{r_c}\right)^{3/2}} \qquad (25)$$

where r_c is the cavity size. This solution yields a rapid growth rate initially which later slows due to the inertia of the surrounding liquid.

In order to calculate the bubble contact time, the bubble departure diameter is first obtained from the results of Fig. 16 at a given pressure. Then, this bubble size is used in the results of Fig. 17 as a function of cavity size and pressure to calculate the growth time needed for the bubble to reach departure size. This growth time is the bubble contact time, t_c, which is shown in Fig. 18 as a function of pressure and cavity size.

III.3.4 Microlayer Heat Transfer

During Phase I while the microlayer is underneath the bubble on the boiling surface, high local rates of heat transfer are present. Heat transfer through this microlayer is governed by the resistances of the liquid layer and of interphase mass transfer. These two resistances act in series, and the overall time-dependent heat transfer coefficient, h(t), may be represented as:

$$h(t) = \frac{1}{\frac{1}{h_i} + \frac{\delta(t)}{k_l}} \tag{26}$$

where h_i is the interphase heat transfer coefficient, and $\delta(t)$ is the microlayer thickness as a function of time, as shown in Fig. 19.

The interphase resistance to heat transfer in sodium is calculated according to the Schrage equation taken from Kroger (17) for interphase mass transfer for small departures from equilibrium:

$$\frac{1}{h_i} = \frac{T_l - T_v}{q_o} = \frac{T_l - T_v}{\left[\frac{2\sigma_e}{2-\sigma_e}\right]\sqrt{\frac{M}{2\pi R T_v}}\, h_{fg}(P_l - P_v)} \tag{27}$$

where σ_e is the accommodation coefficient for evaporation, M is the molecular weight, and R is the universal gas constant.

The heat transfer rate through the microlayer balances the rate of evaporation of the microlayer:

$$-\rho_\ell h_{fg} \frac{\Delta\delta}{\Delta t} = h\left[T_w(0,t) - T_v\right] = h_{eq}\, \theta_w(0,t) \qquad (28)$$

Using $\theta_w(0,t)$ and $\delta(t)$ calculated in the past instant of time Δt, the thickness $\Delta\delta$ which will evaporate in the next instant of time can be calculated with Eq. (28). The cumulative thickness of the microlayer is found by successively subtracting the evaporated thickness in the marching-time solution from the previous thickness $\delta(t)$. If the microlayer has completely evaporated, then heat transfer will be from the solid to the vapor, with a very low heat transfer coefficient.

An estimate of the change in thickness of the microlayer during the time of bubble contact can be made by equating the total heat input to the microlayer during the time of bubble contact, with the total latent heat of the evaporated thickness:

$$q_{t_{max}}\, t_c\, A \cong \rho_\ell h_{fg} A\left[\delta_o - \delta(t_c)\right] \qquad (29)$$

where A is a unit area and δ_o is the initial thickness. An upper limit to the heat flux while the microlayer is on the surface is that $q_{max} = 4\ q_o$, as will be seen in Section III.4. Then, at a value of $t_c = 0.017$ seconds which from Fig. 18 is a longer contact time, a calculation with Eq. (29) for sodium properties and for a

heat flux of q_o = 100,000 BTU/hr-ft^2 yields an evaporated thickness of $\delta_o - \delta(t_c) = 2.3 \times 10^{-5}$ ft, which is only 10% of the initial thickness of the microlayer. Hence, the thickness of the microlayer is assumed to be essentially constant.

For bubble expulsion tests conducted in potassium at 1274°F, Spiller et al. (18) found that the thickness of a liquid layer remaining on the wall was 0.07 mm to 0.23 mm (2.5×10^{-4} ft to 8.1×10^{-4} ft). For a plate lifted out of a liquid, Levich (19) gives the pertinent property of entrained film thickness as $\sqrt{\frac{\mu}{\rho_\ell}}$ which remains practically unchanged when comparing potassium to sodium. At a pressure of 40 mm Hg absolute, a microlayer thickness of 0.15 mm of sodium corresponds to an overall heat transfer coefficient of 37,000 BTU/hr-ft^2-°F, as calculated from

$$h = \frac{1}{\frac{1}{h_i} + \frac{\delta_o}{k_\ell}} \tag{26}$$

In addition, Cooper (20) has theoretically estimated the initial thickness of the microlayer via arguments from fluid mechanics:

$$\delta_o \sim C\sqrt{\frac{\mu}{\rho_\ell} t_c} \tag{30}$$

where C is of order unity. This calculation for sodium properties with C = 1 yields $\delta_o \sim 0.04$ mm for a bubble contact time,

t_c = 0.02 seconds. At a pressure of 40 mm Hg absolute, this corresponds to a value of the overall heat transfer coefficient of 61,000 BTU/hr-ft^2-°F.

The overall resistance to heat transfer for a microlayer thickness of 0.15 mm and for σ_e = 1.0 is shown in Fig. 20 for sodium with k_ℓ = 35 BTU/hr-ft-°F (δ_o/k_ℓ = 1.5 x 10^{-5}hr-ft^2-°F/BTU); it is seen that the interphase resistance makes a significant contribution to the overall resistance at pressures lower than about 100 mm Hg. The same conclusion is true of potassium, for which $1/h_i$ is shown in Fig. 21 with k_ℓ = 18 $\frac{\text{BTU}}{\text{hr-ft°F}}$ and δ_o = 0.15 mm (δ_o/k_ℓ = 2.9 x 10^{-5}hr-ft^2-°F/BTU).

Since there is no valid method available at the present time to predict h with precision, this parameter was lumped into the parameter h_{eq} as discussed in Section III.2.1, and h_{eq} is the parameter in the calculation left to be determined by the experimental data for the bubble period. As seen in Section III.6.3, a magnitude of h_{eq} = 30,000 BTU/hr-ft^2-°F brings the calculated results in reasonable agreement with the measurements. This is the order of magnitude of h as determined from the previously mentioned liquid-layer measurements. Omitting the effect of the vapor temperature being higher than the saturation temperature corresponding to the system pressure, this parameter corresponds to 1/h = 3.3 x 10^{-5} hr-ft^2-°F/BTU, which is the magnitude given by Fig. 21 in the pressure range of 30-100 mm Hg; the pressure range brackets the available data for bubble period

and for temperature amplitude in Section III.6.3.

III.3.5 Calculation Technique

For given time-average heat flux, bubble contact time, and microlayer heat transfer, the method of this marching-time solution is to assume the bubble period, τ, and an initial temperature profile in the solid for the first bubble and then to use the difference equations of Section III.3.1 for Phase I of the boiling cycle. For only the first bubble, it is arbitrarily assumed in order to begin the calculations that the initial temperature profile is linear:

$$\frac{\theta_w(x,0)}{\theta_w(0,0)} = 1 + \frac{q_o X}{k_w \theta_w(0,0)} \qquad (31)$$

At time $t \geq t_c$, the difference equations for Phase II are used, with the solid temperature profile at time $t = t_c$ from Phase I as the initial solid temperature profile for Phase II; the initial liquid temperature is uniform at saturation. As time progresses in Phase II, the solid temperature rises until the surface temperature reaches the wall superheat for nucleation; the time of this event is τ, and the wall temperature profile at τ is used as the initial temperature profile for the cycle of the second bubble. Thus, the bubble period τ is the length of time which has elapsed from nucleation until the wall temperature has risen back to

and wall superheat required for nucleation.

A new value of L for the second bubble is calculated from τ of the first bubble, and the converging calculations are repeated in this manner for successive bubbles. At bubble departure at time $t = t_c$ when relatively cold liquid at saturation temperature rushes to the surface of the heating solid, the liquid temperature for all bubble cycles is always taken as uniform at saturation temperature.

Hence, the calculations are iterated n times for n bubbles, and it is seen that the effect of the assumption of the wall temperature profile for the first bubble is negligible for the nth bubble, as the equations adjust themselves to the periodic nature of the process, just as the physical boiling system itself does when it first begins to boil subsequent to a period of natural convection.

III.4 Calculated Results

The boiling model for a given solid-liquid combination yields the temperature behavior with time and distance in dimensionless form as a function of three operating parameters as shown in Table 1: heat flux, pressure and cavity size. System pressure and cavity size specify the nucleation wall superheat $\theta_w(0,0)$ from Eq. (1), the bubble contact time t_c, and the equivalent microlayer heat transfer coefficient h_{eq}, which are input variables to the model along with the heat flux q_o. The thermophysical properties of sodium were obtained from reference (21), and those of the heating solid

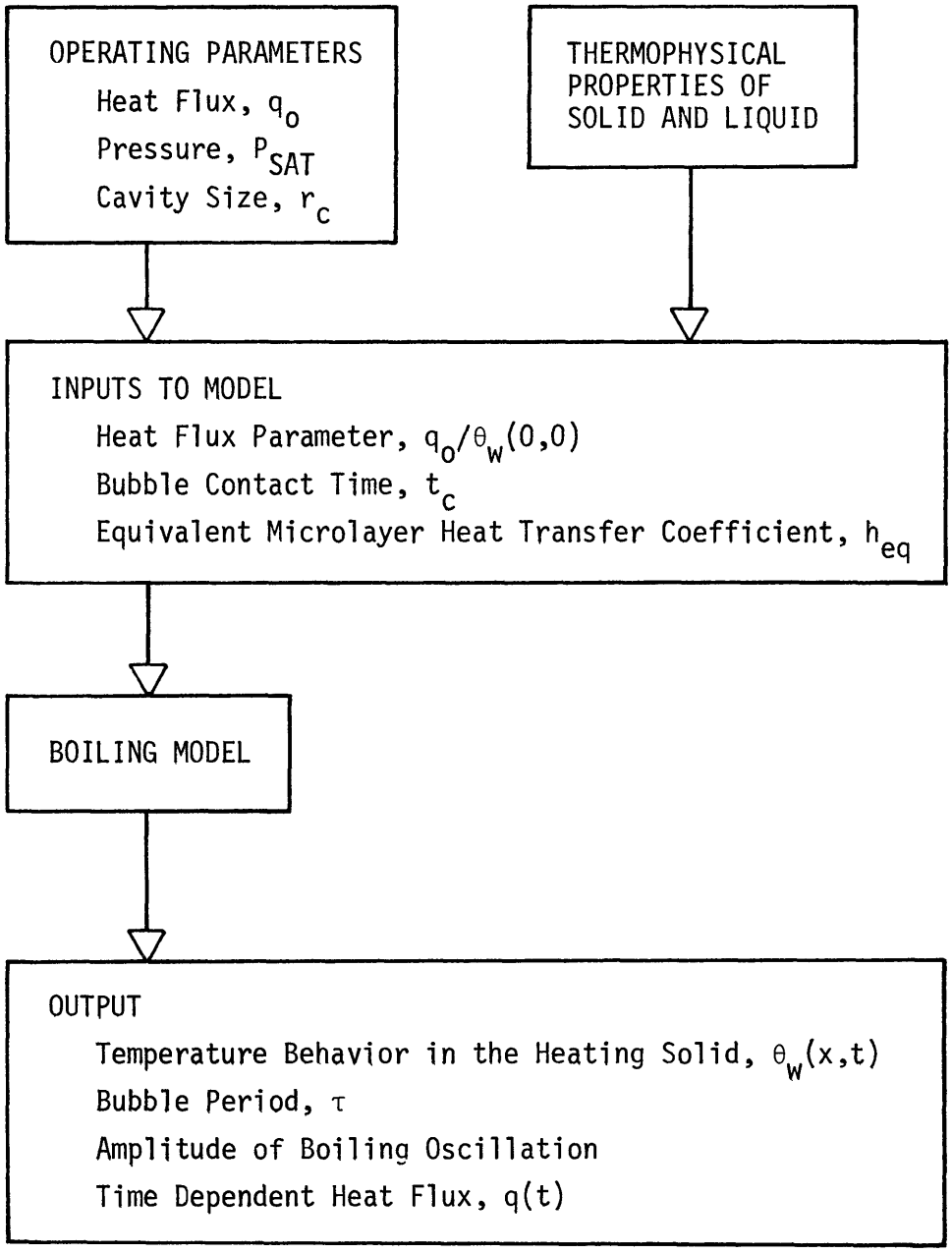

Table 1 Flow Diagram of Boiling Model

from reference (22).

In addition to the temperature behavior, the results of the boiling model include the time-dependent heat flux, the bubble period, and the amplitude of temperature oscillation during boiling.

Typical results of the boiling model are shown in Figs. 22-24 for a sodium-nickel combination with a bubble contact time t_c = 0.0175 seconds, with heat flux parameter $q_o/\theta_w(0,0)$ = 3402 BTU/hr-ft^2-°F, and with microlayer heat transfer h_{eq} = 30,000 BTU/hr-ft^2-°F. The bubble period, τ, for these conditions is 1.06 seconds.

Temperature-time behavior at various positions in the heating solid is given in Fig. 22. At the surface, the temperature drop due to any quenching caused by bubble departure at t/τ = 0.018 is negligible, since there are such steep temperature gradients in the solid at this time. These temperature-time results are cross-plotted in Fig. 23 to show temperatures in the solid along lines of constant time, thereby yielding the envelope of the amplitude of temperature oscillation as a function of position. The transient heat flux at the sodium-nickel interface is plotted in Fig. 24; the high heat transfer during the initial part of the bubble period ($t/\tau \leq 0.018$) is caused by microlayer evaporation. During the time $0.018 \leq t/\tau \leq 1.0$, temperature recovery occurs with liquid on the heating solid before the next bubble begins to grow.

Calculations with the model were done in order to gauge the effect of value of the overall microlayer heat transfer coefficient

on the predicted temperature behavior. Fig. 25 shows the predicted amplitude of oscillation as a function of position for two values of this microlayer heat transfer coefficient, h_{eq} = 30,000 and 60,000 BTU/hr-ft^2-°F. For doubling this coefficient, the predicted amplitude of oscillation increases by about 20% in the vicinity of the thermocouple nearest to the boiling surface (TC 7) at this heat flux, and only 10% for 1/3 the heat flux. In addition, increasing the bubble contact time, t_c, from 0.006 sec. to 0.0175 sec. increases the amplitude of temperature oscillation in the vicinity of TC 7 by 13%, for a value of $q_o/\theta_w(0,0)$ = 3402 BTU/hr-ft^2-°F.

III.5 Experimental Results and Discussion

III.5.1 General Observations

Heat transfer data has been obtained with commercial-grade sodium on each of three horizontal heating surfaces: nickel "A", stainless steel 316, and molybdenum-1/2%-titanium. The range of heat flux in this investigation is from 20,000 to 250,000 BTU/hr-ft^2, and the range of saturation pressure is from 20 to 780 mm Hg absolute. The depth of the pool of sodium in the test section is 3 in.

Three types of heat transfer have been observed: natural convection, stable boiling, and unstable boiling.

At low heat flux, heat transfer to the sodium occurs by natural convection with values of the heat transfer coefficient near

1000 BTU/hr-ft^2-°F. All temperatures in the heating solid are constant with time at each heat flux, and the liquid temperature is superheated with respect to the saturation temperature corresponding to the system pressure.

At high heat flux, heat transfer to the sodium occurs by stable nucleate boiling. Temperatures in the heating solid at locations away from the liquid-solid interface are constant in time; but a steady-state oscillation of wall temperature during boiling exists at locations directly beneath the bubble site and very close to the boiling surface. The magnitude of this oscillation decreases with increased values of heat flux, pressure, or distance from the boiling surface. The liquid temperature is at saturation temperature corresponding to the system pressure.

At intermediate values of heat flux and at low pressures, heat transfer occurs by unstable boiling or "bumping". This unstable mode consists of random alternation between natural convection and boiling; all temperatures in the heating solid are fluctuating erratically between the two extremes of values corresponding to natural convection and boiling heat transfer at the condition of time-average constant heat flux.

III.5.2 Data Reduction

The temperature distribution in the heating solid was obtained by plotting the converted temperatures from the four central thermocouple readings versus their axial position in the heating solid.

A straight line through these temperatures yielded the temperature gradient with which the heat flux was calculated from Fourier's conduction law:

$$q_{to} = k_w \frac{\Delta T}{\Delta X} \tag{32}$$

The thermal conductivity used in this calculation was evaluated at the average temperature of the four central thermocouples. Values of the thermal conductivity, k_w, of the three different materials used as the heating solid in this investigation were obtained from reference (22).

The extrapolated wall temperature $T_w)_{ext}$ for natural convection data was obtained by extrapolating the straight-line temperature distribution to the solid-liquid interface.

For boiling data, if the amplitude of temperature oscillation at thermocouple No. 7 was large enough to be measured, then the bubble period τ was obtained from this periodic temperature variation. Thermocouple No. 7 is close to the boiling surface (see Fig. 3). The maximum and minimum temperatures of thermocouple No. 7 were reduced from the Recording Oscillograph. The calculated results of the boiling model postulated in Chapter III yield the slope of the temperature profile, $\theta'_w(0,0)$, at the solid-liquid interface and at time zero as a function of the bubble period τ. For bubble contact time t_c = 0.0175 seconds and microlayer heat transfer h_{eq} = 30,000 BTU/hr-ft^2-°F, the results of these calculations

for a sodium-nickel system are shown in Fig. 26 as well as for sodium boiling from stainless steel and from molybdenum. It is observed for a straight-line extrapolation to the surface that

$$\theta'_w(0,0) \cong \frac{T_7)_{MAX} - T_w(0,0)}{\Delta X_7} \tag{33}$$

where $T_7)_{max}$ is the maximum temperature of thermocouple No. 7 and Δx_7 is the centerline distance of this thermocouple from the boiler surface; then, by definition from Eq. (2):

$$\theta_w(0,0) \equiv T_w(0,0) - T_{SAT} \tag{2}$$

Substitution of Eq. (33) into Eq. (2) yields after rearrangement:

$$\theta_w(0,0) = \frac{T_7)_{MAX} - T_{SAT}}{1 + \left[\frac{\theta'_w(0,0)}{\theta_w(0,0)}\right]\Delta X_7} \tag{34}$$

Hence, using the value of $[\theta'_w(0,0)/\theta_w(0,0)]$ at the appropriate bubble period τ, this method places a straight line with slope $\theta'_w(0,0)$ through the maximum temperature of thermocouple No. 7 and extrapolates this temperature to the boiler surface; this extrapolation yields the maximum surface temperature, which is the surface temperature required for nucleation.

For boiling data of higher pressures where the amplitude of temperature oscillation is very small, the extrapolated wall temperature $T_w)_{ext}$ was obtained by the extrapolation method for natural convection data.

The saturation temperature was found from the measurement of the thermocouple in the vapor. The saturation temperature corresponding to the system pressure measured by the open-end manometer was calculated with the relationship:

$$\log_{10} P = A - \frac{B}{T} \tag{35}$$

where A and B are empirical constants of the fluid. For sodium, Bonilla et al. (23) gave the values of A = 4.5217 and B = 9396.75 for P in atmospheres and T in degrees Rankine. Recent data (24) for saturation vapor pressure was used directly for comparison with vapor temperature measurements in the range of 19 to 60 mm Hg pressure. This data agrees with Eq. (35) for pressures above 60 mm Hg; the lower limit of pressure for the data used in obtaining Eq. (35) was 40 mm Hg. Good agreement was usually obtained between the two measurements of the saturation temperature, within 3 to 5°F. However, the temperature measured by the vapor thermocouple was always used in data reduction as the vapor temperature.

The other three thermocouples in the boiler plate were not

used in data reduction and served only to check radial temperature distribution. Appendix E discusses the experimental uncertainty in the data and tabulates the microscale boiling data.

III.5.3 Boiling Behavior

Test sections with an artificial cylindrical cavity were used in most of the experiments in order to examine the microscopic behavior of boiling sodium with an instrumented and active bubble site of known geometry.

Boiling data from a drilled cavity of 0.00675 in. radius and 0.10 in. length in a nickel surface are shown in Fig. 27. The three regions of heat transfer observed in this investigation are present: natural convection, bumping and stable boiling. This data demonstrates the effect of pressure on boiling superheat for a cavity radius of known size as predicted by Eq. (1) for boiling wall superheat in liquid metals:

$$\theta_w(0,0) = \frac{T_{SAT}^2}{B} \log_{10}\left[1 + \frac{2\sigma}{r_c P_{SAT}}\right] \qquad (1)$$

where B = 9396.75°R for sodium, an empirical constant of the fluid. Values of the surface tension, σ, were obtained from reference (25). The line of boiling superheat for this artificial cavity is independent of heat flux as indicated by the infinite slope of the boiling data in Fig. 27, since this one cavity of known size is the only active bubble site and is able to perform all of the necessary

heat transfer.

The data of low pressure (32 mm Hg absolute) in Fig. 27 exhibit "bumping" phenomena at intermediate heat fluxes (100,000 BTU/hr-ft^2). This unstable behavior consists of erratic changes in temperature level from that of natural convection to that of boiling, as seen in Fig. 27. The temperature-time trace in Fig. 28 of a thermocouple in the heating solid which is 0.050 in. from the boiling surface shows the typically transient behavior of unstable boiling. An infrequent bubble nucleation causes the temperature level to drop from that of natural convection to that of boiling. The cavity is apparently snuffed out, and the temperature levels rise again. This problem of bumping is discussed further in Chapter V.

Boiling data in Fig. 29 from natural sites in a stainless steel surface exhibit the inverse pressure effect on wall superheats, which correspond to cavity sizes of 0.003 in. radius and smaller. The finite slope of this boiling data indicates that smaller cavities become operative as the heat flux is increased. The natural convection data shows a very slight improvement in heat transfer coefficient at higher pressure.

Boiling data from natural sites in a nickel surface are shown in Fig. 30 as a function of pressure. The lower boiling superheats on this nickel surface when compared to the stainless steel data at the same pressure in Fig. 29 suggest that the identical surface-

grinding process creates larger natural sites of boiling in the soft nickel than in the hard stainless steel.

In addition, a natural cavity in this nickel surface which happened to be very close to a thermocouple was boiling during one of the experiments. Due to the very short distance to which a significant part of the temperature depression penetrates, a thermocouple must be positioned directly beneath the actual site from which boiling occurs if the steady-state temperature oscillation is to be measured. A temperature-time trace of the boiling behavior of this natural cavity is shown in Fig. 31, while the companion trace for an artificial cavity is in Fig. 32. The close similarity of the shapes of these curves for the two different cavities helps to verify the validity of using an artificial cavity in the study of sodium boiling behavior.

The presence of only a single recovery in wall temperature per bubble period suggests that the microlayer has not completely evaporated by the time of bubble departure, Fig. 5.

The wall superheat for boiling, $\theta_w(0,0)$ can be predicted by Eq. (1) as a function of pressure if the radius of the cavity mouth is known:

$$\theta_w(0,0) = \frac{T_{SAT}^2}{B} \log_{10}\left[1 + \frac{2\sigma}{r_c P_{SAT}}\right] \qquad (1)$$

Figs. 33-35 compare the measured wall superheat to the prediction for artificial cavities of different radii in surfaces of nickel, of stainless steel, and of molybdenum as a function of pressure. For data in Figs. 33 and 34, the artificial cavity was always boiling, and the agreement with Eq. (1) is good. Comparison between Figs. 33 and 34 at the same pressure shows the inverse effect of cavity size on wall superheat as predicted by Eq. (1).

However, boiling data in Fig. 35 indicate that an artificial cavity does not always boil and that natural cavities with roughly half the cavity mouth size can preferentially boil at times. The wall superheats of Fig. 35 correspond to cavity radii of 0.0035 in. which are actually available as determined by independent "bubble-meter" tests in Chapter II.

For boiling data shown in Figs. 33 and 34 from artificial cavities, the amplitude of temperature oscillation at thermocouple No. 7 was measurable, and the data was reduced according to the method of Section III.5.2 in conjunction with Fig. 26 at the appropriate value of the bubble period τ. For boiling from natural cavities as shown in Fig. 35, thermocouple No. 7 was not close enough to the bubble site to pick up an oscillation. The data from this thermocouple was reduced by extrapolating to the boiling surface the gradient obtained from the other thermocouples.

Using temperature-time traces of the thermocouple near the boiling surface similar to Fig. 32 for the artificial cavities, the

amplitude of temperature oscillation at TC 7 of steady-state boiling and its bubble period can be determined as a function of pressure and heat flux. This data for a nickel surface with an artificial cavity of radius r_c = 0.00675 in. is shown in Figs. 36 and 37; the peak-to-peak average amplitude of oscillation at a location 0.050 inches from the boiling surface is several degrees Fahrenheit, while the bubble period is on the order of 1 second. Both period and oscillation amplitude decrease with increased heat flux or increased pressure, which is also predicted by the boiling model postulated earlier in this Chapter. The maximum limit of resolution of the available equipment represents 1°F. If the amplitude of oscillation at the higher pressures cannot be measured with the closest thermocouple TC 7 (0.050 in. center-line distance from the boiling surface and 0.041 in. sheath diameter), then the bubble period cannot be obtained either. As seen in Fig. 36, the amplitude of oscillation at TC 7 is small at a pressure of 100 mm Hg.

As mentioned earlier, some data for sodium boiling from a natural cavity was also obtained. The size of this natural cavity was deduced by calculating r_c with Eq. (1) from the measured wall superheat for nucleation $\theta_w(0,0)$ = 67°F at a pressure of 30 mm Hg; this calculation gives r_c = 0.0035 in. The peak-to-peak average amplitude of temperature oscillation at TC 7 for this natural cavity is shown in Fig. 38, and the period of this oscillation is given in Fig. 39.

Similar data for the amplitude of temperature oscillation is

shown in Fig. 40 for sodium boiling from an artificial cavity in a molybdenum surface; the cavity radius is r_c = 0.00675 in.

Prediction of the amplitude of temperature oscillation at any point in the heating solid is available from the results of the boiling model as presented earlier in this Chapter. The results of comparing the nickel amplitude data of Fig. 36 with calculations for the cavity size and operating pressure from the boiling model for a position 0.050" from the boiling surface are shown in Fig. 41; the values of the calculation parameters used for the sodium-nickel system are equivalent microlayer heat transfer coefficient h_{eq} = 30,000 BTU/hr-ft^2-°F, and bubble contact time t_c = 0.0175 sec. for data at a pressure of 30 mm Hg, and 0.015 sec. at 100 mm Hg, respectively. Reasonable agreement is found.

However, as discussed in Appendix D, an error in the measurement of these periodic temperature oscillations is caused by the contact coefficient of heat transfer, h_c, between the thermocouple and its well in the heating solid. This measurement error is small for long bubble periods, but it becomes significant at the shorter bubble periods as seen in Fig. 55. Using a single value of h_c = 120 BTU/hr-ft^2-°F, an amplitude reduction factor is obtained from Fig. 55 as a function of bubble period for each data point; the amplitude data corrected for this thermocouple error is shown in Fig. 41 by the solid points. The same value of h_c = 120 BTU/hr-ft^2-°F is consistently used to correct the amplitude data in Figs. 42-44 for this thermocouple error. Actually, a different value of the

contact coefficient would be expected for the set of data in each of Figs. 41-44. The removable thermocouple was freshly installed in its well for each different test section, and a different degree of contact can exist for each installation.

The magnitude of contact coefficient of around 120 BTU/hr-ft^2-°F appears to be a reasonable one for the installation used here, in the light of measured contact coefficients for zero or very light loading (39). The magnitude of this h_c would be expected to be different for each apparatus and for each reassembly of any given apparatus.

The amplitude data for the natural cavity in the nickel surface are shown in Fig. 42 with the prediction of the boiling model. The solid points represent the amplitude data corrected for the thermocouple error discussed above. The value of the equivalent microlayer heat transfer coefficient was taken as h_{eq} = 30,000 BTU/hr-ft^2-°F; the bubble contact time was taken as t_c = 0.015 sec.

The same comparison for the molybdenum amplitude data of Fig. 40 between the predicted and the measured amplitudes is made in Fig. 43. The value of the equivalent microlayer heat transfer coefficient was taken as h_{eq} = 30,000 BTU/hr-ft^2-°F; the value of the bubble contact time was taken from Fig. 19 and for r_c = 0.00675 in. to be t_c = 0.0175 sec. for data at a pressure of 30 mm Hg, and t_c = 0.0130 sec. for data at 60 mm Hg and at 100 mm Hg.

In addition, these amplitude predictions with the appropriate operating parameters of equivalent microlayer heat transfer

coefficient h_{eq} = 30,000 BTU/hr-ft^2-°F, and bubble contact time t_c = 0.0175 sec. for data at a pressure of 40-65 mm Hg, and 0.006 sec. for data at 105 mm Hg, respectively, were performed for the data points from the work of Shai (5) for which amplitude data was presented for boiling sodium from an artificial cavity in a nickel surface. The same comparison between the data and this model is shown in Fig. 44.

The nickel data in Fig. 44 has a long period (1 second and longer), and the correction from Fig. 55 due to thermocouple error is small. However, the molybdenum data in Fig. 43 have a short period (1 second and shorter) and this correction is significant.

The favorable comparison in Figs. 41 and 44 of both the magnitude and trend of the data with the boiling model of this Chapter tend to substantiate the importance of the microlayer in a model for boiling sodium.

Experimental data for the bubble period τ for sodium boiling from an artificial cavity in a nickel surface is shown in Fig. 45 as a function of the parameter $q_o/\theta_w(0,0)$. The theoretical result from the boiling model of Chapter III for a sodium-nickel combination is also shown, and the data straddles this theoretical prediction. The calculation parameters of this curve are bubble contact time t_c = 0.0175 seconds and equivalent microlayer heat transfer coefficient h_{eq} = 30,000 BTU/hr-ft^2-°F.

Similarly, Fig. 46 shows bubble period data for sodium boiling from an artificial cavity in a molybdenum surface. This experimental

data also straddles the theoretical prediction of this Chapter. The calculation parameters for this sodium-molybdenum system are equivalent microlayer heat transfer coefficient h_{eq} = 30,000 BTU/hr-ft^2-°F and bubble contact time t_c = 0.0175 sec. at a pressure of 30 mm Hg, and t_c = 0.0130 sec. at a pressure of 60 mm Hg.

III.5.4 Summary of Assumptions and Constants Deduced from the Data

This section summarizes the assumptions and the constants which have been deduced from examination of the data presented in the previous section.

First, nucleation occurs and bubble growth begins when the superheat at the nucleating cavity is given by Eq. (1):

$$\theta_w(0,0) = \frac{T_{SAT}^2}{B} \log_{10}\left[1 + \frac{2\sigma}{r_c P_{SAT}}\right] \qquad (1)$$

Second, a microlayer exists underneath the bubble while it is attached to the heating surface, and heat transfer through the microlayer can be represented as:

$$q = h_{eq}\left[T_w(0,t) - T_{SAT}\right] \qquad (4)$$

Third, the bubble contact time, t_c, is established by an inertia-controlled bubble growth (Fig. 17) and bubble departure size given by Eq. (21).

Fourth, after bubble departure, heat transfer to the liquid close to the wall can be treated as pure conduction.

Fifth, during the temperature transient, heat transfer between the thermocouple and its well in the heating solid can be represented by a contact coefficient of heat transfer, h_c, as given by Eq. (D1):

$$qA = h_c \pi d \left[T_w(x=0.05\,\text{in.}, t) - T_7 \right] \qquad \text{(D1)}$$

With these assumptions, the temperature behavior in the heating solid can be determined for various magnitudes of h_{eq}. The experimental data compared with the calculated results suggest the appropriate magnitudes of h_{eq} and h_c. Since the period of the temperature oscillation is not affected by the magnitude of the contact coefficient h_c, the data for the bubble period is used to deduce that $h_{eq} \cong 30{,}000$ BTU/hr-ft^2-°F.

The amplitude of the temperature oscillation is directly influenced by the magnitude of h_c; hence, the amplitude data suggests with Fig. 55 the magnitude of h_c = 120 BTU/hr-ft^2-°F.

The magnitude of h_{eq} = 30,000 BTU/hr-ft^2-°F is shown in Section III.3.4 to be a reasonable one by comparison with liquid-layer measurements. The magnitude of h_c = 120 BTU/hr-ft^2-°F is

shown to be a reasonable one by comparison of measured contact coefficients for zero or very light loading (39).

III.5.5 Conclusions

The results discussed above lead to the following conclusions:

1. During stable nucleate boiling of sodium, the presence of the microlayer directly beneath the growing bubble on the heating surface causes a wave of temperature depression to penetrate into the heating solid; this local temperature drop is due to the evaporation of this thin layer of liquid into the bubble, and is much larger than the temperature drop due to any surface quenching at the time of bubble departure.
2. During stable nucleate boiling of sodium, the wall temperature at the solid-liquid interface varies periodically. The maximum temperature is that required to cause nucleation of the sodium-vapor bubble at the cavity. The minimum temperature is determined by the evaporative cooling of the microlayer during the bubble contact time, and is a function of the thermophysical properties of the liquid and of the solid.
3. Boiling from an artificial cavity is similar to boiling from a natural cavity, and the use of artificial cavities is a valid method for the study of the mechanism of boiling heat transfer to the alkali liquid metals.

4. The wall superheat for nucleation from a single cavity is independent of heat flux and is predicted by Eq. (1).
5. The bubble period for stable boiling is a function of the heat flux, the system pressure, the cavity size, and the thermophysical properties of the liquid and of the solid.
6. Stable boiling from natural cavities can exist at atmospheric pressures and at low heat fluxes.
7. Unstable boiling or "bumping" is present only at low pressures.

IV. CAVITY DEACTIVATION BY PRESSURE - TEMPERATURE HISTORY

The real problem in connection with nuclear reactor safety is that of cavity deactivation during a pressurization and subcooling time period of up to 3 years (expected lifetime of fuel rod).

The pressure-temperature history is believed (7,8) to be a critical variable in determining the size range of the cavities which will be deactivated during pressurization and subcooling conditions. For alkali liquid metals, the size of the largest active cavity governs the incipient wall superheat to nucleate due to the low temperature gradient caused by high thermal conductivity. For the reactor application, the sodium subcooling with respect to local pressure will be greater than 500 °F, and the operating pressures will be greater than 1 atmosphere.

IV.1 Previous Work

There have been two recent investigations (7,8) into the effect of pressure-temperature history on incipient wall superheats to boil. Holtz and Singer (7) investigated the effect of pressure-temperature history for sodium in pool boiling with transient heat flux; a great deal of scatter existed in the experimental results. Chen (8) investigated the incipient wall superheat to initiate the boiling of potassium in forced convection; in addition to the fairly large scatter in the experimental results, a semi-empirical correction attributed to the presence of inert

gas was applied to correlate the data. In contrast to Chen, the presence of an inert gas was neglected in the analysis by Holtz and Singer although their experimental technique did not rule out the possibility. Varying amounts of inert gas for the different runs in the experiments of both investigators could explain the observed scatter.

In addition, the data of Holtz and Singer exhibited a suspicious effect of heat flux on incipient wall superheats to boil. One explanation (26) of the observed phenomenon is that nucleation may have occurred at a cavity which is not in the heating zone but is in the unheated wall at a finite distance from the heating zone. Conduction along the wall during the transient can explain why a thermocouple in the heated zone yields higher readings at incipience as the magnitude of the step change in heat flux is increased. The data of Holtz and Singer after re-examination in light of the above discussion actually indicate that the same cavity outside of the heated zone could have been nucleating in all of their experiments. More recently, Holtz and Singer (27) have reversed their earlier no-gas stand, and they now attribute this heat flux effect to varying amounts of inert gas in the nucleating cavity.

Earlier theoretical work by Bankoff (28) suggested the physical mechanisms of "flipping" of contact angle from wetting to non-wetting and back, which is the basic concept of the two recent cavity deactivation models of Holtz and Singer (7) and of Chen (8). Chen extended the work of Holtz and Singer to account for the presence of a non-condensible gas.

Chen's model states that, subsequent to the filling operation and during the deactivation conditions of pressure P_ℓ' and temperature T_ℓ' as shown in Fig. 47a and 47b, the vapor-liquid interface moves into the cavity with a non-wetting contact angle on the cavity wall which is covered with surface oxide. Thus, mechanical equilibrium at deactivation requires:

$$P_\ell' - (P_v' + P_g') = \frac{2\sigma'}{r_d} \tag{36}$$

where P_v' = vapor pressure at the deactivation temperature T_ℓ'

P_g' = partial pressure of non-condensible gas trapped in the cavity

σ' = surface tension at the deactivation temperature T_ℓ'

r_d = deactivation radius.

Therefore, if P_g' is known, r_d can be calculated from deactivation conditions P_ℓ' and T_ℓ'. Then, as the system is heated at its boiling pressure as shown in Fig. 47c, Chen's model postulates that the vapor-liquid interface flips from a non-wetting contact angle to a wetting contact angle ($\beta \sim 0°$) and subsequently nucleates at the previous deactivation radius, r_d, when sufficient superheat is available. Thus, mechanical equilibrium at the nucleation condition requires:

$$(P_v + P_g) - P_\ell = \frac{2\sigma}{r_d} \tag{37}$$

where P_v = vapor pressure at the boiling temperature T

P_g = partial pressure of non-condensible gas trapped in the cavity

σ = surface tension at temperature T

P_ℓ = liquid pressure.

Hence, if P_g' and P_g are known, the wall superheat for incipient nucleation subsequent to a specified deactivation history can be

predicted. Chen relates P_g' and P_g to the cavity size via the perfect gas law:

$$P_g' = \frac{G_o T'}{r_i^3} \quad , \quad P_g = \frac{G_o T}{r_i^3} \tag{38}$$

where G_o is a constant characteristic of the experimental conditions and the filling procedures; the order of magnitude of G_o is estimated, but the final value of $G_o = 8 \times 10^{-17}$ in.-lbf/^oR used to correlate the data is obtained empirically.

Chen attributes G_o as being due to gas trapped in the cavity at the time of fill, and he justifies its constancy with arguments of low diffusion rates of argon in potassium as preventing its diffusion out of the cavities over the time period of his experiments. The argument of diffusion out of the cavity as not being of consequence seems highly suspect, and turbulent bubble ejections during boiling would further deplete the argon supply in time.

Using new equilibrium solubility data for argon in sodium (29) the reduction in superheat afforded by the equilibrium content of argon can be calculated (30), and the magnitude of this reduction is small. For example, a reduction of about 6 °F from 60 °F can be expected at cavities with radii of 10^{-4} in. at a boiling pressure of 1.7 atmospheres. In addition, the effect diminishes at smaller cavity sizes which correspond to increasingly severe deactivation conditions.

However, a different non-equilibrium effect has been found by Bersin et al. (31) in flow-boiling potassium experiments; the single-phase liquid metal apparently picked up inert gas bubbles from the accumulator. To investigate the effect of these bubbles

on the incipient superheat to initiate boiling, a non-condensible gas separator was installed; incipient wall superheat data was taken as a function of operating time of the separator. This superheat increased from 100 °F to 200 °F at a boiling pressure of 36 psia after the separator had been run for 800 hours. Gas bubbles of the proper size present in the liquid metal stream could facilitate bubble formation by acting as nuclei; this could beneficially reduce the incipient superheat for boiling, thereby minimizing fluid expulsion from the channel in the eventuality of a reactor accident. Therefore, it is possible that non-equilibrium gas bubbles could overshadow wall nucleation sites in flow-boiling incipience. Bersin et al. appear to be the only investigators with published results to examine this effect, and their attention to it was strictly as a sidelight.

In another investigation, the effect of increased velocity in a forced convection sodium loop was found (32) to reduce bulk superheat at incipience; in fact, little or no superheating was reported for flow velocities above 4 ft./sec. in the pressure range of 2-8 psia. This effect can also be attributed to the presence of inert gas bubbles, which have less time to separate from the stream of liquid metal at the higher velocities.

IV.2 Model for Deactivation of Re-entrant Cavities

The findings of Addison et al. (33) support the view that cylindrical and conical cavities can be deactivated by the wetting by sodium of the cavity walls. Their investigation indicates that sodium assumes a zero contact angle in time (less than 1 minute)

and above a certain temperature (800 °F), on both nickel and stainless steel surfaces. All of their observations were consistent with the assumption that sodium reduces the invisible oxide that would be present after abrasion to a mirror surface finish in air. Thus, this deactivation process is limited by the seepage rate of the liquid metal into the cavity, and is therefore expected to be time dependent.

Secondly, theoretical arguments (34) show that if the liquid temperature is reduced to saturation temperature or lower, then all cylindrical and conical cavities are flooded for zero contact angle in the static case if no inert gas is present.

Thirdly, experimental work on potassium (35) without a cover gas indicates that deactivation can occur without any mentioned subcooling or pressurization; otherwise, large incipient superheats would not be required to initiate boiling in the second and succeeding runs of a given series.

The above investigations are consistent with each other, and it is concluded that the assumptions of the recent deactivation models with conical cavities (7,8) appearing in the literature do not entirely describe the real problem of the prediction of boiling incipience.

A model is presently delineated which avoids the above-mentioned problems. First, it is allowed that the contact angle through the liquid, β , is equal to zero. Second, re-entrant cavities are assumed to be present over a range of cavity sizes in the boiling surface, and typical geometry is shown in Fig. 48. Recent photomicrograph studies (36) on extruded tubing show that both re-entrant

and cylindrical cavities do exist on natural surfaces.

Cavity deactivation is governed by the internal mouth. This requires that at the maximum allowable conditions (subcooling, pressurization) for the cavity to remain active, the vapor-liquid interface hangs on the lower lip. At zero contact angle, mechanical equilibrium requires

$$P_\ell' - \left[P_v' + P_g'(t)\right] = \frac{2\sigma' \sin\phi}{r_d} \qquad (39)$$

where $P_g'(t)$ = the time-dependent partial pressure of inert gas in the cavity at temperature T_ℓ'.

Cavities with mouth sizes greater than r_d will be deactivated, while those with smaller sizes can remain as active sites. Then subsequent nucleation is governed by the internal mouth, since this is the condition of the smallest radius which requires the highest superheat; mechanical equilibrium requires:

$$\left[P_v + P_g(t)\right] - P_\ell = \frac{2\sigma}{r_d} \qquad (40)$$

where $P_g(t)$ = the time-dependent partial pressure of inert gas in the cavity at temperature T.

Thus, the same general equations result from consideration of re-entrant cavities as result from a conical non-wetting cavity, but sounder rationale can be applied to obtain the results. In addition, the interpretation of $P_g'(t)$ and $P_g(t)$ is different and is based upon examination of the actual situation, as discussed below.

When the heat transfer system with a cover gas is at boiling temperature and pressure, the equilibrium conditions of the partial pressures of the sodium and the helium (or other cover gas) obtain as shown in Fig. 49a. The equilibrium partial pressure of the helium in the cavity is small, and helium is slowly diffusing out

of the cavity due to the possible slight partial pressure gradient.

However, when the system is at deactivation conditions in Fig. 49b, the partial pressure gradient is reversed and vastly steeper; helium diffuses into the cavity. At the liquid interface, the partial pressure of the sodium vapor is determined by the deactivation temperature, T_ℓ' ; the partial pressure of the helium is the difference between the total pressure and the sodium vapor pressure. At the cavity, the partial pressure of the helium begins roughly at the previous equilibrium value and is increasing due to diffusion of helium into the cavity caused by the helium gradient. Thus, P_g' and P_g are expected to be time-dependent. In addition, convective mixing in the liquid would augment the rate of deposition of helium at the cavity entrance, thereby increasing the helium accumulation rate.

Therefore, the partial gas pressure, P_g' , could increase with time; incipient boiling would be affected by the diffusion rate and by the solubility of the cover gas in the liquid. At the present time, no data exist for either the solubility or diffusion coefficient of helium in sodium.

In view of these considerations, the presence of an inert cover gas can reduce the incipient superheats for boiling; the magnitude of this reduction can vary with time and with the specific cover gas.

IV.3 Experimental Incipient Superheats

Additional experiments were run to investigate the effect of pressure-temperature history on incipient boiling superheats. For

these experiments, the apparatus was brought up to operating temperatures over several hours; then, boiling occurred from the test section for one hour before imposing the controlled deactivation conditions of pressurization and subcooling.

The system was cooled to the deactivation temperature, T_1' , of 1475^{o} F and then pressurized to its deactivation pressure, P_1' ; in 5 of the experiments, the duration of these deactivation conditions was 15 minutes, and it was 2 hours in 2 of the experiments. The data for incipient wall superheat required to initiate boiling at a saturation temperature of 1620^{o} F is shown in Fig. 50 as a function of deactivation pressure and for a constant deactivation temperature. The no-gas prediction of incipient superheat of Eq. (40) is shown as is the Chen correlation for gas content (see Section IV.3) which described his argon-potassium results. The data fall well below these predictions.

The discrepancy between theory and experiments is believed to be due to the presence of the inert cover gas, helium, in the natural cavities. As discussed in Section IV.2, this gas would lower the incipient superheat for boiling. Helium is probably more soluble in sodium than argon, due to its smaller molecule. Hence, the gas effect would be enhanced by the use of helium instead of argon. No data is available in the literature on the solubility of helium in sodium; consequently, a quantitative estimate of its effect is difficult. During one test, argon was substituted for helium as the cover gas; but the density of argon is greater than that of sodium vapor, and the resultant convection instability did not allow steady state conditions to obtain.

The incipient data for the tests where the deactivation conditions were in effect for 2 hours show slightly lower superheats. This indicates an increased amount of helium in the cavity due to a longer time for diffusion of this gas into the cavity. This observation is consistent with the discussion of partial pressures of helium in Section IV.2.

IV.4 Conclusions

The results discussed in this Chapter lead to the following conclusions:

1. Re-entrant cavities can remain active during periods of subcooling and pressurization and still meet the requirement of zero contact angle through the liquid.
2. The presence of non-condensible gas in a cavity can significantly reduce the incipient superheats for boiling. The source of this gas is diffusion during the deactivation period from the cover gas over the liquid; the amount of this gas in the cavity is time-dependent which affects the incipient superheat.

V. UNSTABLE BOILING

V.1 General Considerations

A number of investigators (2, 3, 4, 5, and others) have observed the phenomenon of unstable boiling, so-called "bumping". However, scant consideration in the literature has been given to the physical cause of this unsteady boiling, although it has been attributed (5) to the transient presence of inert gases. A typical temperature-time trace during unstable boiling at low pressure was shown earlier in Fig. 28.

Only Collier and Kosky (1) have examined the leak rate of an inert gas after its being trapped in a cavity during the filling operation by advancing liquid. The objective of their analysis is to determine whether inert gas would be present over sustained periods of time, thereby lowering the wall superheat required for nucleation. Their analysis evaluated at zero contact angle through the liquid shows that all gas has diffused out of the cavities within several hours in a conservative estimate, or within one hour if the cover gas is evacuated immediately after filling. As a matter of interest, the filling procedure of many investigations (including the present one) is to evacuate the system before filling, which reduces the amount of inert gas which could be trapped initially. This analysis of Collier and Kosky (1) does not consider the problem of outgassing of the heating solid. In addition, it has been observed by the present writer and others (4, 5)

that bumping may be present over long periods of time.

V.2 Analysis of Unstable Boiling

The analysis presented herein shows that there is a finite and steady source of gas at the nucleation site which stems from the very slow and continuous degassing of the heating solid over long periods of time. The standard solution for the concentration profiles and the flow rate of the transient diffusion problem in a semi-infinite medium is presented, and its applicability to this problem is verified.

V.2.1 Mathematical Formulation of the Diffusion Problem

The problem of transient diffusion of gas from the heating solid (nickel) is examined. The problem as shown in Fig. 51 may be handled by solving the transient diffusion equation for a semi-infinite medium:

$$\frac{\partial c}{\partial t} = D \frac{\partial^2 c}{\partial x^2} \tag{41}$$

At time zero, the solid is initially at uniform gas concentration, c_o:

$$t = 0 \quad c(x,0) = c_0 \text{ for all } x$$

and the ambient concentration, c_a, at the interface is zero at all times:

$$t > 0 \quad c_a = 0 \text{ at } x = 0$$

This condition implies no resistance to mass transfer at the interface, and is a reasonable assumption since the diffusion coefficient in the liquid (sodium) is several orders of magnitude

larger than that in the solid.

The solution to this problem is known (37), and the concentration profile is:

$$\frac{C}{C_o} = \text{erf}\left[\frac{X}{2\sqrt{Dt}}\right] \tag{42}$$

and the mass flux out of the solid is:

$$\frac{W}{A} = C_o\sqrt{\frac{D}{\pi t}} \tag{43}$$

Significant amounts of these various gases, CO_2, CO, H_2, N_2, have been found (38) to be present in commercial-grade nickel. A conservative number for c_o from reference (38) is

c_o = 0.10 cm^3 gas (STP)/cm^3 nickel.

The value of the diffusion coefficient, D, is conservatively deduced via exponential extrapolation from the available data (38) to be

D = 3.1 x 10^{-12} cm^2/sec (or 1.2 x 10^{-11} ft^2/hr) at 1200 °F.

These material properties yield from Eq. (43) a time-dependent mass flux out of the solid of:

$$\frac{W}{A} = \frac{5.9 \times 10^{-4}}{\sqrt{t}} \quad \frac{cm^3 \text{ gas (STP)}}{cm^2\text{-hr}} \quad \text{with t in hours} \tag{44}$$

In order to clarify the magnitudes of the numbers, the volume of gas at standard temperature and pressure (STP) evolved per unit surface area in the 15 minutes immediately subsequent to the 15th hour of operation may be calculated after a nominal integration of Eq. (44) over time to be: 3.9 x 10^{-5} cm^3 gas (STP)/cm^2 surface. The perfect gas law yields the pressure temperature correction of: V(1200 °F, 0.1 atm) = 31 V (STP), so the true volume of gas evolved per unit surface area in this specified time is: 1.2 x 10^{-3} cm^3 gas/cm^2 surface. A typical length of a natural

cylindrical cavity is about 10 times its mouth radius, or a length of roughly 0.02 in. (or 0.05 cm). Hence, the fraction of cavity volume which is filled by gas in the specified 15 minutes is:

$$\frac{1.2 \times 10^{-3} \text{ cm}^3 \text{ gas}}{0.05 \text{ cm} \quad \text{cm}^2 \text{ surface}} = 2.5 \times 10^{-2} \text{ or } 2.5\% \text{ by volume}$$

which is a conservative calculation; this accumulated gas fraction in the cavity is much lower than the initial concentration of gas in the nickel. This calculation shows that a finite amount of gas relative to the cavity size can be slowly evolved from the heating solid.

The volume fraction of cavity filled by gas is independent of cavity diameter, and is inversely proportional to the characteristic cavity length. This implies that the effect of system outgassing would be greater for the smaller cavities which would tend to be of shorter length.

The gas flow rate is shown to have two properties: it is small but finite, and it continues over long periods of time. The meaning of this result is that there is a continuous source of gas which is able to act as a nucleation site for bubbles if the liquid superheat at the wall is adequate. Alternatively, this gas could reduce the superheat required to nucleate an active cavity of smaller radius.

It must be assumed that the diffused gas remains trapped in the cavity and does not immediately diffuse out of the cavity into the liquid; this is valid if the gas is trapped in a re-entrant cavity. As discussed in Section IV.2, photomicrograph evidence (36) verifies the existence of both re-entrant cavities and cylindrical cavities.

A logical explanation of the "bumping" phenomenon is now given. During bumping, it has been observed in this investigation that the system can remain in natural convection for extended periods of time; this implies that the cavities are not immediately active as bubble nucleation sites. The small cavities require a large superheat which is not available, as the system can remain in steady-state natural convection and still transfer heat at the required rate. In addition, these cavities could have been de-activated by the wetting of the cavity walls by sodium. Then, gas molecules which appear in the natural cavity via transient diffusion from the heating solid are able to act as a nucleation site in the superheated liquid; this gas can cause the nucleation of a bubble with the associated large drop in wall temperatures. This single nucleation can re-activate larger cavities if the bubble pushes vapor into the top of a larger cavity. Any accumulated gas in the nucleating cavity would be carried away by the bubble ejections.

At low pressures where bumping is usually observed, the density of the vapor is very low; and hence the heat capacity of the vapor in the cavity is also very low, relative to the same volume of heating solid. A small perturbation in the local heat flux or evaporative cooling by the microlayer could condense this vapor and snuff out the cavity; this perturbation can reasonably occur, for example, if the bubble remains at the cavity only momentarily beyond its expected contact time. If the cavity is snuffed out, then the mode of heat transfer returns to

natural convection. The heating solid will remain in natural convection until the gas is again able to trigger random nucleation, wherein the erratic behavior discussed above is repeated. This inert gas would be diffusing into many cavities, and nucleation could be triggered from a succession of cavities, thereby allowing time for replenishment of the gas content in the cavity by diffusion. This is the phenomenon known as unstable boiling, and the gas source functions as an erratic nucleation site.

If the cavity is not snuffed out during the normal cyclical temperature drop during stable boiling, then the cavity is an active nucleation site, and steady boiling continues on the surface. The nucleation dynamics during steady boiling carry the gas away as fast as it diffuses into the cavity, so that no gas effect is expected on stable-boiling superheats.

V.2.2 Validity of Assumption of Semi-Infinite Medium for Diffusion

In order to assume a semi-infinite medium, it must be shown that a boundary layer thickness in the concentration profile does not extend past the actual width of the nickel heating solid. This means that the location where $c/c_o = 0.99$ must be calculated. For $\frac{c}{c_o} = 0.99 = \text{erf}\left[\frac{x}{2\sqrt{Dt}}\right]$, then $\left[\frac{x}{2\sqrt{Dt}}\right] = 1.82$. For time, it is assumed that $t = 1000$ hours. Then, with $D = 3.1 \times 10^{-12}$ cm^2/sec, a calculation yields $x = 4.7 \times 10^{-3}$ in. as the depth of boundary layer penetration in 1000 hours; the actual thickness of the nickel heating solid is 0.85 in. Therefore, the treatment of the problem as that of a semi-infinite solid is valid.

V.3 Experimental Results and Discussion

A typical temperature-time trace during unstable boiling at low operating pressure was shown earlier in Fig. 28. This trace shows that the mode of heat transfer during bumping randomly alternates between boiling and natural convection. In order to trigger the boiling, a nucleation site must become active. Gaseous diffusion from the heating solid into a potential nucleation site can cause this cavity to become active as a nucleation site. As discussed in Section V.2.1, this gas source is available from the slow but finite outgassing of the heating solid at the operating conditions of the system.

Fig. 52 shows another temperature-time trace during unstable boiling at low pressures. At the time when boiling is triggered on this trace, the liquid superheat is not at its highest value. This behavior indicates that the activation of the nucleation site is dependent upon time; this observed time-dependence is consistent with the fact that gaseous diffusion into the cavity is time-dependent.

It has also been observed that the system can remain in natural convection for extended periods of time, before a bubble nucleation is triggered. This indicates that the nucleation site corresponding to the available superheat is not immediately active and that its activation is time-dependent.

These two observations give strength to the supposition that transient diffusion of non-condensible gas from the heating solid can act as an erratic nucleation site.

Referring to Fig. 29, the small arrows near the 100 mm Hg data ("circles") indicate the heat flux history. As the heat flux was increased, the mode of heat transfer switched to stable boiling from natural convection and no bumping was observed. The heat flux was increased further and then decreased; no bumping was observed in this 100 mm data or for the higher pressure data in Fig. 29.

Similarly, for the 100 mm data in Fig. 30, as the heat flux was increased, the mode of heat transfer switched to boiling and no bumping was observed, both at increased and decreased heat flux. However, bumping existed at 30 mm Hg. Bumping was not observed for data at pressures greater than 200 mm Hg and only occasionally at a pressure of 100 mm Hg. This indicates that bumping is a characteristic of low-pressure operation.

Earlier discussion in Section V.5.2 indicates that outgassing of the heating solid can trigger nucleation at a previously inactive site. The data from (38) for gas concentration in a solid was obtained by outgassing a solid into a vacuum; for a solid heated in a non-vacuum environment, however, the driving force for outgassing is less, and a lower gas flow rate is expected. Hence, at higher operating pressures, the effect of outgassing would be diminished, and the direction of gas flow may even be reversed at atmospheric pressure; these are consistent with the observation that bumping occurred only at low pressure.

V.4 Conclusions

The results discussed in this Chapter lead to the following conclusions:

1. Unstable boiling or bumping can be caused by outgassing of the heating solid into a previously inactive site; this gas can act as an erratic nucleation site.
2. Bumping is a characteristic of low-pressure operation, since the gas flow rate from the heating solid decreases as the pressure is increased and at some pressure will cease altogether.

VI SUMMARY OF CONCLUSIONS AND RECOMMENDATIONS

The conclusions were previously given at the end of each Chapter and are listed here for convenience.

Nucleate Boiling Heat Transfer

1. During stable nucleate boiling of sodium, the presence of the microlayer directly beneath the growing bubble on the heating surface causes a wave of temperature depression to penetrate into the heating solid; this local temperature drop is due to the evaporation of this thin layer of liquid into the bubble, and is much larger than the temperature drop due to any surface quenching at the time of bubble departure.
2. During stable nucleate boiling of sodium, the wall temperature at the solid-liquid interface varies periodically. The maximum temperature is that required to cause nucleation of the sodium-vapor bubble at the cavity. The minimum temperature is determined by the evaporative cooling of the microlayer during the bubble contact time, and is a function of the thermophysical properties of the liquid and of the solid.
3. Boiling from an artificial cavity is similar to boiling from a natural cavity, and the use of artificial cavities is a valid method for the study of the mechanism

of boiling heat transfer to the alkali liquid metals.

4. The wall superheat for nucleation from a single cavity is independent of heat flux and is predicted by Eq. (1).
5. The bubble period for stable boiling is a function of the heat flux, the system pressure, the cavity size, and the thermophysical properties of the liquid and of the solid.
6. Stable boiling from natural cavities can exist at atmospheric pressures and at low heat fluxes.
7. Unstable boiling or "bumping" is present only at low pressures.

Incipient Superheats

1. Re-entrant cavities can remain active during periods of subcooling and pressurization and still meet the requirement of zero contact angle through the liquid.
2. The presence of non-condensible gas in a cavity can significantly reduce the incipient superheats for boiling. The source of this gas is diffusion during the deactivation period from the cover gas over the liquid; the amount of this gas in the cavity is time-dependent which affects the incipient superheat.

Unstable Boiling

1. Unstable boiling or bumping can be caused by outgassing of the heating solid into a previously inactive site;

this gas can act as an erratic nucleation site.

2. Bumping is a characteristic of low-pressure operation, since the gas flow rate from the heating solid decreases as the pressure is increased and at some pressure will cease altogether.

Recommendations

1. Fundamental investigation of sodium bubble growth is needed to provide experimental information on bubble growth rate, thickness of microlayer, and bubble departure diameter; visual techniques with x-rays would be desirable.
2. A definitive set of experiments should be run to clarify the magnitude of the gas effect on incipient superheats for boiling subsequent to deactivation pressurization and subcooling.

REFERENCES

1. Collier, J.G. and Kosky, P.G., "Natural Convective Boiling of the Alkali Metals - A Critical Review," AERE-R 5436, 1967.

2. Lyon, R.E., Foust, A.S. and Katz, D.L., "Boiling Heat Transfer with Liquid Metals," Chem. Engr. Prog. Symposium Series No. 17, vol. 51, 1955.

3. Madsen, N. and Bonilla, C.F., "Heat Transfer to Boiling Sodium-Potassium Alloy", Chem. Engr. Prog. Symposium Series, No. 30, Vol. 56, 1959.

4. Marto, P.J. and Rohsenow, W.M., "The Effect of Surface Conditions on Nucleate Pool Boiling Heat Transfer to Sodium," M.I.T. Engineering Projects Laboratory Report No. 5219-33, 1965.

5. Shai, I. and Rohsenow, W.M., "The Mechanism of Nucleate Pool Boiling Heat Transfer to Sodium and the Criterion for Stable Boiling," M.I.T. Engineering Projects Laboratory Report No. 76303-45, 1967.

6. Bobrovich, G.I., Avksentyuk, B.P. and Mamontova, N.N., "On the Mechanism of Boiling of Liquid Metals," J.S.M.E. Semi-International Symposium, Tokyo, Japan, Sept. 4-8, 1967.

7. Holtz, R.E. and Singer, R.M., "On the Initiation of Pool Boiling in Sodium," A.I.Ch.E. Preprint 15 for Tenth National Heat Transfer Conference, August, 1968.

8. Chen, J.C., "Incipient Boiling Superheats in Liquid Metals," Journal of Heat Transfer, Vol. 90, 1968, pp. 303-312.

9. Brown, W.T., Jr., "A Study of Flow Surface Boiling," Ph.D. Thesis, Mech. Eng. Dept., M.I.T., 1967.

10. Dina, J.L., "Determination of Nucleation Sites for Pool Boiling," M.S. Thesis, Mech. Eng. Dept., M.I.T., 1968.

11. Cooper, M.G. and Lloyd, A.J.P., "Transient Local Heat Flux in Nucleate Boiling," Proceedings of the Third International Heat Transfer Conference, Chicago, Vol. III, pp. 193-203, 1966.

12. Carslaw, H.S. and Jaeger, J.C., Conduction of Heat in Solids, Oxford Press, 1959.

13. Eckert, E.R.G. and Drake, R.M., Heat and Mass Transfer, McGraw-Hill, 1959.

14. Lien, Y.-C. and Griffith, P., "Bubble Growth Rates at Reduced Pressure," to be submitted to Int. Journal Heat Mass Transfer; also, Lien, Y.-C., "Bubble Growth Rates at Reduced Pressure," Sc.D. Thesis, Mech. Eng. Dept., M.I.T., 1969.

15. Cole, R. and Rohsenow, W.M., "Correlation of Bubble Departure Diameters for Boiling of Saturated Liquids," A.I.Ch.E. Preprint 25 for Tenth National Heat Transfer Conference, 1968.

16. Wichner, R.P. and Hoffman, H.W., "Vapor-Bubble-Growth Rates in Superheated Liquid Metals," ORNL-TM-1413, 1966.

17. Kroger, D.G., "Heat Transfer During Film Condensation of Potassium Vapor," M.I.T. Engineering Projects Laboratory Report No. 75239-42, 1966.

18. Spiller, K., Grass, G. and Perschke, D., "Superheating and Single Bubble Ejection with the Vaporization of Stagnating Liquid Metals," Atomkernenergie, Vol. 12, 1967, pp. 111-114.

19. Levich, V.G., Physicochemical Hydrodynamics, Prentice-Hall, 1967.

20. Cooper, M.G., and Lloyd, A.J.P., "The Microlayer in Nucleate Pool Boiling," Int. Journal Heat Mass Transfer, Vol. 12, No. 8, 1969, pp. 895-913.

21. Weatherford, W.D., Tyler, J.C. and Ku, P.M., "Properties of Inorganic Energy-Conversion and Heat-Transfer Fluids for Space Applications," WADD Technical Report 61-96, 1961.

22. Touloukian, Y.S., ed., Thermophysical Properties of High-Temperature Solid Materials, Macmillan, 1967.

23. Bonilla, C.F., Sawhney, D.L. and Makansi, M.M., "Vapor Pressure of Alkali Metals, III Rubidium, Cesium, and Sodium-Potassium Alloy up to 100 Pounds per Square Inch," Proceedings of 1962 High-Temperature Liquid-Metal Heat Transfer Technology Meeting, BNL-756, 1962.

24. Vinogradov, Y.K. and Volyak, L.D., "Experimental Determination of the Saturated Vapor Pressure of Sodium and Potassium," High Temperature (Soviet), Vol. 4, No. 1, 1966, p. 43.

25. Solov'ev, A.N. and Makarova, P.O., "Study of the Surface Tension of Liquid Sodium and Potassium," High Temperature (Soviet), Vol. 4, No. 2, 1966, pp. 187-192.

26. Rohsenow, W.M. and Deane, C.W., Discussion of A.I.Ch.E. Preprint 15 for Tenth National Heat Transfer Conference, 1968, to appear in A.I.Ch.E. Journal.

27. Singer, R.M. and Holtz, R.E., Discussion, Journal of Heat Transfer, Vol. 91, 1969, p. 199.

28. Bankoff, S.G., "Ebullition from Solid Surfaces in the Absence of a Pre-Existing Gas Phase", Heat Transfer and Fluid Mechanics Institute, 1956.

29. Veleckis, E., et al., "Solubility of Argon in Liquid Sodium", in ANL-7325, 1967, pp. 128-131.

30. Judd, A.M., "Sodium Boiling and Fast Reactor Safety Analysis", AEEW-R561, 1967.

31. Bersin, G.W., Horan, J. and Costales, D., "Forced Convection Boiling Potassium Experiments", PWAC-430, 1964.

32. "Quarterly Technical Progress Report", Atomics International, AI-AEC 12680, Jan-March, 1968, pp. 59-68.

33. Addison, C.C., Iberson, E. and Manning, J.A., "The Role of Oxide Films in the Wetting of Iron, Cobalt and Nickel by Liquid Sodium, and by Solutions of Barium and Calcium in Liquid Sodium", Journal Chem. Soc., 1962, pp. 2699-2705.

34. Petukhov, B.S., Kovalev, S.A. and Zhukov, V.M., "Study of Sodium Boiling Heat Transfer", Proceedings of the Third International Heat Transfer Conference, Chicago, Vol. III, pp. 80-91, 1966.

35. Edwards, J.A. and Hoffman, H.W., "Incipient and Stable Boiling Superheat for Potassium on a Surface Containing Re-entrant Cavities," ORNL-P-3083, 1966.

36. Pan, C.H.T., Eighth Monthly Letter Progress Report on "Study of Thermo-Hydraulic Oscillations in Boiling Systems Employing Liquid Metal Working Fluids," Mechanical Technology Incorporated, Latham, New York, September, 1968.

37. Rohsenow, W.M. and Choi, H.Y., Heat, Mass, and Momentum Transfer, Prentice-Hall, 1961.

38. Dushman, S. and Lafferty, J.M., Scientific Foundations of Vacuum Technique, Wiley, 1962.

39. Mikic, B.B. and Rohsenow, W.M., "Thermal Contact Resistance," M.I.T. Engineering Projects Laboratory Report No. 74542-41, 1966.

40. Wilcox, S. J. and Rohsenow, W. M., "Film Condensation of Liquid Metals-Precision of Measurement", M.I.T. Engineering Projects Laboratory Report No. 71475-62, 1969.

APPENDIX A

EQUIPMENT

The apparatus for this investigation was originally built and used by Marto (4); Shai (5) used the apparatus in his subsequent investigation. Fig. 1 shows a diagram of the whole apparatus. The important details of the various system components are described below.

A.1 Boiler-Condenser

The boiler-condenser section shown in Figs. 53 and 54 is a vertical pipe, stainless steel 316, 40-inches long with 2-1/2 in. inside diameter. The horizontal boiling surface is the bottom of this pipe, while the plate at the top of the pipe contains two temperature-probe fittings and two inlet pipes.

The two stainless-steel temperature probes of 1/4-in. diameter are each in a "Conax" packing gland with a teflon sealant; the tightness of the teflon sealant was checked and maintained during the experiments at half-hour intervals. One probe contains the liquid thermocouple and is also the sensor for the minimum sodium level (see Section A.7). The other probe contains the vapor thermocouple.

One of the inlet pipes is used for pumping sodium into the test section (Section A.4), while the other pipe is for controlling the pressure of the helium cover gas (Section A.5).

The boiler section is a 9 in. length of 2-1/2 in. inside diameter pipe which is welded with 5 in. diameter flanges to the condenser section which extends through the vacuum-chamber cover as seen in Figs. 53 and 54. The end piece at the bottom of this vertical pipe is the horizontal boiling surface; the specifications of the various boiling surfaces used in this investigation are given in Chapter II.

In order to change boiler surfaces, the weld which attaches the boiler section to the condenser section as seen in Fig. 54 must be ground off, and the new test section welded into place.

The condenser section is a 31 in. length of 2-1/2 in. inside diameter pipe with 18 vertical copper fins silver-soldered to the outside. A concentric jacket of mild steel fits over this condenser pipe which channels air over the copper fins as shown in Fig. 53. A 120-CFM centrifugal air blower attaches to the top of the condenser and a coil of Chromel "A" resistance wire is used to preheat the air. The air exits at the bottom of the condenser section into the MIT exhaust system.

A.2 Main Heater and Guard Heater

The main heater shown in Fig. 54 consists of three tantalum-10%-tungsten corrugated filaments clamped into series; the dimensions of the filaments are 0.010 in. thick x 1 in. wide x 4 in. long, with the internal angle of the corrugations at 30°.

The filaments operate near 4000°F and require the use of a high vacuum system to prevent oxidation embrittlement caused by the coarse grain structure of tantalum; the melting point of tantalum-10%-tungsten is near 5300°F. The heater is reliable, and failure of the filaments was avoided by vacuum operation at better than 0.3 microns at the highest power levels.

Each filament is secured in position by pressing it between two 1/4 in. thick tantalum clamps machined to fit the filament corrugations; the assembly is then riveted together with tantalum wire of 1/16 in. diameter. This construction insures good electrical contact at all times.

These tantalum clamps are bolted to 1/8 in. thick molybdenum electrodes with tantalum screws. These molybdenum pieces are then fastened with stainless steel bolts to "L" shaped molybdenum electrodes which are slotted vertically for adjustment of the overall height of the filaments. These "L" shaped electrodes are bolted to 3/8 in. thick horizontal copper bus bars as shown in Fig. 54.

Water-cooled vertical copper electrodes are silver-soldered to the underside of the horizontal bus bars. They are fabricated by silver-soldering a 1/2 inch pipe inside a 1 in. pipe (Fig. 54); cooling water flows up the inside of the 1/2 in. pipe, then down and out the annulus. These electrodes are electrically insulated from the vacuum-chamber base plate by teflon collars which are pressed between stainless-steel flanges silver-soldered to the electrodes.

Water-cooled copper coils are installed locally in grooves machined in the underside of the base plate to protect the teflon from high temperature.

High temperature electrical insulators made of aluminum oxide and of lava channel the current so that the three filaments are connected in series. A DC power supply rated at 1000 amperes, 15 volts is connected through flexible copper leads to the vertical copper electrodes.

Eight concentric radiation shields of 0.019 in. thick stainless steel 304 are used to increase the thermal efficiency of the main heater. These shields are 12 in. high with diameters varying on the half inch from 9-1/2 in. to 13 in. Also, ten horizontal radiation shields of stainless steel, 0.019 in. thick x 3 in. wide x 6 in. long are beneath the tantalum filaments.

A new concentric guard heater shown in Fig. 54 was installed about the test section for active reduction of heat losses from the liquid sodium. During the previous investigations of Marto (4) and Shai (5), operation at atmospheric pressure with sodium at its saturation temperature and also at low heat flux was not possible due to the high heat losses. The guard heater consists of two semi-cylindrical Lindberg "Hevi-duty" heaters of 6-1/2 in. diameter, each rated at 850 watts. They have a heating element of nickel wire and a ceramic shell; "Kanthal" wire electrodes passing through a Conax gland with Lava sealant supply electricity from a variable

power source. The heaters are supported vertically in slings made from strips of "Kanthal" which hang from the 5 in. flange attaching the boiler section to the condenser section.

A.3 High Vacuum System

The high vacuum system which contains the heaters and the boiler is a stainless steel 316 vacuum chamber of dimensions 14 in. O.D. x 1/8 in. thick x 18 in. long. This vessel is fabricated by heliarc-welding flanges (3/4 in. thick x 16-3/4 in. diameter) to the top and bottom of the cylinder and by bolting plates (3/4 in. thick x 16-3/4 in. diameter) to these flanges. Twelve stainless steel cap screws (1/2 in. diameter x 2 in. long) with bolts are used with each flange. A single copper "O"-ring of 14-1/4 in. diameter provides a vacuum seal on each flange; the "O"-rings are silver-soldered from 0.125 in. diameter wire. Three Conax glands are heliarc-welded into the vacuum chamber cover to provide vacuum seals for the thermocouples and the electrodes for the guard heater. The teflon collars provide excellent seals for the main-heater copper electrodes. A vacuum of better than 10^{-5} mm Hg can be attained with the system. The entire vacuum chamber is covered with 1-1/2 in. of Fiberfrax thermal insulation to reduce heat losses. The vacuum chamber is raised and lowered with two hydraulic jacks and a steel support ring.

The high vacuum line is a horizontal stainless steel pipe of 4 inches diameter which is welded to the wall of the vacuum chamber

at a level 11 inches above the base plate. This pipe is connected to a National Research Corporation type HS4-750 diffusion pump. A Welch Duo-Seal type 1402B Mechanical pump is connected in series with the diffusion pump and is used as the roughing and backing pump. No cold trap or separate roughing lines are used.

A.4 Helium Cover-Gas Line

The helium cover gas is dried and filtered by flowing through a molecular-sieve bed at liquid nitrogen temperatures in order to maintain the sodium as free of oxides as possible; pellets of 1/16 in. diameter of an alkali-metal alumino silicate from Linde Co. were packed firmly in a stainless steel cylinder (2 in. diameter x 10 in. long). The helium gas line is 1/4 in. stainless steel 316 tubing, and all valves are Hoke type TY440.

A Cenco-Magavac mechanical vacuum pump is connected to the helium system through a standard ice trap where the 1/4 in. stainless steel tubing is joined to a series of 1/4 in. copper coils.

A large stainless steel 316 pressure tank is attached to the helium system above the condenser section; it is an 8 in. pipe of 18 in. length with caps welded at both ends. Six brass baffles are silver-soldered on the inside of the tank, and water-cooled copper coils are soldered on the outside. The tank functions as a reservoir to damp any pressure fluctuations during boiling and also as a cold trap for possible sodium vapor. All breakable joints are stainless

steel Parker Triple-lok or Swagelok fittings, and all permanent joints are stainless steel Parker Braze-lok fittings.

A.5 Sodium Fill System

The sodium fill-tank is made from stainless steel 316 of dimensions 4-1/2 in. O.D. x 6 in. high. This tank is flanged at the top and is sealed with a Viton "O"-ring of size 4-1/2 in. I.D. x 0.139 in. thick. A steel-sheathed Calrod heater of 0.260 in. diameter is cemented around the tank. This heater is rated at 1.25 KW. Thermal insulation on the tank consists of an inner layer of Fiberfrax alumina-silica fibers of half-inch thickness and an outer layer of standard fiberglass strips of half-inch thickness.

The sodium fill line is made from 3/8 in. diameter stainless-steel 316 tubing. This line goes from the fill tank through an Anaconda flexible stainless steel section (3/8 in. diameter x 12 in. long) to the condenser section through the top of the condenser. Briskeat heating tapes are wrapped around this line and are insulated. Sodium is filtered before entering the boiler section by going through a stainless steel cup (1-1/2 in. O.D. x 3 in. long) which is packed with fine-grade stainless steel wool and which is kept near 350°F during sodium transfer. All valves are Hoke type TY445, and all breakable joints are either Parker Triple-lok or Swagelok fittings.

A.6 Containment and Safety Equipment

The high vacuum system acts as a primary containment for possible sodium leakage since the boiler section is within the 14 in. O.D. vacuum chamber.

Furthermore, the entire heat transfer apparatus is enclosed within a 5 ft. x 5 ft. x 8 ft. cell which is constructed from 20-gauge steel sheets bolted to a welded framework. Rubber stripping is used between the sheets and framework to provide a pressure-tight seal in the event that an inert atmosphere is necessary. A plexiglass window (22 in. x 16 in. x 1/4 in.) is in the top half of the front side of the cell; a hinged door of size 5 ft. x 4-1/2 ft is below this window. All valve handles extend through the steel sheets to permit operation from the outside. The cell is vented through a 3-in. duct to exhaust possible fumes.

Safety equipment includes an Ansul MET-L-X fire extinguisher, a safety helmet, safety glasses, a plexiglass face shield, and asbestos-lined leather gloves.

A.7 Safety Controls

A semi-automatic control system is used for safe operation of the apparatus. This system monitors the sodium level in the boiler, the condenser air flow rate, the main electrode cooling-water flow rate, and the pressure in the main vacuum system. If the sodium level drops beneath a set value, or if there is loss of air flow or loss of vacuum or loss of water circulation, then this system

activates a buzzer and one of four control-panel lights. The system is semi-automatic because control of the equipment is manual even though detection is automatic. A master stop button on the control panel is used to shut off the main power supply in case of emergency.

Each sensing device operates an electrical relay which controls a common buzzer and an individual light. The sensor for the sodium level uses the vertical liquid-thermocouple probe; a 110-volt DC power supply is connected to this probe which is electrically insulated from the condenser by a Conax electrode gland with a teflon sealant. The sodium level acts as a switch, making or breaking the contact when the level is below or above the switch. The sensor for the air flow rate is a mercury switch attached to a butterfly valve inside the air duct. The sensors for both the water flow rate and the high vacuum system are standard pressure diaphragms attached to micro-switches.

APPENDIX B

INSTRUMENTATION

Eight chromel-alumel Conax thermocouples with magnesium-oxide insulation are used in the test surface. Ceramic insulation beads are placed on exposed portions of the thermocouples. Six of these thermocouples have 0.067 in. diameter inconel sheaths with ungrounded tips. Special calibration of all eight thermocouples was done by the Conax Corporation at 1200°F, 1500°F, and 1800°F. The other two thermocouples have 0.041 in. diameter inconel sheaths with grounded tips and a time constant of 0.04 seconds. In addition, two chromel-alumel thermocouples with 1/16 in. diameter stainless steel sheaths with magnesium-oxide insulation are used in the two vertical liquid and vapor temperature probes. These thermocouples were calibrated at 1200°F, 1300°F, and 1400°F.

Primary thermocouple measurements are made with a Leeds and Northrup type K-2 precision potentiometer with an external standard cell, battery, and galvonometer. These thermocouples are connected through a Leeds and Northrup 16-pole rotary switch. The reference junction for these thermocouples was chosen at room temperature; this reference value is recorded for each data point with a 30-gauge chromel-alumel glass-insulated thermocouple which is read against an ice junction.

In addition, a second circuit is used to record on light-sensitive paper any time-dependent behavior of the temperatures during

stable boiling. Two Leeds and Northrup millivolt potentiometers (No. 8690) are used to provide reference millivolt levels and are connected in series with the thermocouples to a recording oscillograph (Consolidated Electrodynamics Corp. No. 5-125) run at a chart speed of 0.25 in./second. The maximum sensitivity obtainable with the galvanometers is near 30 °F/in.

The liquid and the vapor thermocouples are connected through a selecting switch to one of those potentiometers. The thermocouples in the boiler test plate are connected through a selecting switch to the other potentiometer.

These two potentiometers provide a reference temperature level and only temperature variations about this level are recorded. This arrangement increases the sensitivity, and the use of two potentiometers permits simultaneous recording of temperature variation of a single thermocouple in the boiler plate with either the liquid or the vapor temperature.

A number of other thermocouples are used in the apparatus to monitor system operation. They are 30-gauge iron-constantan glass-insulated thermocouples and are connected directly to a Minneapolis-Honeywell Brown 20-point recorder with a range of 0-1000 °F.

Pressure in the helium line is measured with an open-end mercury manometer and with a Marsh compound pressure gauge. The pressure at the top of the condenser section is measured by a Taylor high-temperature volumetric pressure transducer which had been previously calibrated against the mercury manometer down to a

pressure of 40 mm Hg.

The main-heater voltage drop is measured with a 0-25 volt DC voltmeter, and the main current is determined by observing the voltage drop across a National Bureau of Standards shunt on a 0-50 millivolts meter, with 50 millivolts equalling 1000 amperes. All line heaters are monitored with variacs and ammeters in each circuit.

The pressure in the high vacuum system is determined with two thermocouple gauges and an ionization gauge. All three gauges are connected to an NRC type 710B gauge control, and the vacuum is monitored from 1 mm Hg down to 10^{-5} mm Hg.

A phonograph crystal cartridge is taped directly to the high vacuum line to pick up boiling noise from the test section. Because the crystal is limited to temperatures below 140°F roughly, the pickup is positioned about 2 in. from the wall of the vacuum chamber and is protected by water-cooled coils. The boiling noise is transmitted directly to this cartridge, and the electrical signal goes to an oscilloscope for qualitative observation.

APPENDIX C

EXPERIMENTAL PROCEDURES

C.1 Preparation of System

A lengthy procedure was followed when changing test sections. The old test section was removed by grinding off the weld, and then the new test section was welded in its place.

First, all water and electrical lines were disconnected from the vacuum chamber. Two hydraulic jacks with a steel support ring were placed under the vacuum chamber and were raised until they began to carry the heavy load. The top and side flanges of the vacuum chamber were opened, and the vacuum chamber was slowly lowered to the floor by the jacks. This chamber was then pushed to one side of the enclosure. The thermocouples were removed from the test surface and bent away from the boiler flange. A portable grinder was used to grind off the weld on the boiler flange. Helium at 3 psig pressure was maintained inside the boiler during this grinding operation which lasted one-half hour. When the crack between the two flanges was visible around the entire circumference, the weld was opened with hammer and chisel. The boiler section containing the sodium was removed; the sodium was covered with mineral oil and later reacted with n-butyl alcohol in a 55 gallon drum. All burrs on the edge of the top flange and all traces of sodium were removed. This took about two minutes during which helium was purged through the system in order to prevent oxidation of the sodium inside the apparatus.

A new boiler was then clamped in place with the thermocouple holes in the test plate oriented in the same direction as for the previous boiler. This new weld was completed in 15 minutes, and the system was immediately pumped down to less than 1 mm Hg pressure and re-pressurized with 5 psig of helium. The boiler flange was then leak tested; when it was tight, the thermocouples were inserted into the test plate, the vacuum chamber with a new copper "O" ring was raised, and the top and side vacuum flanges were tightened until a vacuum of 10^{-5} mm Hg was obtainable. High temperature lubricant, "silver goop", was used on the thermocouples and on all bolts in hot zones.

Periodically, the condenser and all the connection lines were removed and were reacted in the drum of n-butyl alcohol. Then, all parts were thoroughly washed with denatured alcohol and with hot water, degreased with trichloroethylene, furnace-dried, and re-assembled in place.

Whenever the apparatus had been completely dismantled and re-assembled after cleansing, thorough leak testing would take place. The sodium system was pressurized to 10 psig with Freon, and all previously opened joints were checked with a halogen leak detector; the sodium system was considered tight if a vacuum of 650 mm Hg held overnight without any change occuring in the open-end manometer after correction for changes in atmospheric pressure.

The vacuum system over the tantalum heaters was leak-tested

after assembly until a vacuum of 10^{-5} mm Hg existed. Leaks were checked by spraying all joints with acetone and watching the response of the thermocouple gauge for a vacuum between 10^{-2} and 10^{-3} mm Hg and of the ionization gauge for a vacuum below 10^{-3} mm Hg.

To charge the system with a new batch of sodium, the fill tank was disconnected and opened. All remaining sodium was removed mechanically and the tank was thoroughly cleaned as described above. A cylindrical brick of sodium, 2-1/4 in. diameter x 3-5/8 in. long, was placed in the fill tank after surface oxides had been scraped off. The cover, with a new viton "O" ring, was bolted in place; and the fill tank was connected to the system. The apparatus was then evacuated to 1 mm Hg pressure and re-pressurized to 5 psig with helium. At this stage, the system was ready for the next experiment.

C.2 Method of Operation

An experiment began with the sodium system at a pressure of 5 psig helium and the vacuum chamber at a vacuum of 10^{-5} mm Hg. Then, the heaters for the fill tank, the fill line, and the pressure line were turned on; the main heater, the guard heater, and the air heater were also turned on. These heaters were kept on for about 2 hours until the fill tank was at 400°F, the lines at 450°F, and the boiler plate at 400°F; the strainer was kept at 350°F. When these parts of the system were at temperature, the boiler-condenser

section was evacuated to 1 mm Hg pressure, keeping the fill tank at a pressure of 5 psig. Then, the sodium-fill-line valve was opened, and sodium flowed into the boiler. During this transfer operation, all temperatures were recorded. The transfer was completed in a few seconds. To clean the lines of any trapped sodium, the fill tank was evacuated while the boiler-condenser section remained under pressure with the fill-line valve closed. Then this valve was opened, and helium flowed from the boiler through the fill line to the fill tank, thereby cleaning the lines. When this blow-back was completed, the fill-line valve was closed, and the heaters for the fill tank and for the part of the fill-line up to the valve were shut off. While keeping the other lines at a temperature of 350°F and the top of the condenser at 225°F, the main power was gradually increased. The system was kept at a pressure of 5 psig until the desired temperature level was obtained; then it was evacuated to the desired operating pressure.

Natural convection data was taken first. When nucleate boiling began, the condenser air blower was turned on; this action lowered the condenser air-inlet temperature to 125°F. The other heaters maintained the auxiliary lines at 350°F.

For a given heat flux level, equilibrium conditions were reached after 15 minutes and the following measurements were made: the barometric pressure, the compound pressure gauge, the open-end mercury manometer, and the power input to the main heater were all read. Then, all thermocouples were read twice, including the

reference temperature, by the Leeds and Northrup type K-2 potentiometer. During boiling, the temperature of the two thermocouples close to the surface was usually oscillating, and a reading was not possible with the type K-2 potentiometer; these temperatures were recorded on the Recording Oscillograph.

After the set of measurements was completed in 15 minutes, the power to the main heater was changed. Data for both increasing and decreasing heat flux were taken.

The system was shut down by turning off the main heater and the guard heater, and by pressurizing the system to 5 psig with helium. After 1 hour when the temperature of the liquid had cooled to 1000°F, the line heaters and the diffusion pump were turned off. The entire system cooled overnight, and the sodium solidified in the boiler. The mechanical vacuum pump was shut off when the system was at room temperature.

APPENDIX D

TRANSIENT THERMOCOUPLE RESPONSE TO A PERIODIC TEMPERATURE VARIATION

This appendix shows that the magnitude of a thermocouple response to a periodic temperature variation is less than the actual temperature variation. This reduction is shown to be a function of the period of the oscillation and is caused by poor contact between the thermocouple and its well in the heating solid.

A transient energy balance on a unit length of cylindrical thermocouple of sheath diameter, d, and at temperature, T_7, with negligible internal temperature gradients yields:

$$q_+ A = h_c \pi d \left[T_w(x=0.05\ \text{in.}, t) - T_7 \right] = \rho c_p \frac{\pi d^2}{4} \frac{dT_7}{dt} \qquad (D1)$$

where h_c is the contact coefficient of heat transfer between the thermocouple sheath and its well in the heating solid, and where T_w is the temperature of the heating solid at the well.

As seen in the experimental temperature-time traces for stable boiling in Figs. 32 and 33, a reasonable representation of the temperature behavior at thermocouple No. 7 is a sinusoid. For a sinusoidal variation of the solid temperature with period, τ (bubble period), and amplitude T_o,

$$T_w = T_o \sin t/\tau \qquad (D2)$$

the solution of Eq. (D1) for the transient temperature of thermocouple, T_7, is given by:

$$T_7 = T_o\left[\cos\delta_r \sin\delta_r + \frac{T_i}{T_o}\right]e^{-\frac{4h_c}{\rho c_p d}t} + T_o \cos\delta_r \sin\left[\frac{t}{\tau} - \delta_r\right] \qquad (D3)$$

where T_i is the initial temperature of the thermocouple and where δ_r is defined as:

$$\delta_r \equiv \tan^{-1}\left[\frac{\rho c_p d}{4h_c \tau}\right] \qquad (D4)$$

The first term of Eq. (D3) is the initial start-up transient which dies out with time, while the second term represents the temperature measurement of the periodic solid temperature, T_w, by the thermocouple. The amplitude measured by the thermocouple is $T_o\cos\delta_r$, which is less than the actual amplitude of oscillation T_o.

The specifications of the thermocouple used to measure the amplitude of temperature oscillation (TC 7) in the experiments described in Section III.5.3 are: d = 0.04 in., ρ = 190 lbm/ft^3, c_p = 0.23 BTU/lbm-°F; the values of ρ and c_p are for the magnesium-oxide insulation in the thermocouple.

Calculations of the amplitude reduction factor, $\cos\delta_r$, are shown in Fig. 55 as a function of the bubble period, τ, for two values of the contact coefficient, h_c. For long bubble periods

(τ = 4 sec.), the thermocouple measurement is only slightly lower than the actual temperature variation. However, for short bubble periods, a significant difference between the thermocouple measurement and the actual temperature variation is seen to exist. This error in the measurement of the periodic temperature variation is caused by the poor contact between the thermocouple and its well in the heating solid.

APPENDIX E

DISCUSSION AND TABULATION OF MICROSCALE BOILING DATA

This appendix discusses the experimental uncertainty in the data and tabulates the microscale boiling data. An estimate of the probable error in the measurement of the heat flux due to the uncertainty of the position of the thermocouple in its well is given by Wilcox and Rohsenow (40). Using the thermocouple size and the positions of the thermocouple in the heating solid used for this investigation and as given in Fig. 3, the probable error in heat flux is estimated at $\pm$ 4.7%.

Their analysis also gives an estimate of the error in temperature measurement caused by the uncertainty in the position of the thermocouple in its well in the nickel heating solid. For the geometry of the nickel test section, the probable error in temperature measurement at TC 7 is $\pm$ 3°F at a heat flux of q_o = 100,000 Btu/hr-ft^2. This measurement error varies inversely with the thermal conductivity of the heating solid. The temperature measurement error at TC 7 is taken as the error in wall temperature measurement, since the two locations are very close to each other. The measurement error due to the calibrated precision potentiometer and the calibrated thermocouples is estimated to be about $\pm$ 2°F. Assuming these two individual uncertainties in the wall-temperature measurement to be independent, then the total estimated uncertainty in wall temperature can be calculated as: $\sqrt{(3°F)^2 + (2°F)^2} = \pm$ 3.6 °F for a heat flux of 100,000 BTU/hr-ft^2 from a nickel heating solid.

The following procedure was used in determining the average magnitudes of the bubble period τ and the amplitude of temperature oscillation of TC 7. The average peak-to-peak amplitude of temperature oscillation at TC 7 was obtained by numerically averaging twenty values of the peak-to-trough temperature variation from a representative section of the recorder chart as shown typically in Fig. 32. The typical range of the amplitude data for two different operating conditions is given in Figs. 56 and 57 as a function of its frequency of occurrence in this sample of twenty points; this sample is representative of the data at a given operating condition, and the average values are seen to be close to the most-frequently-occurring values. In addition, the statistical nature of boiling causes the maximum temperature of TC 7 to vary by about $\pm$ 3°F.

Similarly, the average bubble period was obtained by numerically averaging twenty values of the time elapsed between successive peaks of the temperature variation from a representative section of the recorder chart as shown typically in Fig. 32. The typical range of the period data for the two operating conditions discussed above is given in Figs. 58 and 59 as a function of its frequency of occurrence in this sample. Again, the average values are seen to be close to the most-frequently-occurring values.

The microscale boiling data are tabulated in Table 2. The values of the bubble period τ and of the amplitude of temperature oscillation at TC 7 presented in this table are average values as discussed earlier in this appendix.

Table 2 Tabulation of Microscale Boiling Data

Stable Boiling of Sodium from an Artificial Cavity in a Nickel Surface, r_c = 0.00675 in., 0.10 in. deep

Run-Point	P_{sat} (mm Hg)	T_{sat} (°F)	q_o (BTU/hr-ft^2)	$\theta_w(0,0)$ (°F)	τ (sec)	Temperature Amplitude at TC 7 (°F)
2-5	100.6	1280	85,500	16	0.84	1.5
2-6	102.2	1279	103,000	19	0.79	1.6
2-7	102.6	1280	75,700	18	0.84	1.4
3-10	31.5	1142	92,000	40	2.16	7.4
3-11	33.3	1144	107,000	41	2.01	4.6
3-12	33.5	1145	121,000	38	1.56	4.0
3-14	34.8	1146	135,000	38	1.17	2.8
3-15	34.0	1143	157,000	39	0.81	3.2
3-16	34.0	1143	182,000	39	0.77	2.9
3-17	33.4	1142	225,000	39	0.65	2.7
3-18	33.1	1139	125,000	40	1.71	5.4
3-19	31.8	1136	113,000	41	1.94	9.7

Stable Boiling of Sodium from a Natural Cavity in a Nickel Surface, r_c 0.0033 in.

14-16	30.2	1126	201,000	67	1.88	8.2
14-17	29.3	1125	166,000	72	2.32	10.2
14-18	29.1	1122	173,000	69	3.66	11.2

Stable Boiling of Sodium from an Artificial Cavity

in a Molybdenum Surface, r_c = 0.00675 in., 0.10 in. deep

Run-Point	P_{sat}	T_{sat}	q_o	$\theta_w(0,0)$	τ	Temperature Amplitude at TC 7
	(mm Hg)	(°F)	(BTU/hr-ft^2)	(°F)	(sec)	(°F)
33-5	31.1	1137	87,600	37	0.74	7.2
33-6	31.1	1137	102,000	43	0.57	4.5
33-7	31.3	1142	142,000	44	0.68	5.3
33-8	60.3	1215	137,000	30	0.34	2.7
33-9	60.7	1216	118,000	25	0.51	2.4
33-10	60.7	1216	100,000	23	0.46	1.9
33-11	60.5	1213	85,000	24	0.54	2.5
33-12	60.7	1213	72,900	28	0.59	2.5
33-14	101.	1282	71,300	18	0.70	1.5
33-15	103.	1283	90,100	21	0.47	1.5
33-16	103.	1282	71,400	22	0.50	1.6

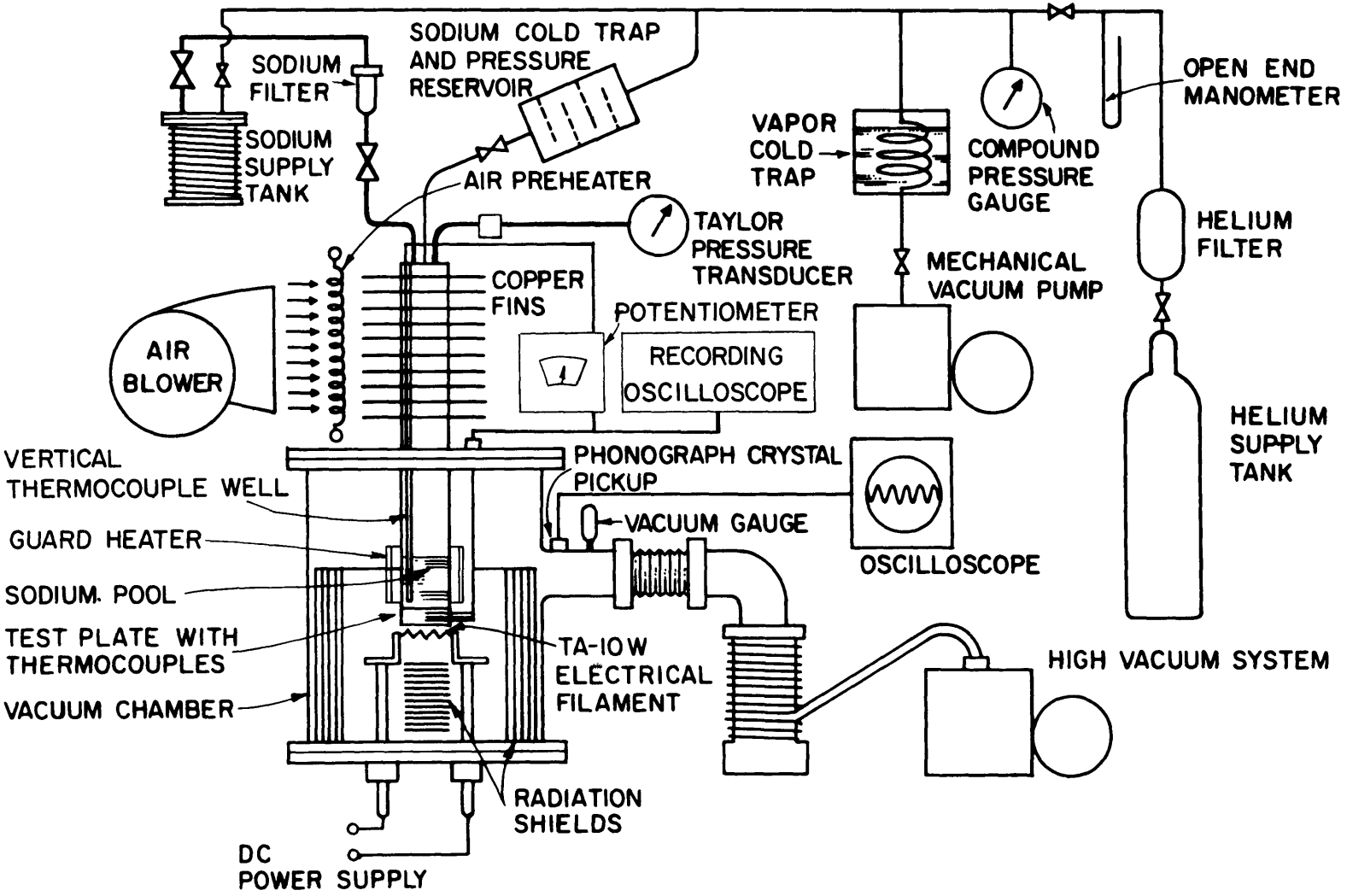

Fig. 1 Diagram of Equipment

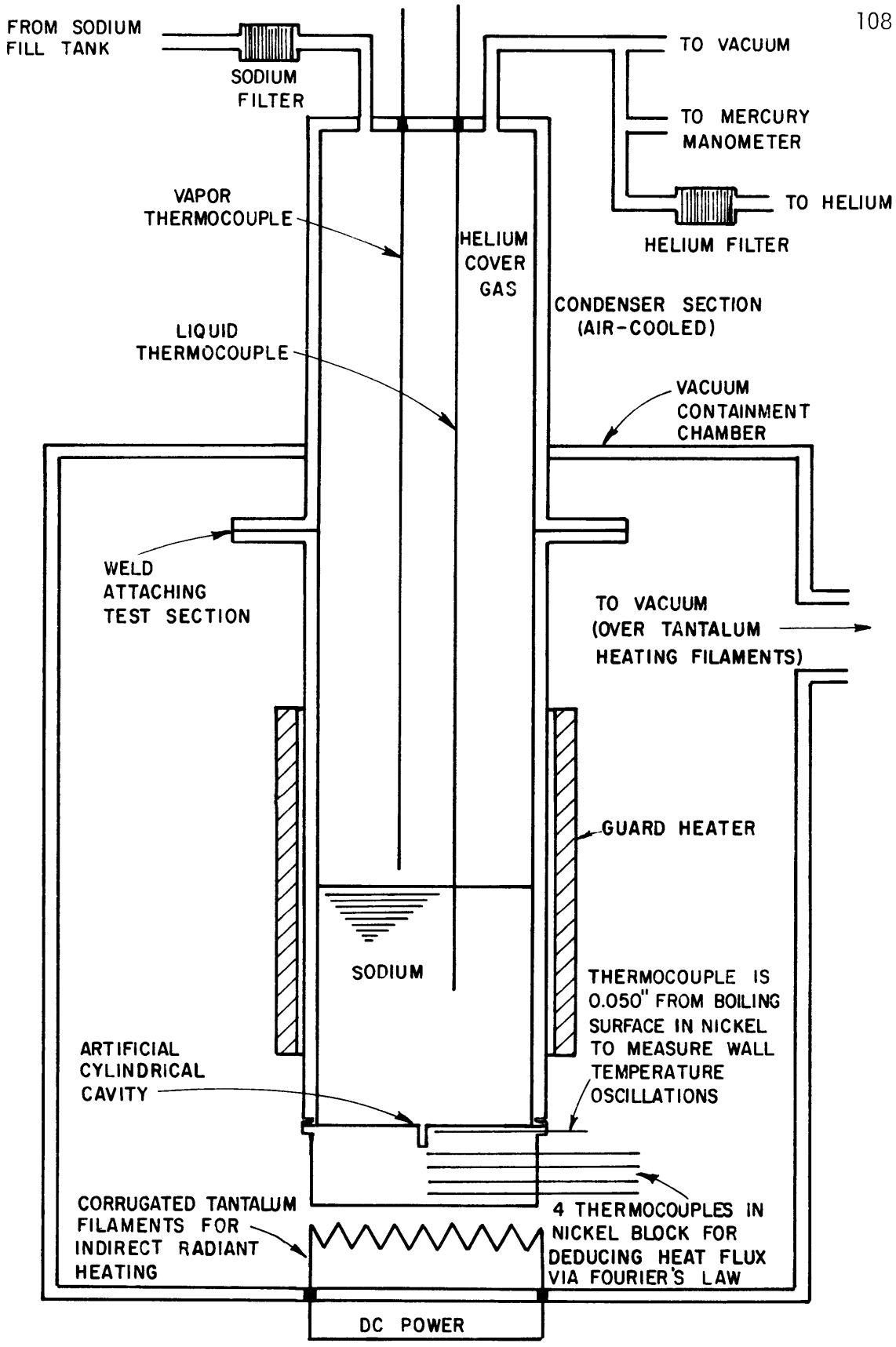

Fig. 2 Simplified Diagram of Test Section

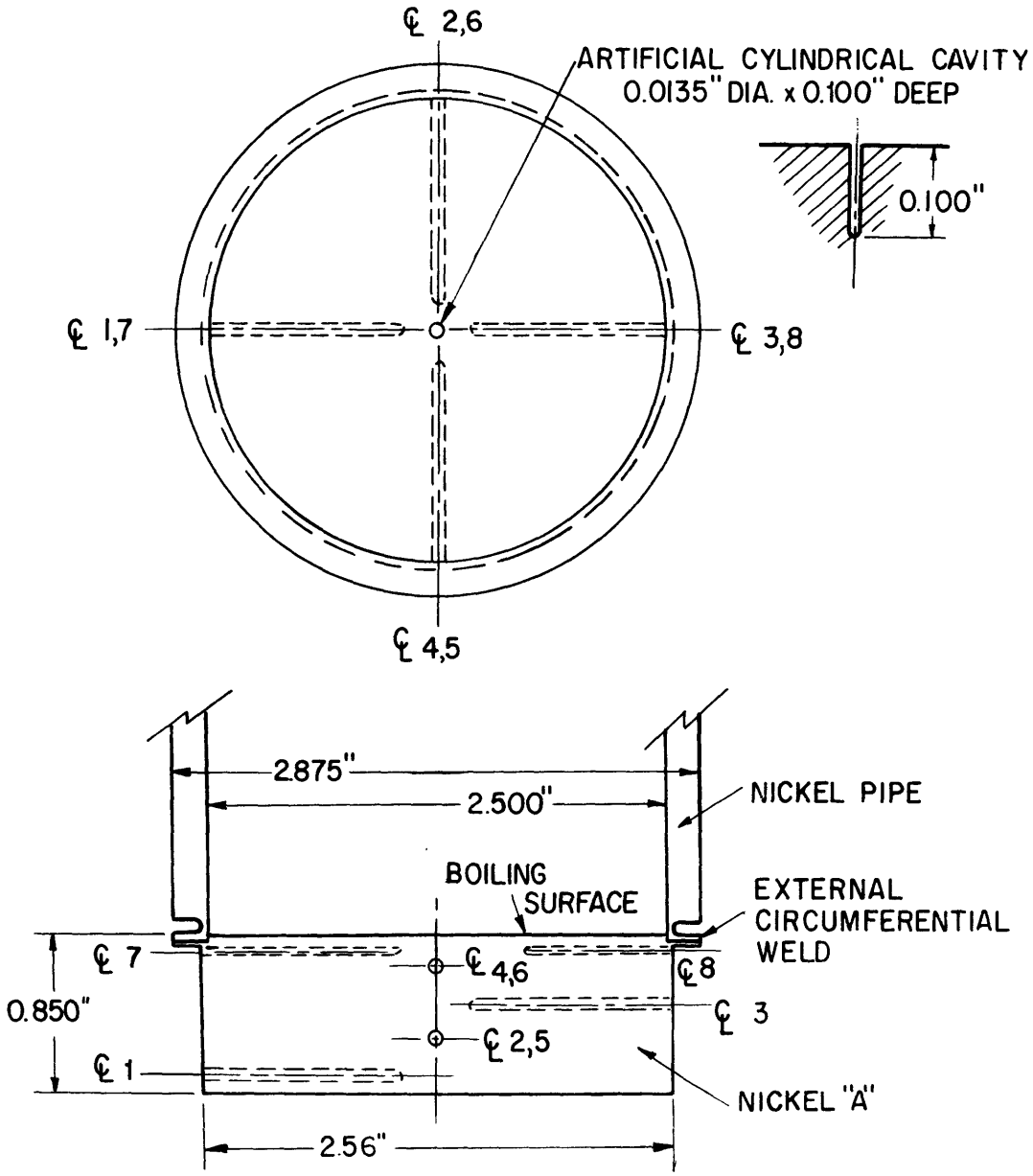

TC No.	Diameter (in.)	Immersion Depth (in.)	℄ Distance from Surface (in.)
1	0.0625	1.100	0.750
2	0.0625	1.100	0.550
3	0.0625	1.100	0.350
4	0.0625	1.100	0.150
5	0.0625	0.650	0.550
6	0.0625	0.650	0.150
7	0.040	1.100	0.050
8	0.040	0.800	0.050

Fig. 3 Geometry of Test Section of Nickel and of Stainless Steel 316

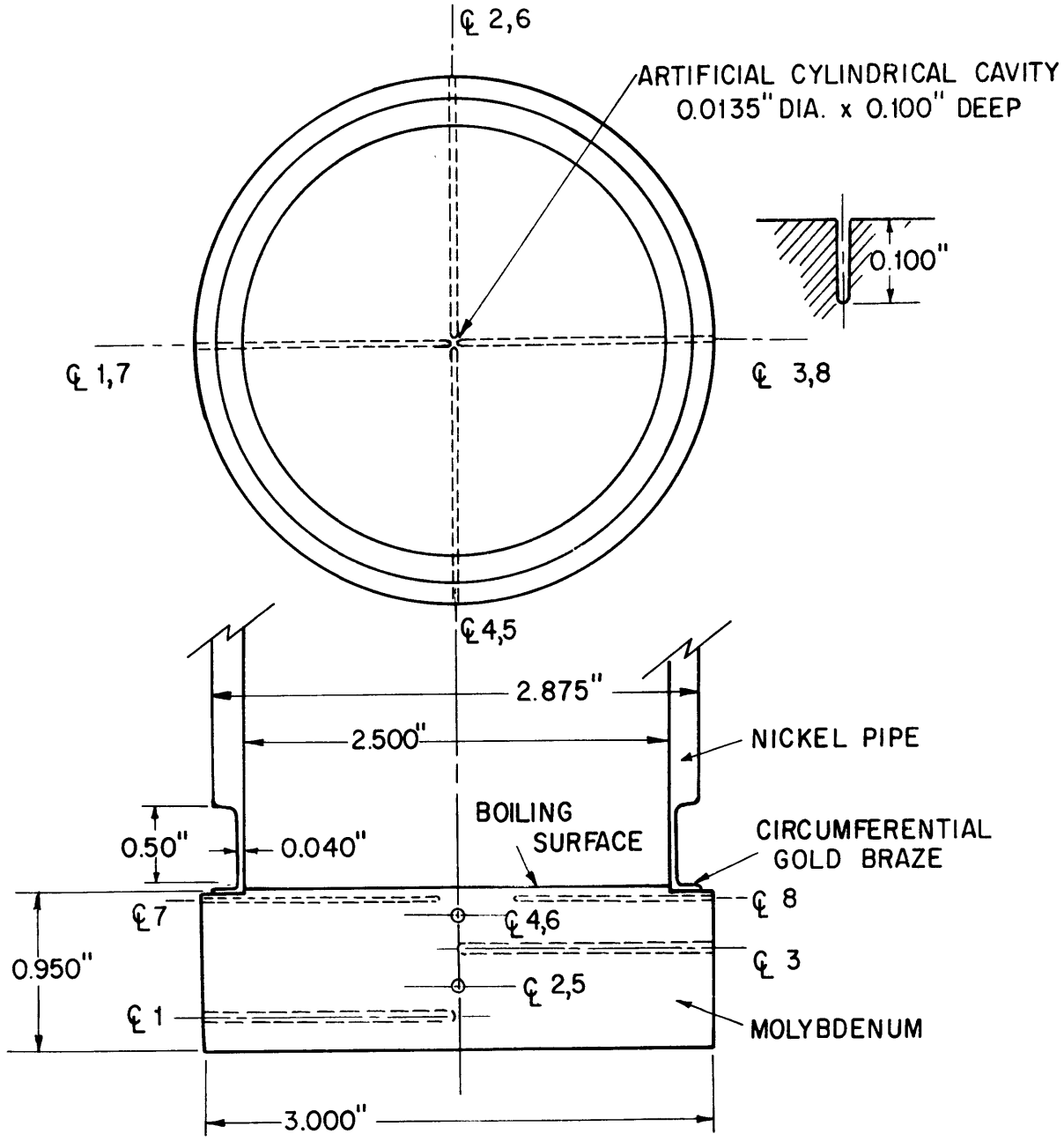

TC No.	Diameter (in.)	Immersion Depth (in.)	℄ Distance from Surface (in.)
1	0.067	1.500	0.750
2	0.067	1.500	0.550
3	0.067	1.500	0.350
4	0.067	1.500	0.150
5	0.067	0.813	0.550
6	0.067	0.813	0.150
7	0.041	1.350	0.050
8	0.041	1.000	0.050

Fig. 4 Geometry of Test Section of Molybdenum-1/2%-Titanium

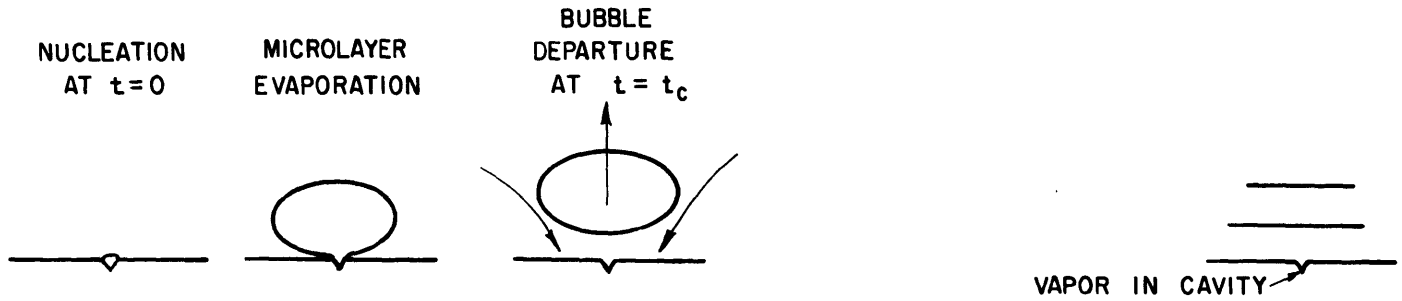

5a. BUBBLE BEHAVIOR

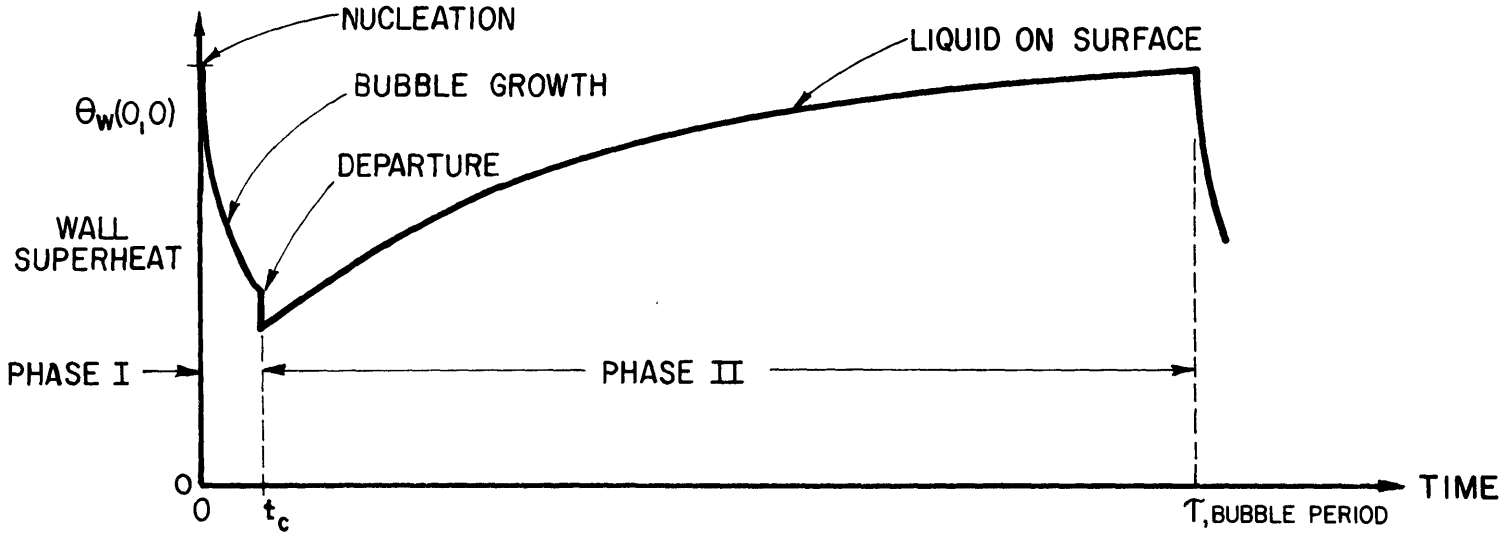

5b. WALL TEMPERATURE – TIME BEHAVIOR, MODIFIED FROM COOPER & LLOYD (11) FOR THE CASE OF SODIUM.

Fig. 5 Model of Periodic Boiling Behavior

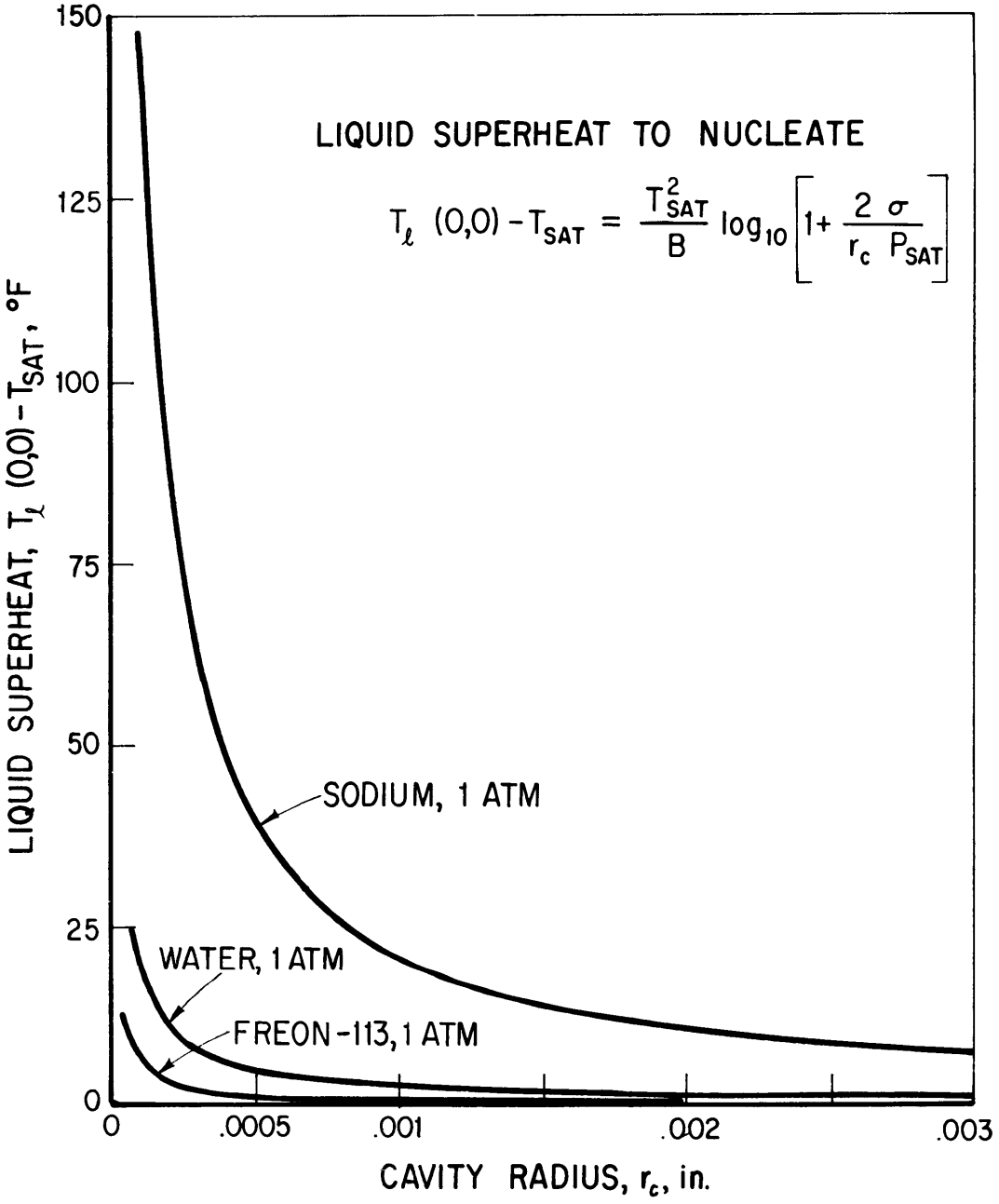

Fig. 6 Liquid Superheat for Nucleation for Several Fluids at Atmospheric Pressure

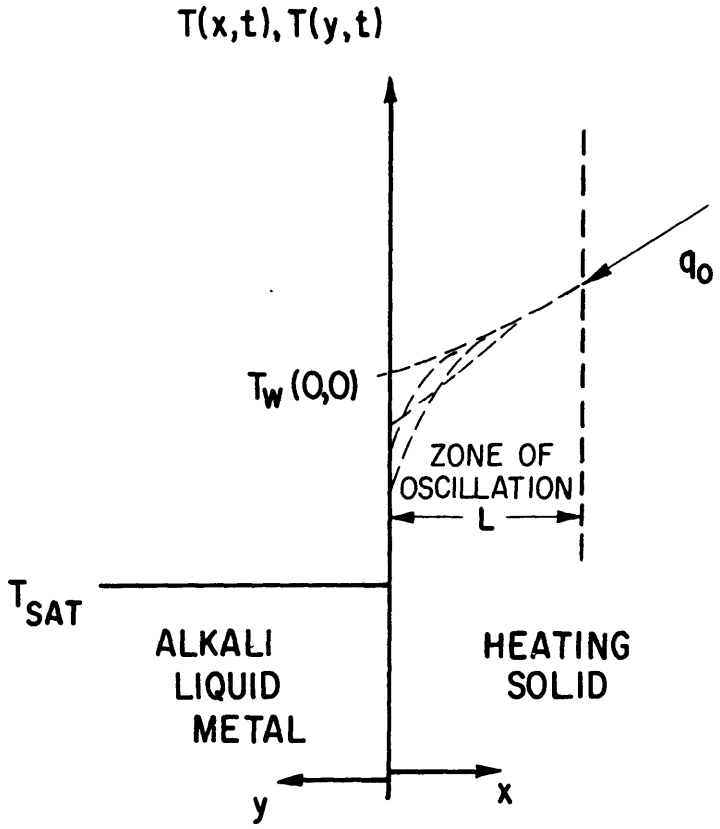

Fig. 7 Fundamental Geometry of the Problem of Boiling Heat Transfer to the Alkali Liquid Metals

PHASE I: BUBBLE AT CAVITY

$0 \le t \le t_c$

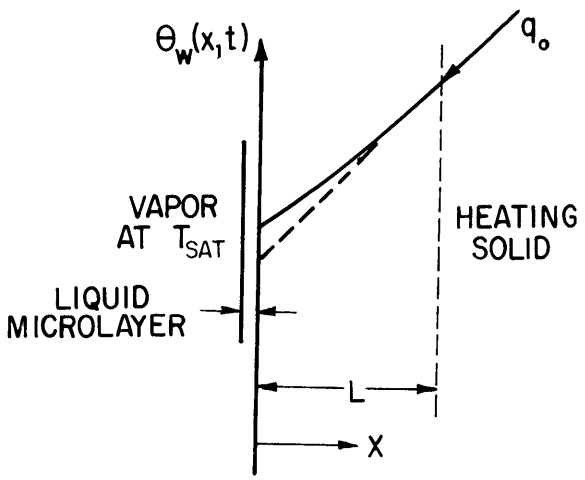

CONDUCTION EQ IN SOLID

$$\frac{\partial^2 \theta_w(x,t)}{\partial x^2} = \frac{1}{\alpha_w}\frac{\partial \theta_w(x,t)}{\partial t}$$

INITIAL TEMPERATURE PROFILE

$\theta_w(x,0)$ from $t=\tau$ of Phase II

INTERFACE CONDITION

$$k_w \frac{\partial \theta_w(0,t)}{\partial x} = h_{eq}\theta_w(0,t)$$

CYCLIC CONDITION

$$\theta_w(0,\tau) = \theta_w(0,0)$$

PHASE II: LIQUID ON SURFACE

$t_c \le t \le \tau$

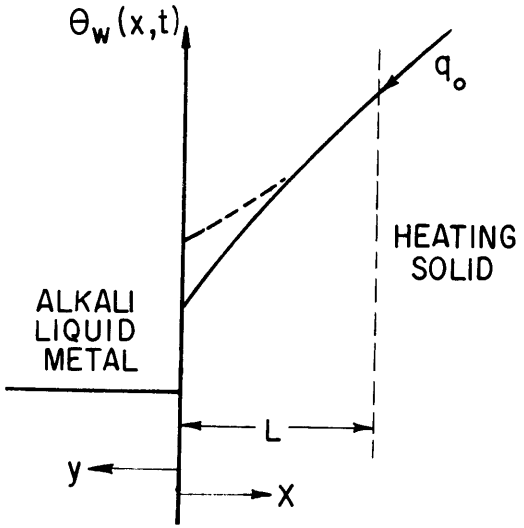

CONDUCTION EQ IN LIQUID

$$\frac{\partial^2 \theta_\ell(y,t)}{\partial y^2} = \frac{1}{\alpha_\ell}\frac{\partial \theta_\ell(y,t)}{\partial t}$$

INITIAL TEMPERATURE PROFILE

$$\theta_\ell(y,t_c) = 0$$

CONDUCTION EQ IN SOLID

$$\frac{\partial^2 \theta_w(x,t)}{\partial x^2} = \frac{1}{\alpha_w}\frac{\partial \theta_w(x,t)}{\partial t}$$

INITIAL TEMPERATURE PROFILE

$\theta_w(x,t_c)$ from $t=t_c$ of Phase I

INTERFACE CONDITIONS

$$\theta_\ell(0,t) = \theta_w(0,t) \quad \text{TEMPERATURE CONTINUITY}$$

$$-k_\ell \frac{\partial \theta_\ell(0,t)}{\partial y} = k_w \frac{\partial \theta_w(0,t)}{\partial x} \quad \text{FLUX CONTINUITY}$$

Figure 8 Mathematical Formulation of Boiling Model

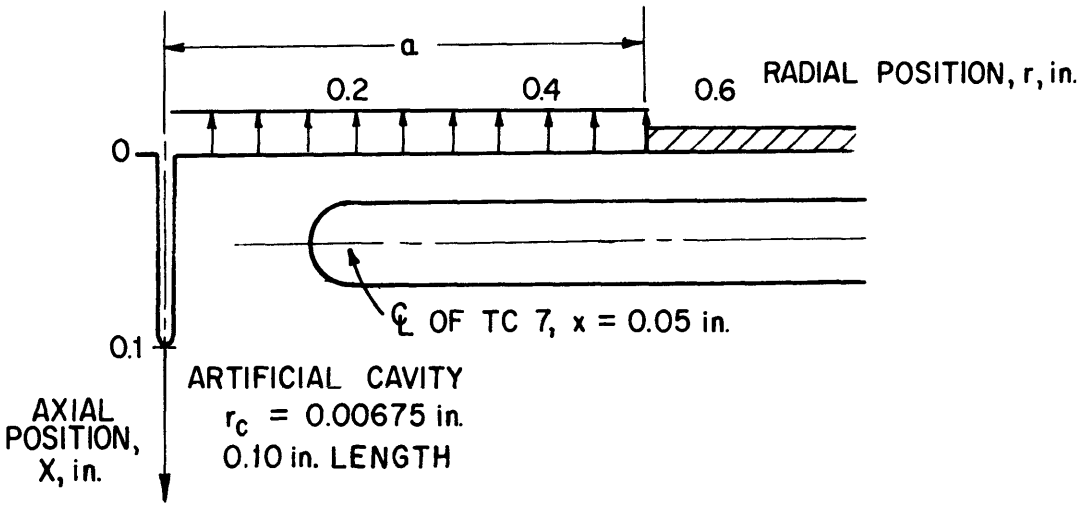

Fig. 9 Geometry of "Cold-Spot" Disc and Thermocouple 7

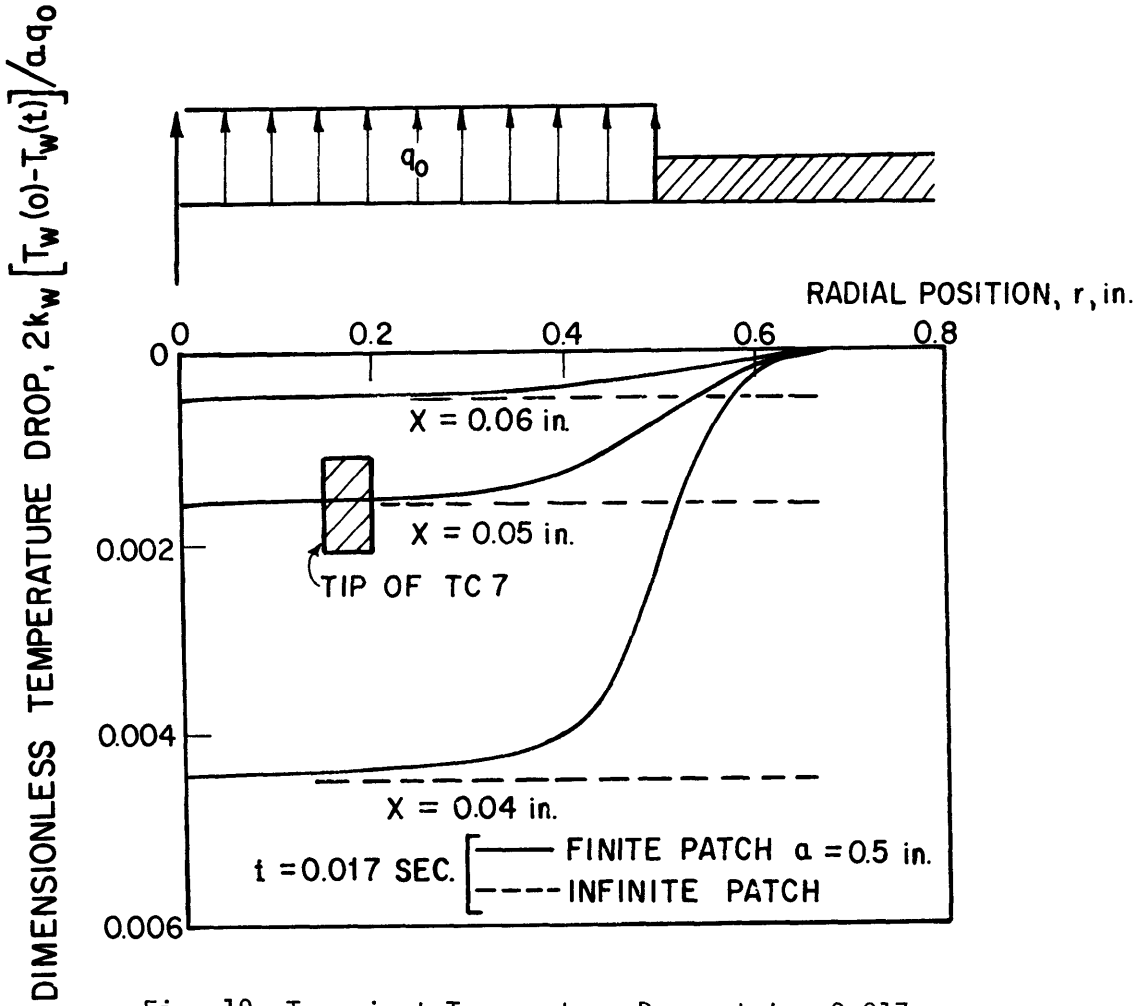

Fig. 10 Transient Temperature Drop at t = 0.017 sec. due to "Cold-Spot" Disc of Constant Heat Flux on Surface

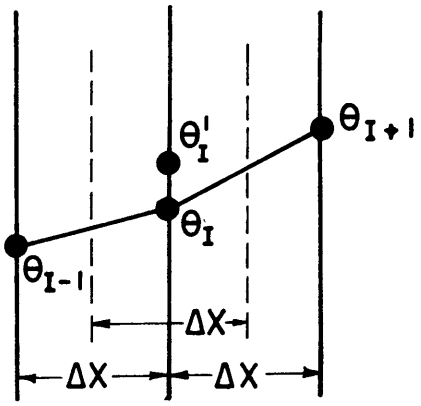

Fig. 11 Internal Node of Finite Difference Equation

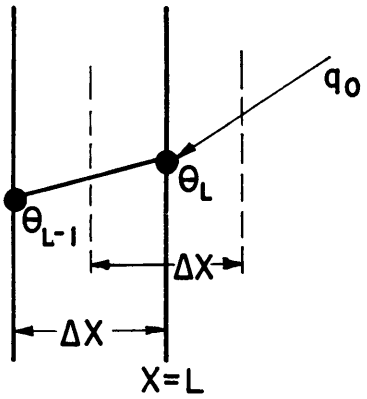

Fig. 12 Node at Position X=L, at the Edge of the Oscillation Zone

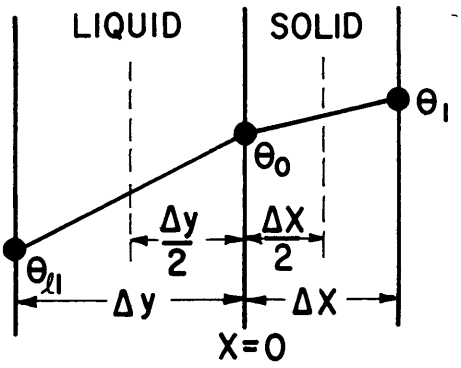

Fig. 13 Node at Interface of Heating Solid and Liquid Metal

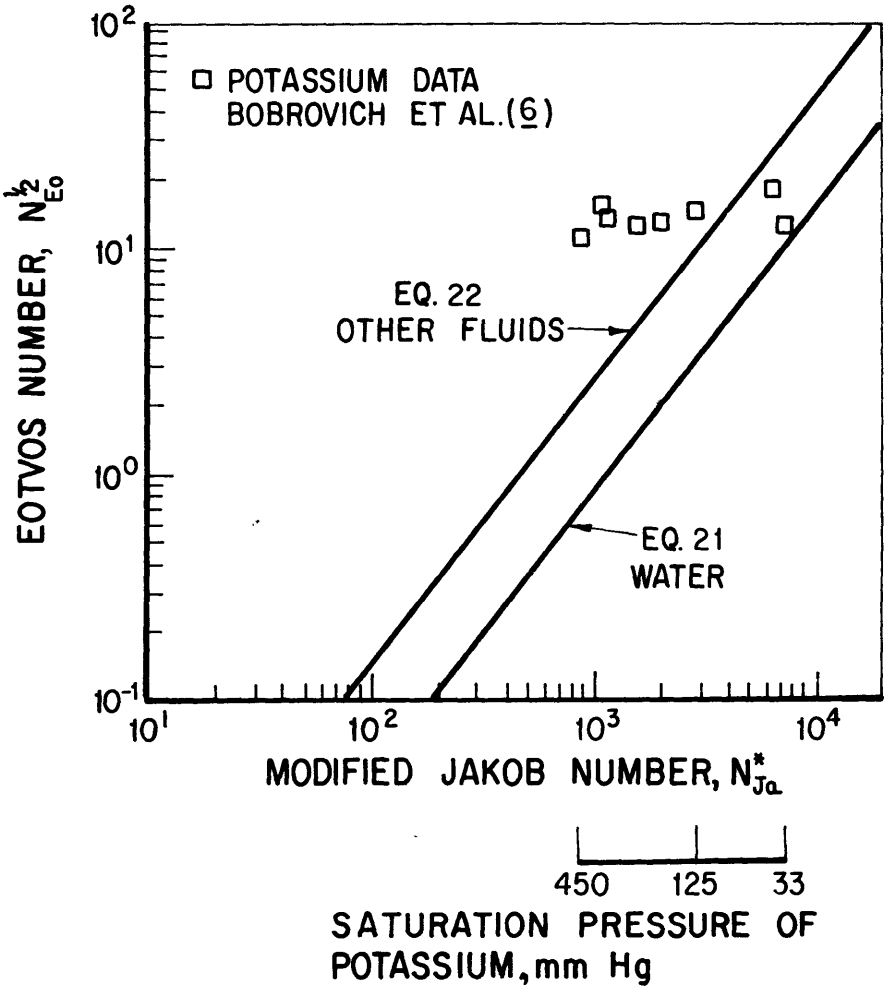

Fig. 14 Data on Bubble Departure Diameter (6) in Potassium Compared with Correlations (15) for Water and for Other Fluids

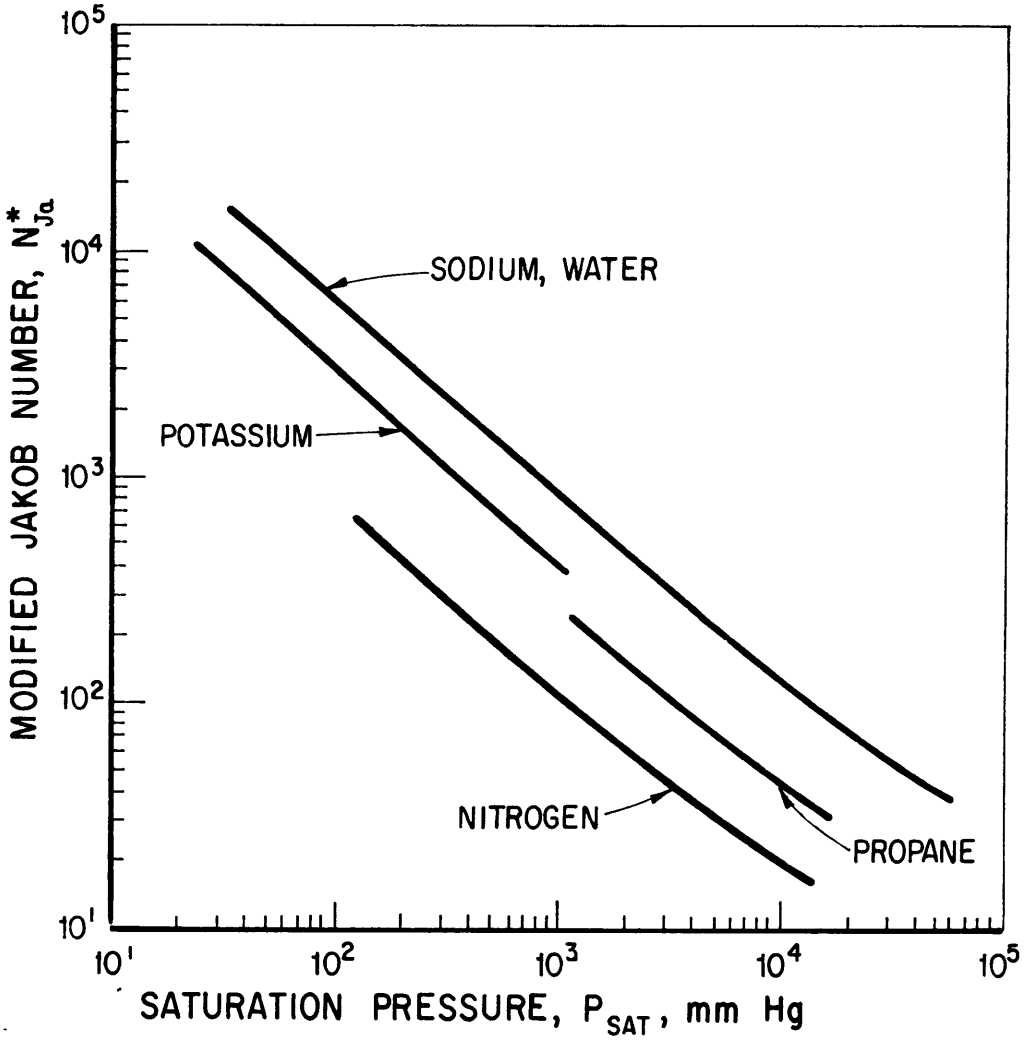

Fig. 15 Variation of Modified Jakob Number with Pressure

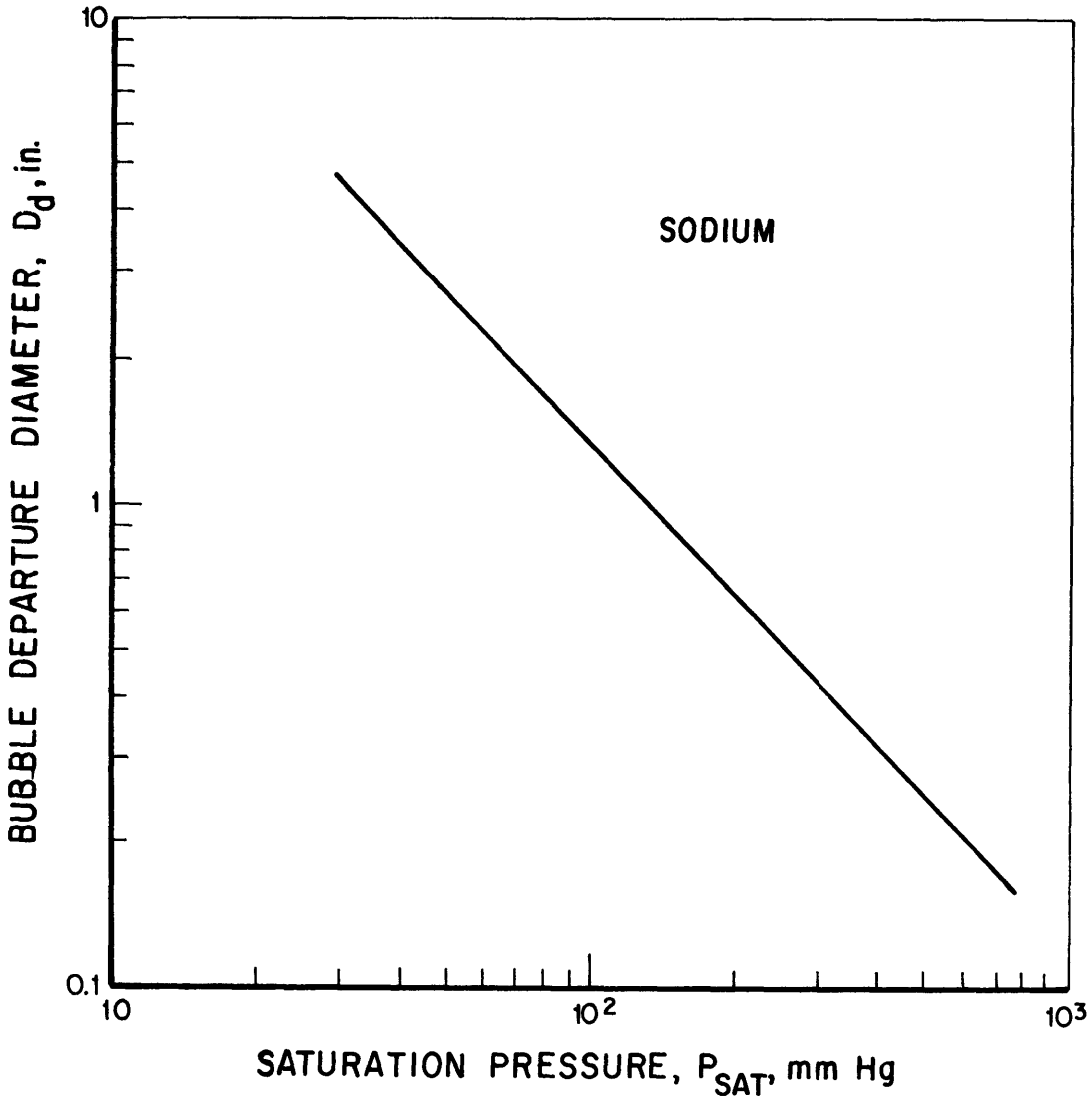

Fig. 16 Sodium Departure Diameter
Calculated with Eq. (21)

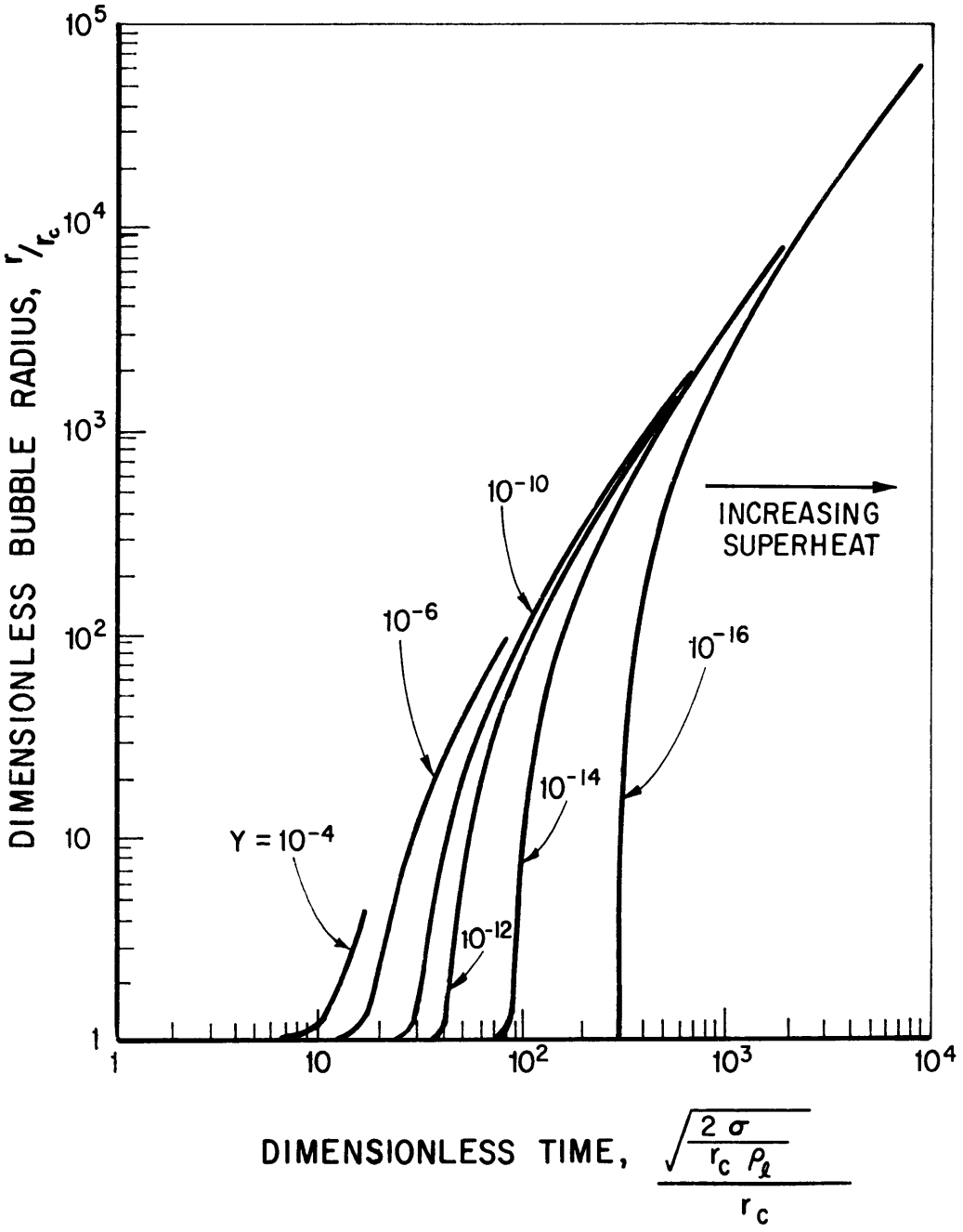

Fig. 17 Bubble Radius Versus Time Elapsed from Nucleation as Calculated from the Theoretical Model of Wichner and Hoffman (16) for Liquid Metals

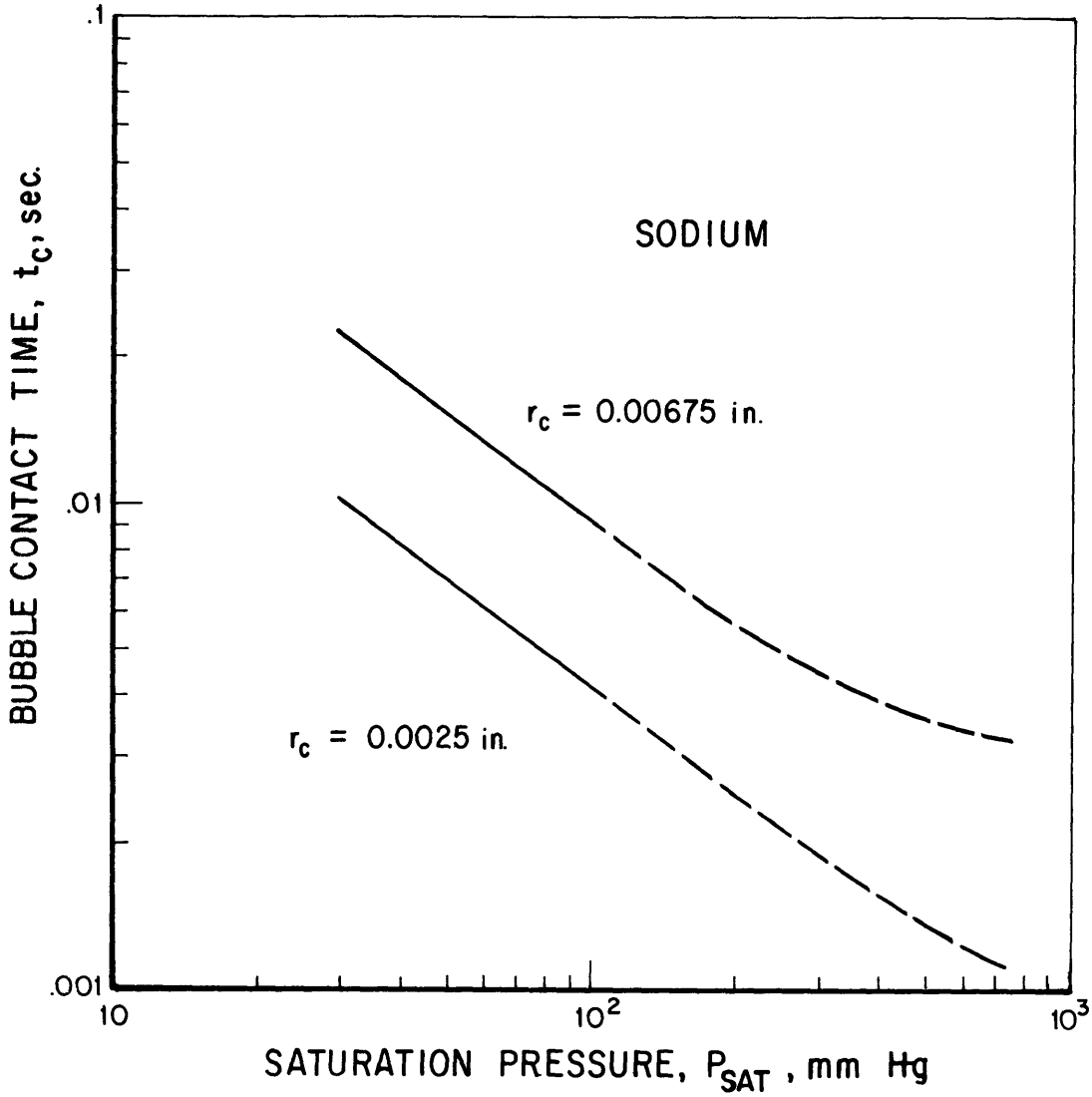

Fig. 18 Bubble Contact Time for Sodium Calculated from Inertia-Controlled Model (16)

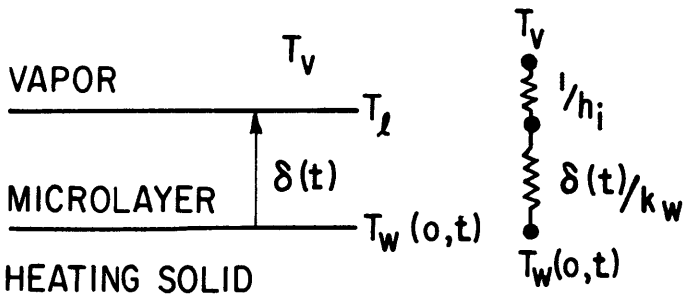

Fig. 19 Heat Transfer Resistance
Through the Microlayer

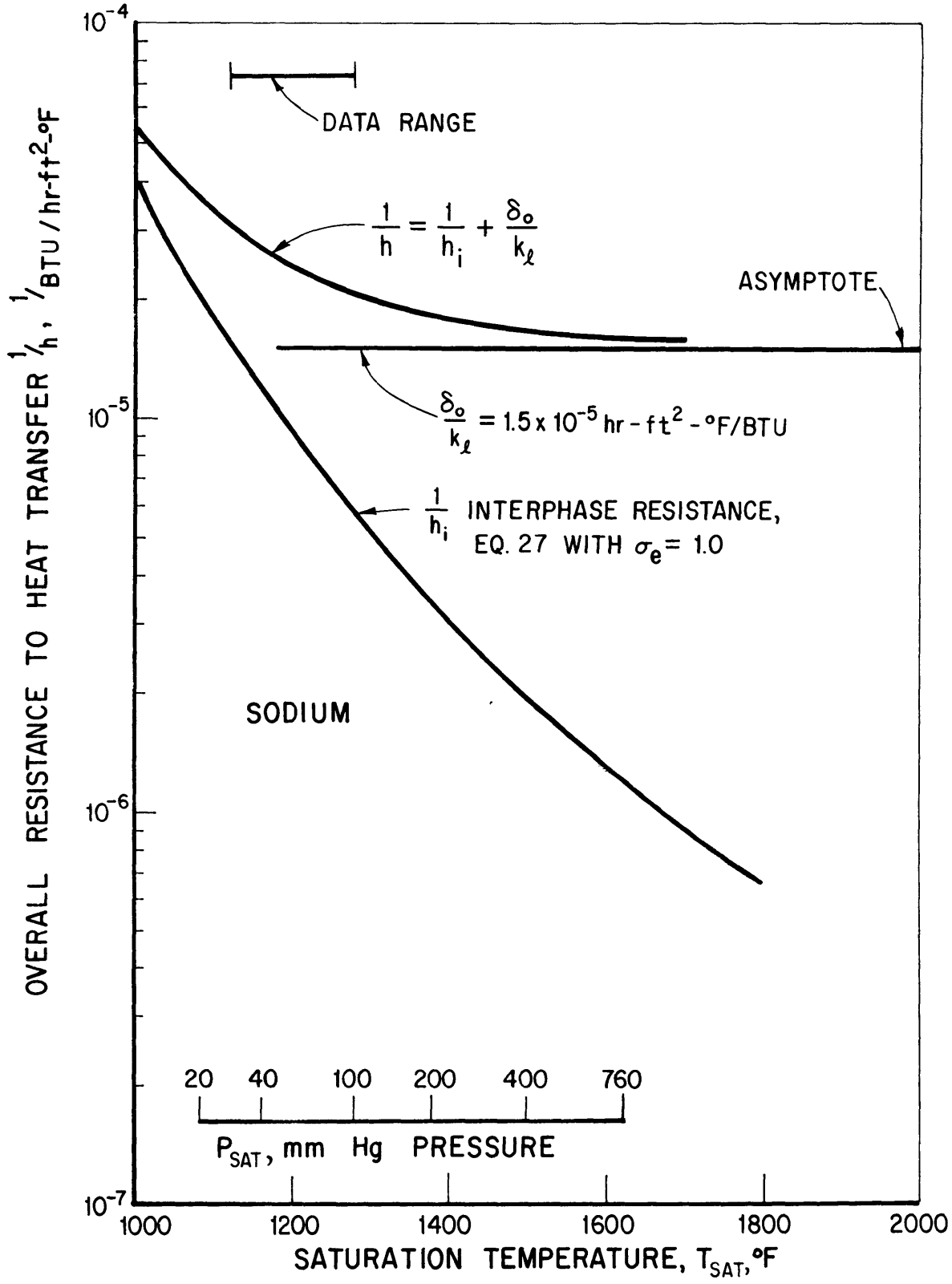

Fig. 20 Overall Resistance to Heat Transfer Through a Sodium Microlayer

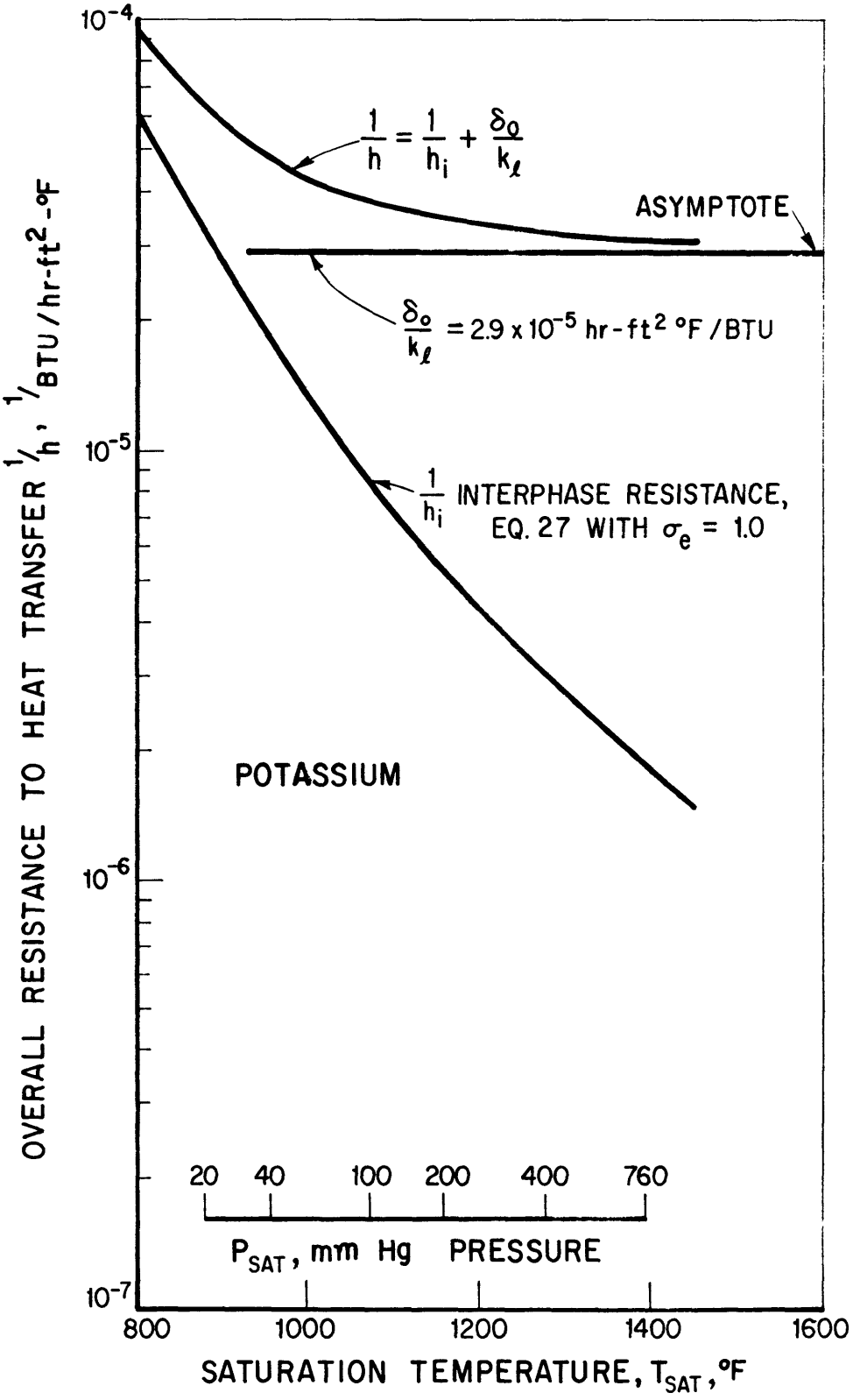

Fig. 21 Overall Resistance to Heat Transfer Through a Potassium Microlayer

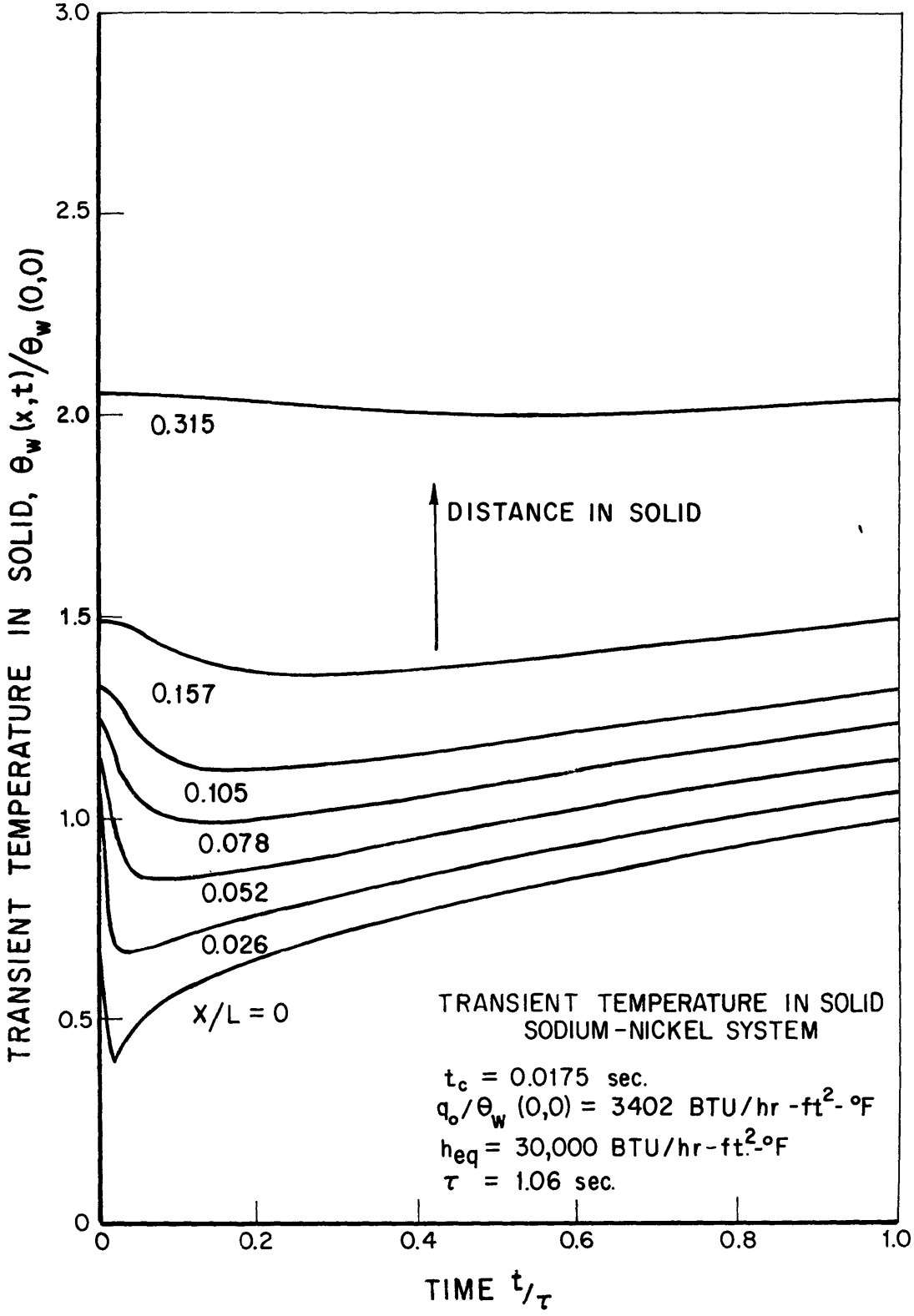

Fig. 22 Transient Temperature in the Solid at a Position, Sodium-Nickel System

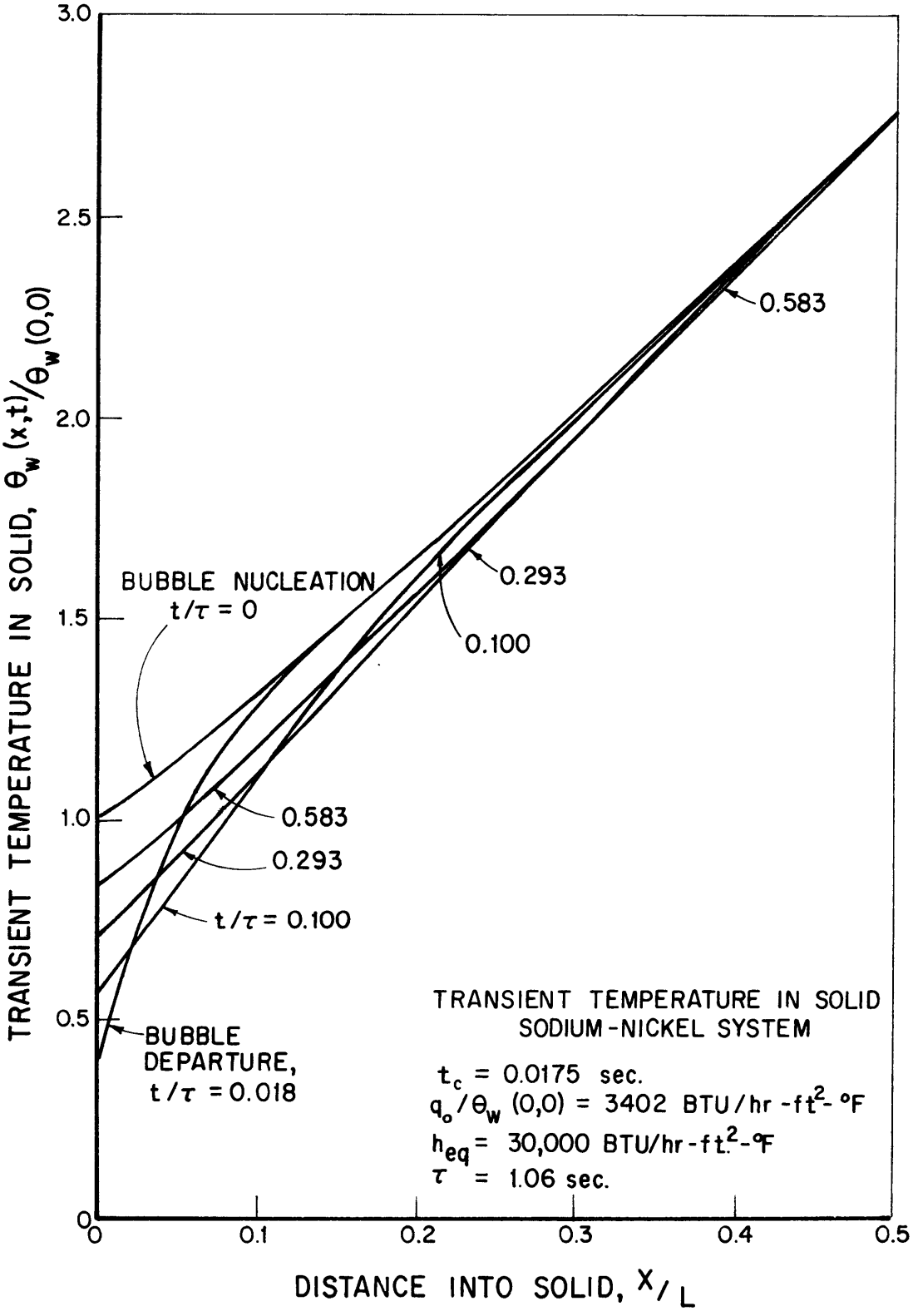

Fig. 23 Transient Temperature in the Solid on Lines of Constant Time, Sodium-Nickel System

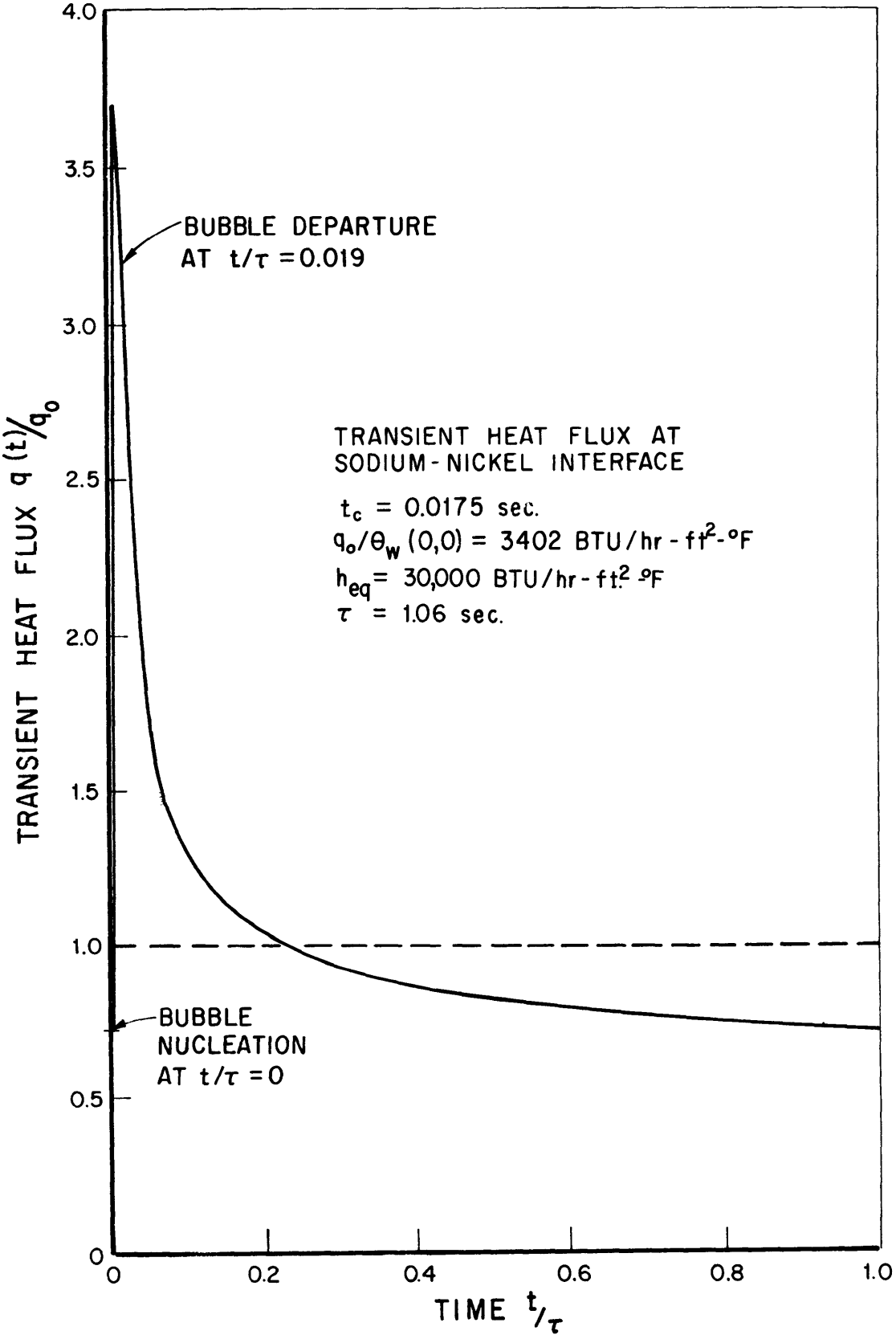

Fig. 24 Transient Heat Flux at Sodium-Nickel Interface

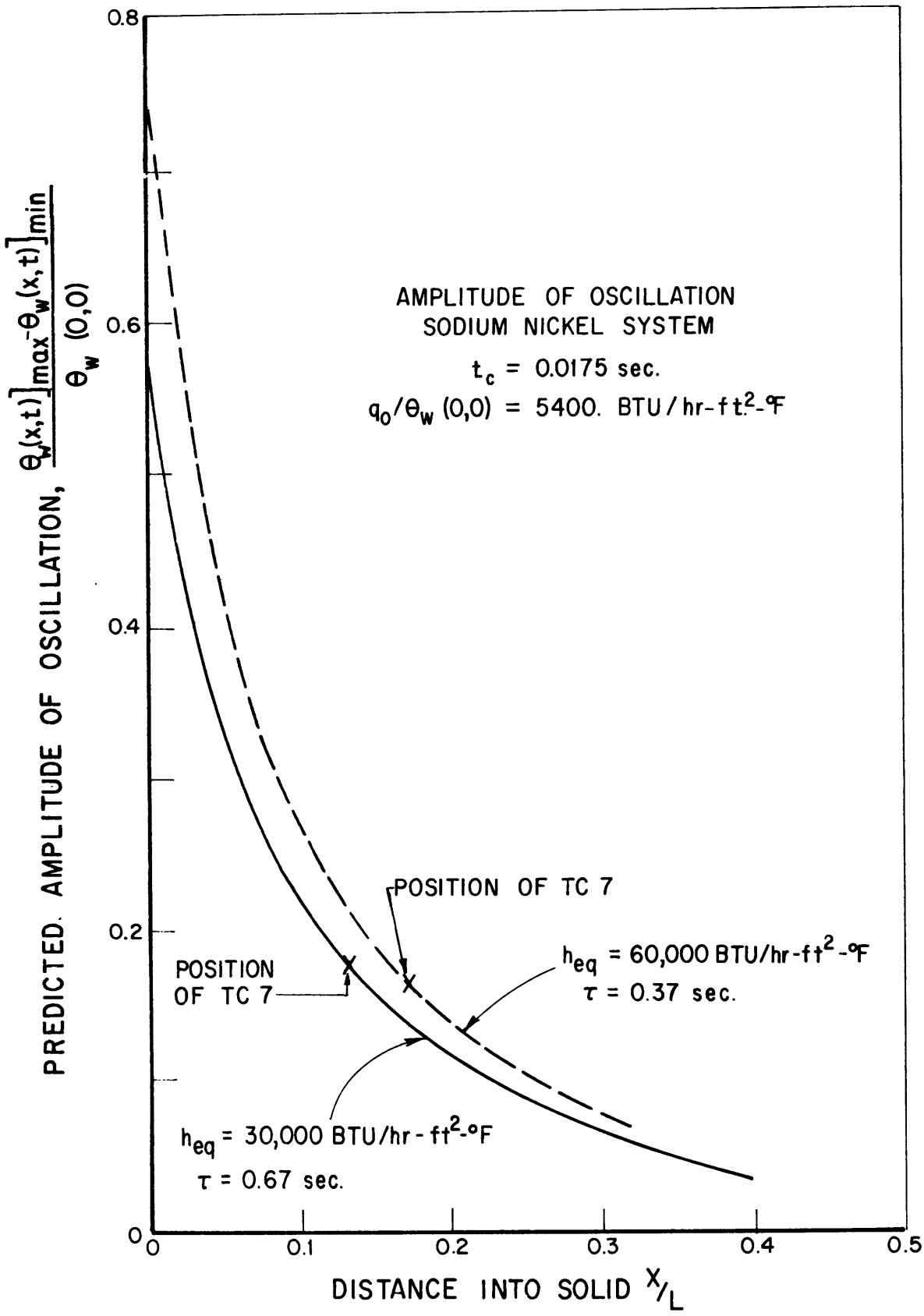

Fig. 25 Variation of Prediction of Amplitude of Temperature Oscillation with Microlayer Heat Transfer, Sodium-Nickel System

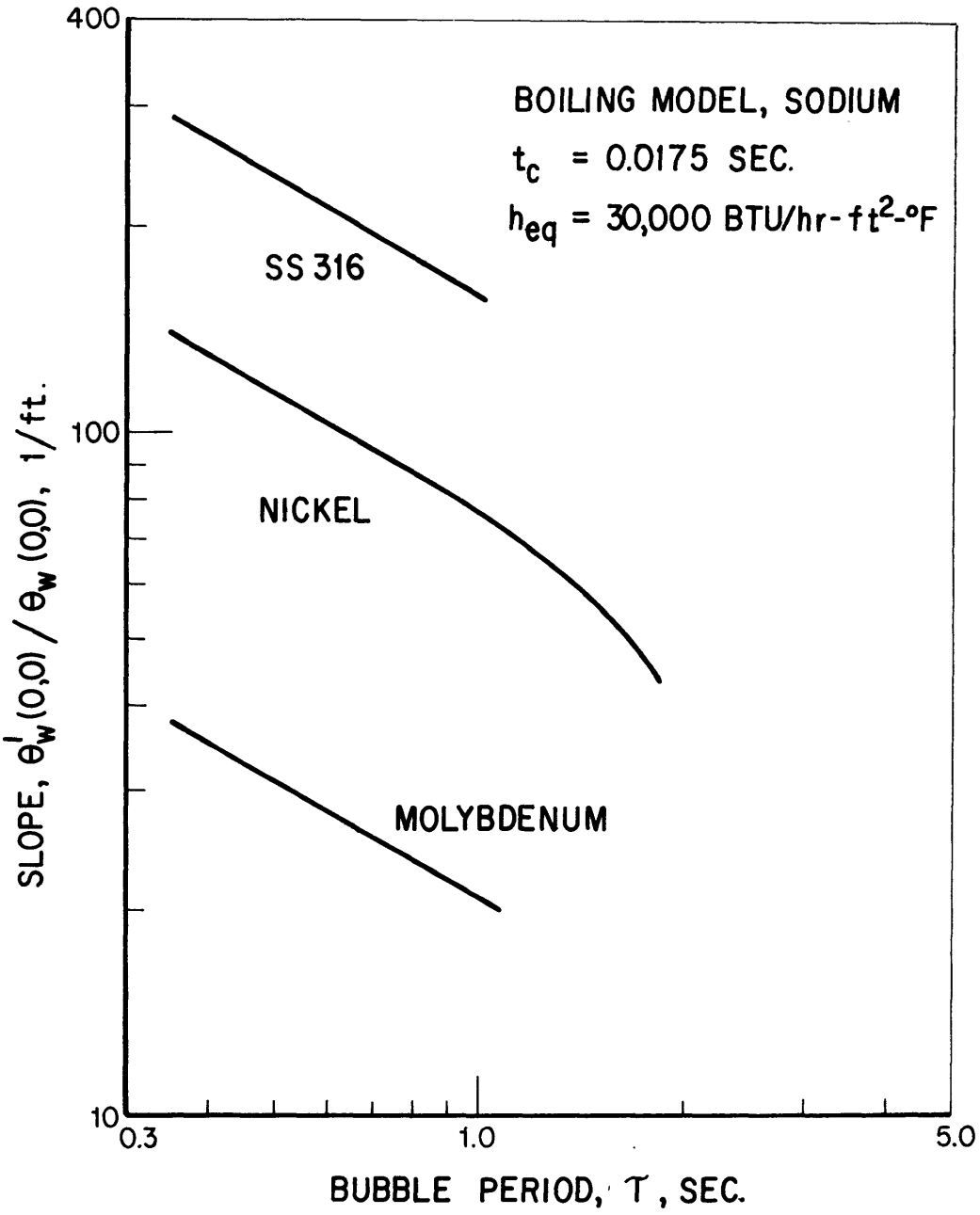

Fig. 26 Temperature Slope at Surface and at Nucleation as a Function of the Bubble Period

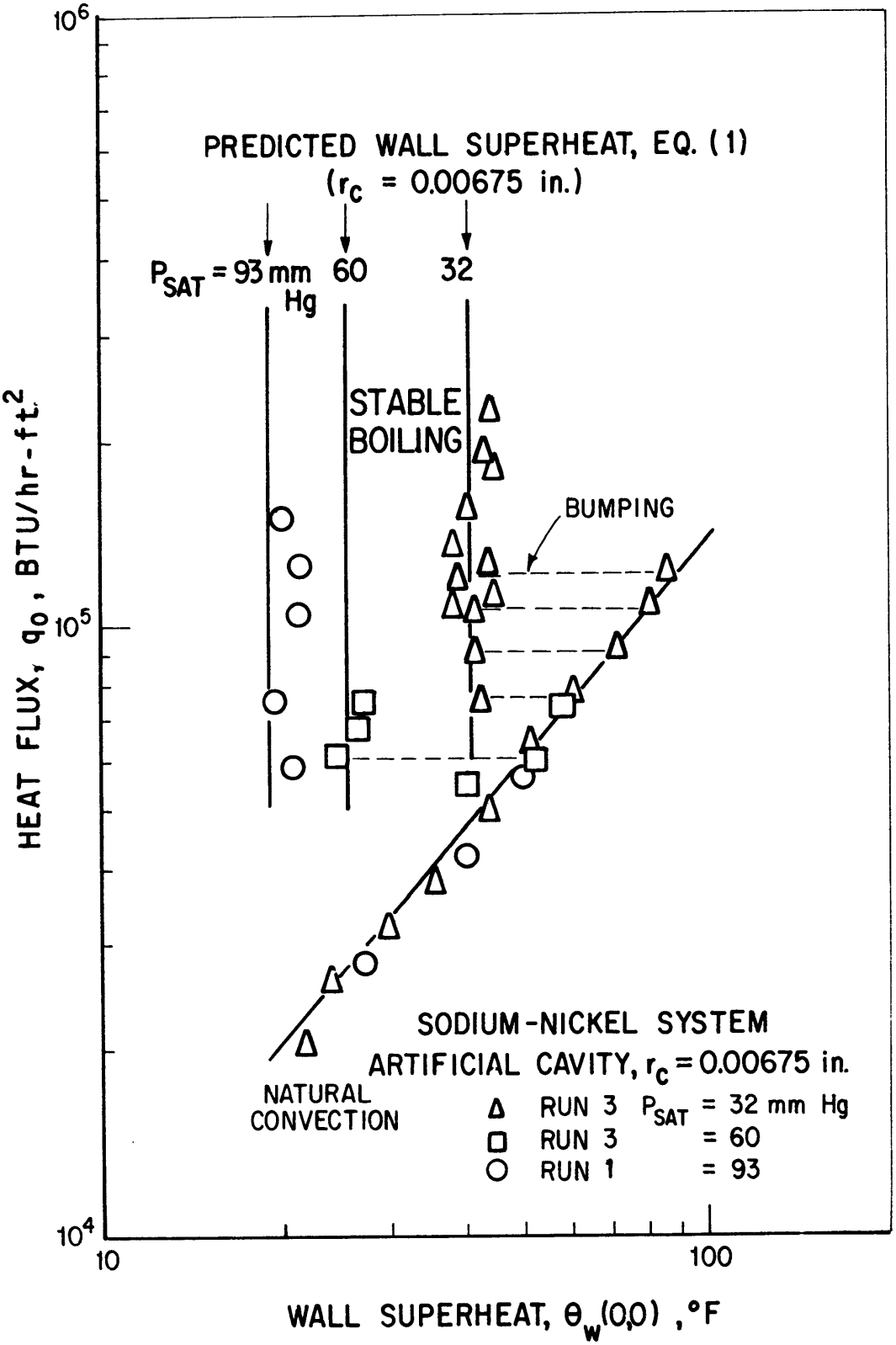

Fig. 27 Effect of Pressure on Nucleate Boiling of Sodium from an Artificial Cavity in Nickel Surface

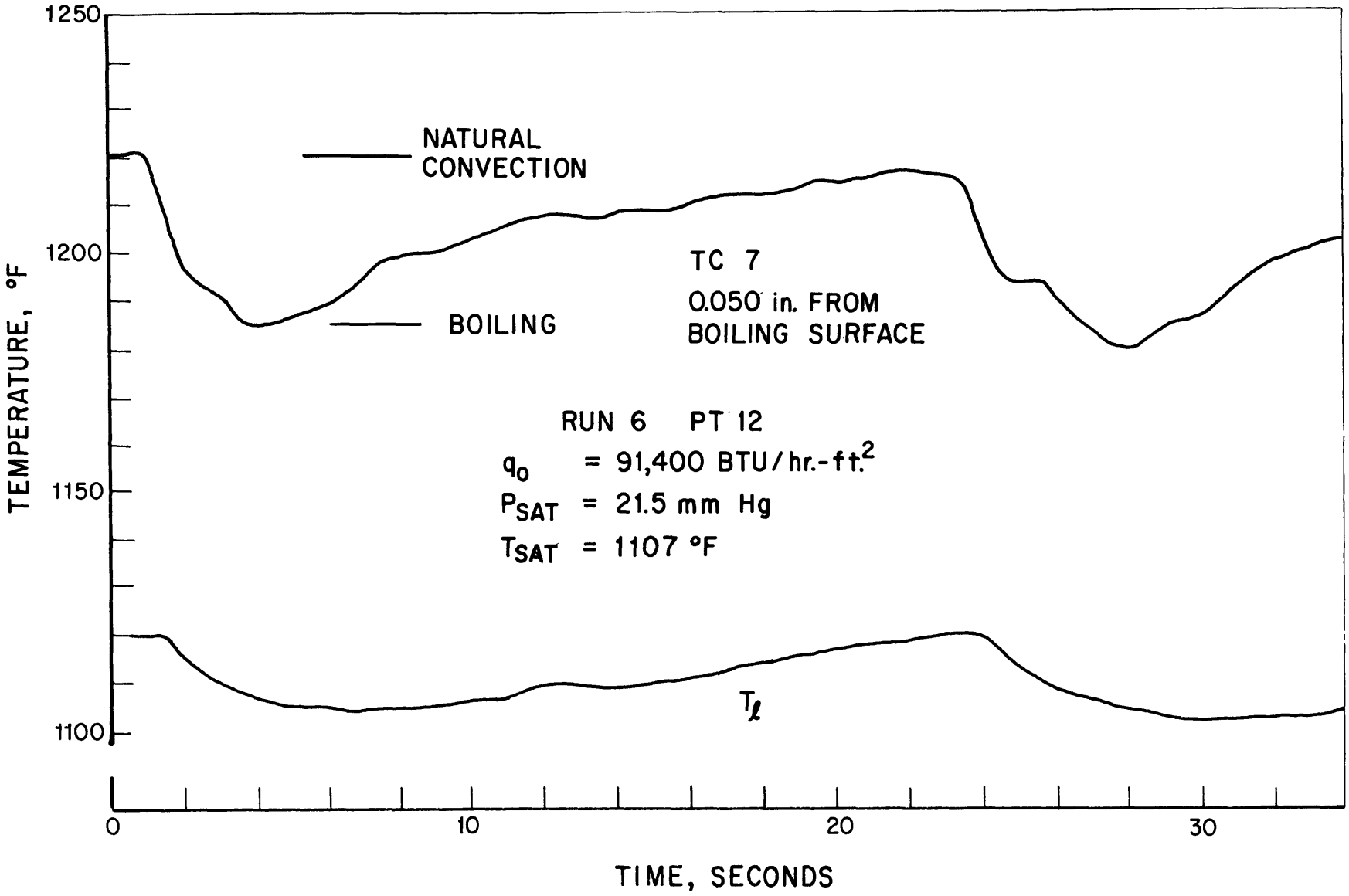

Fig. 28 Unstable Boiling at Low Pressure on Stainless-Steel Surface

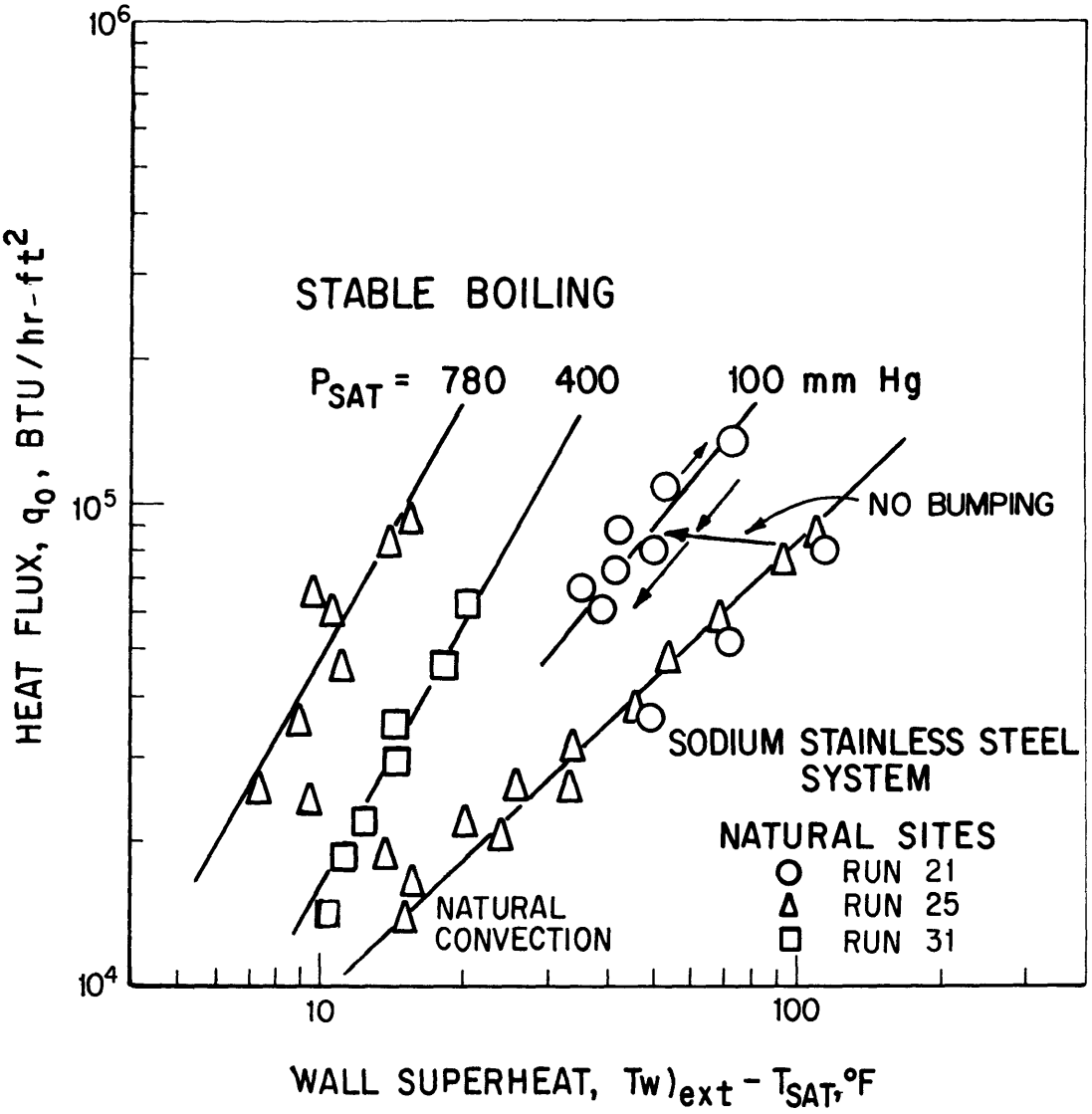

Fig. 29 Effect of Pressure on Nucleate Boiling of Sodium from Natural Sites in Stainless-Steel Surface

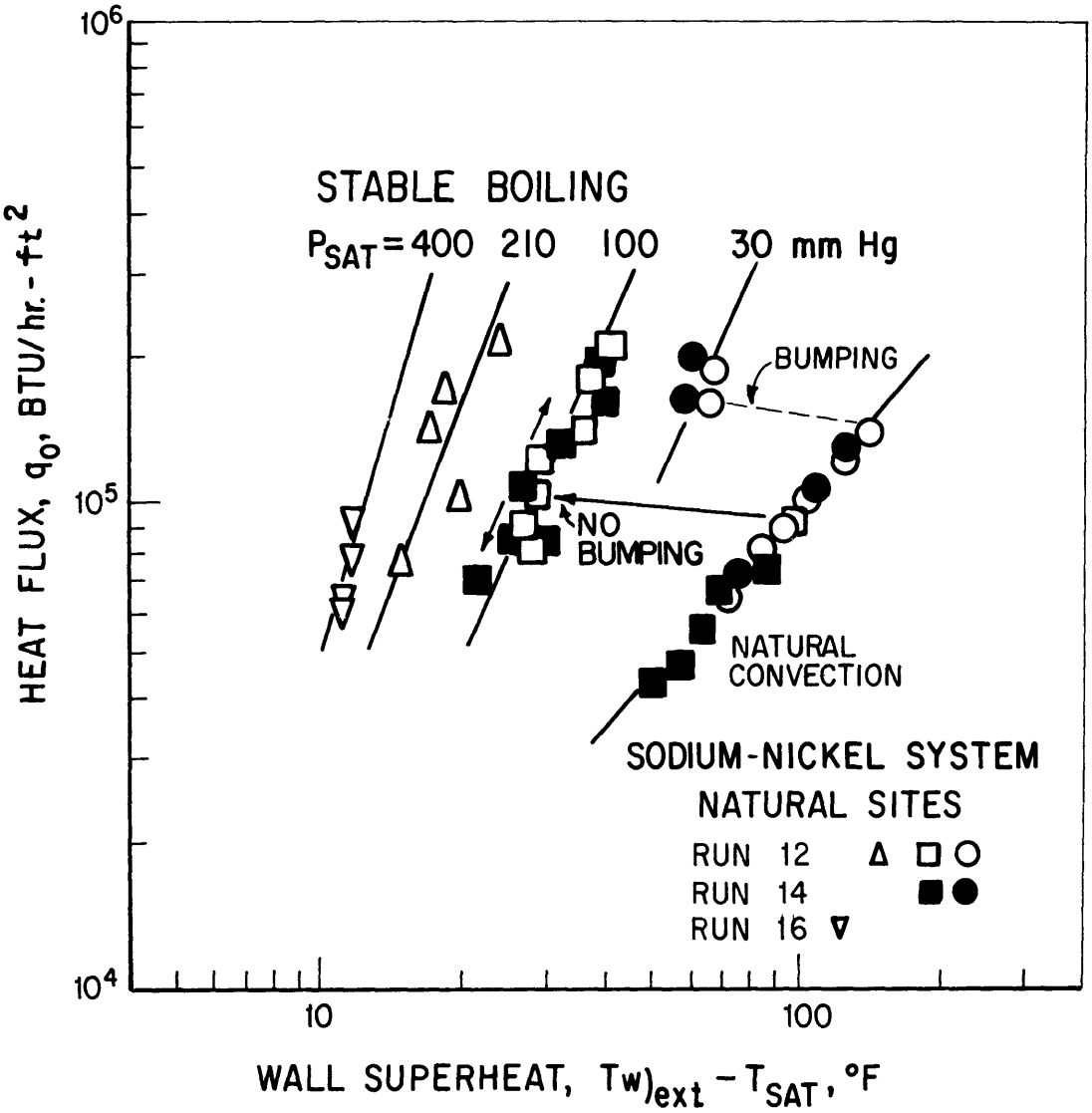

Fig. 30 Effect of Pressure on Nucleate Boiling of Sodium from Natural Sites in Nickel Surface

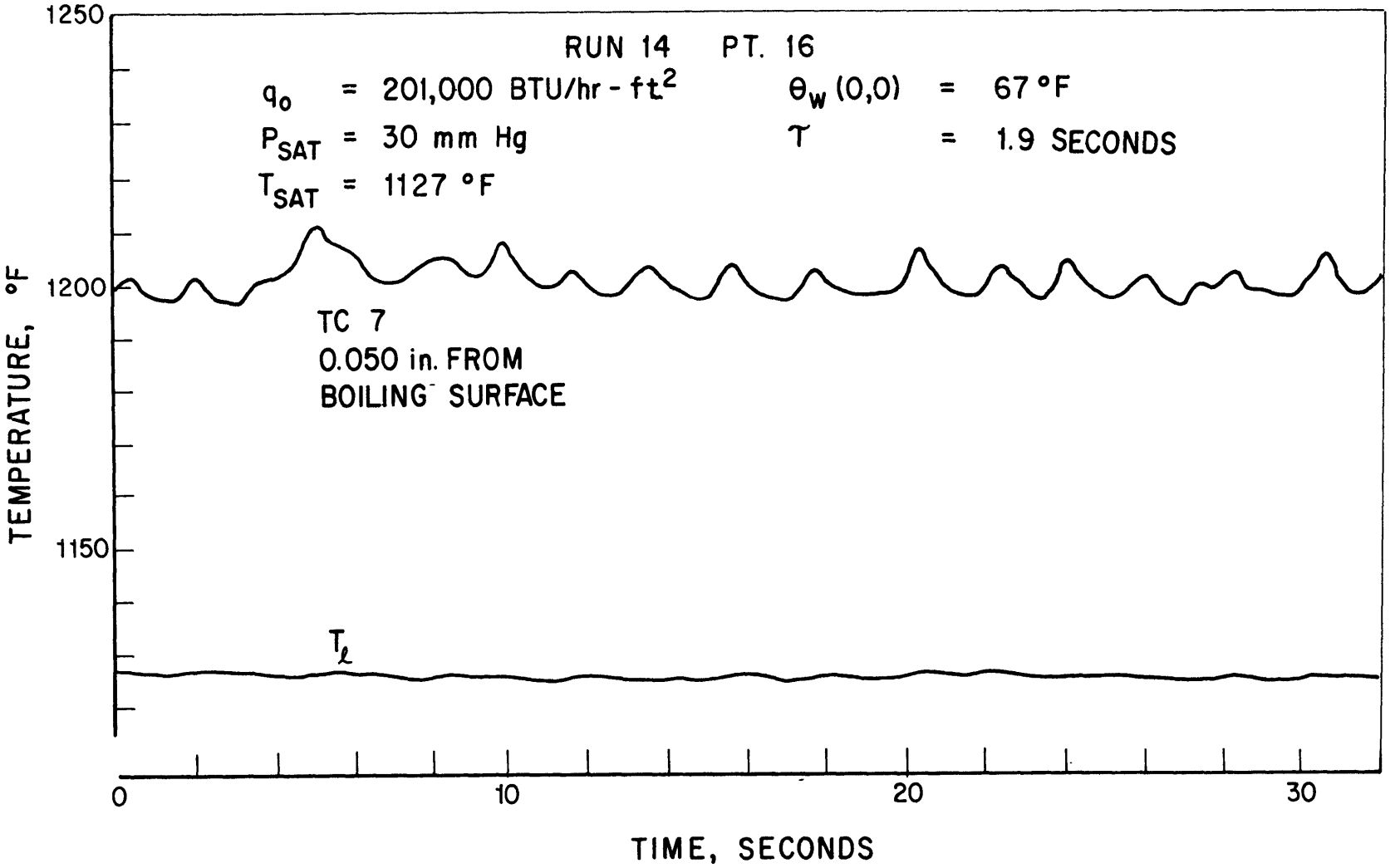

Fig. 31 Stable Boiling at Natural Site in Nickel Surface

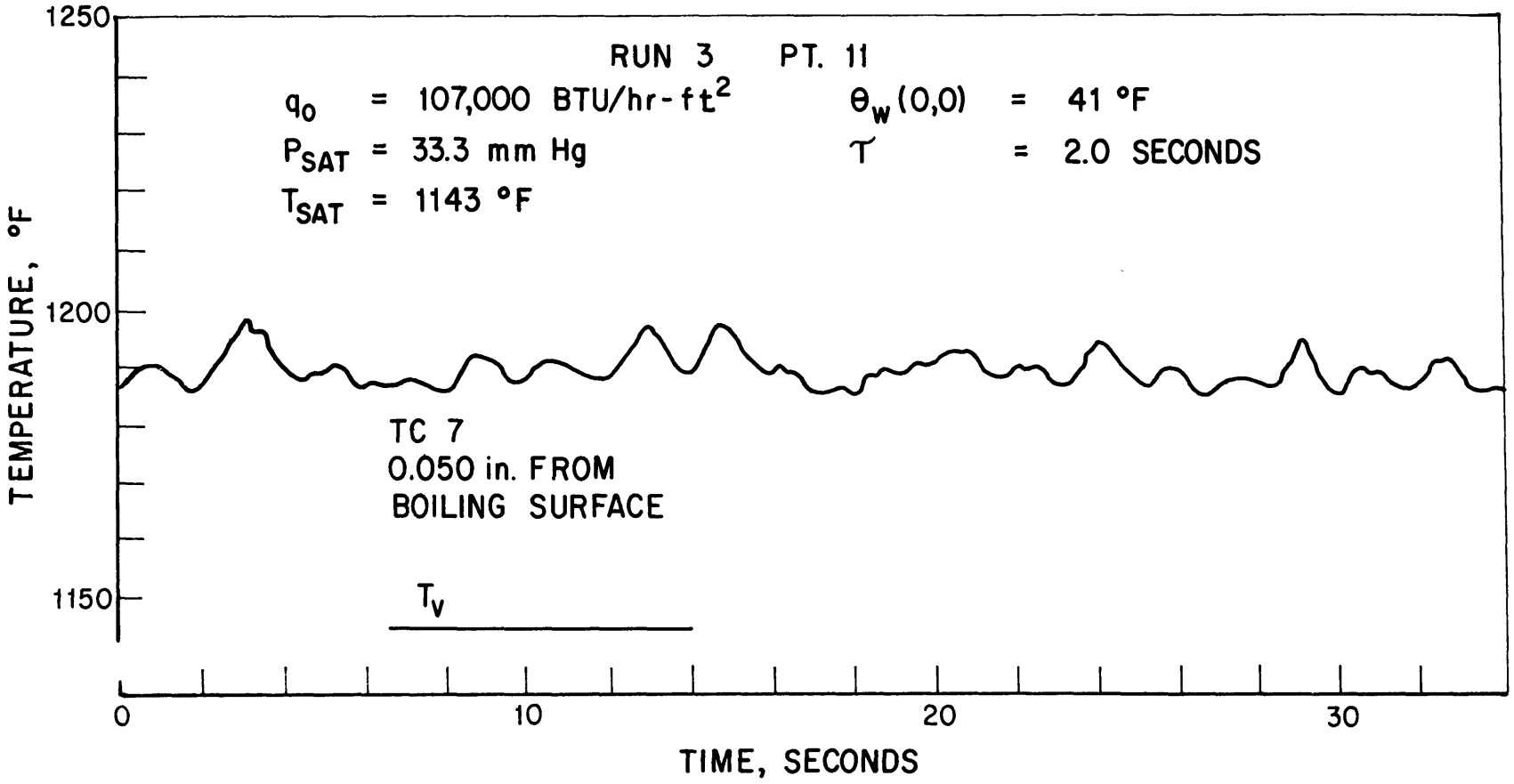

Fig. 32 Stable Boiling at Artificial Cavity in Nickel Surface

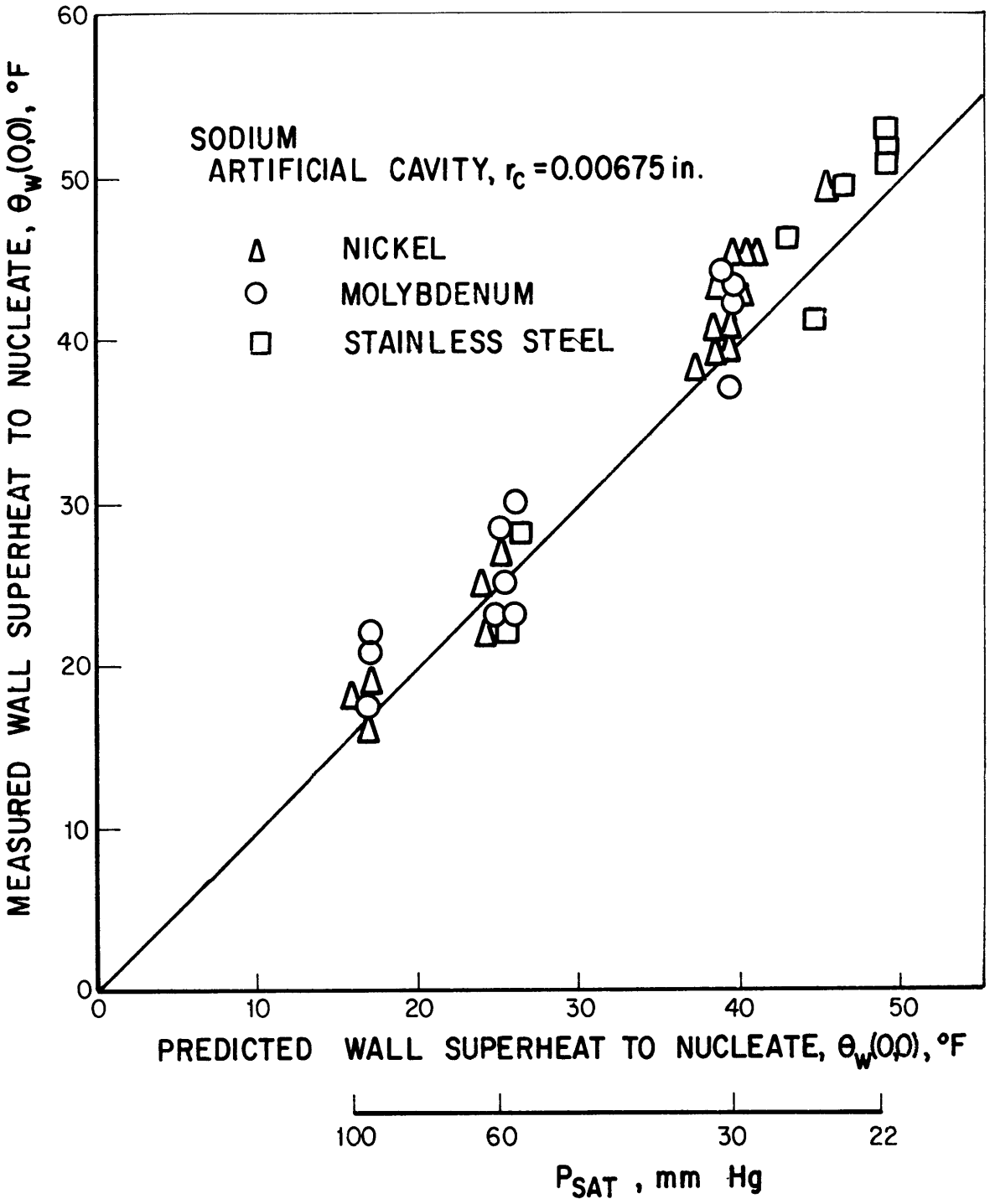

Fig. 33 Prediction of Wall Superheat for Nucleation of Boiling Sodium from an Artificial Cavity in Nickel, Molybdenum, and Stainless Steel

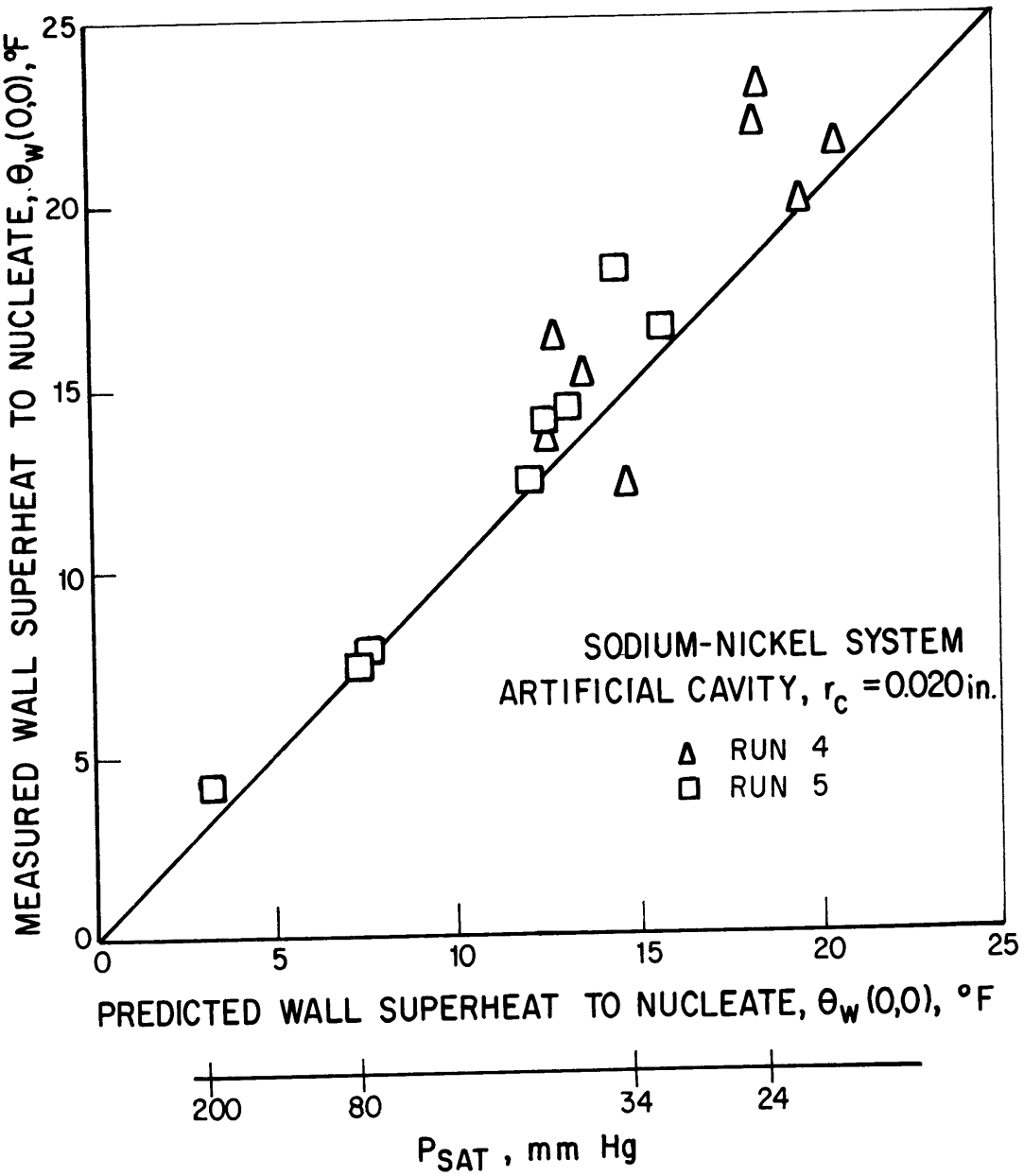

Fig. 34 Prediction of Wall Superheat for Nucleation from an Artificial Cavity in Nickel Surface

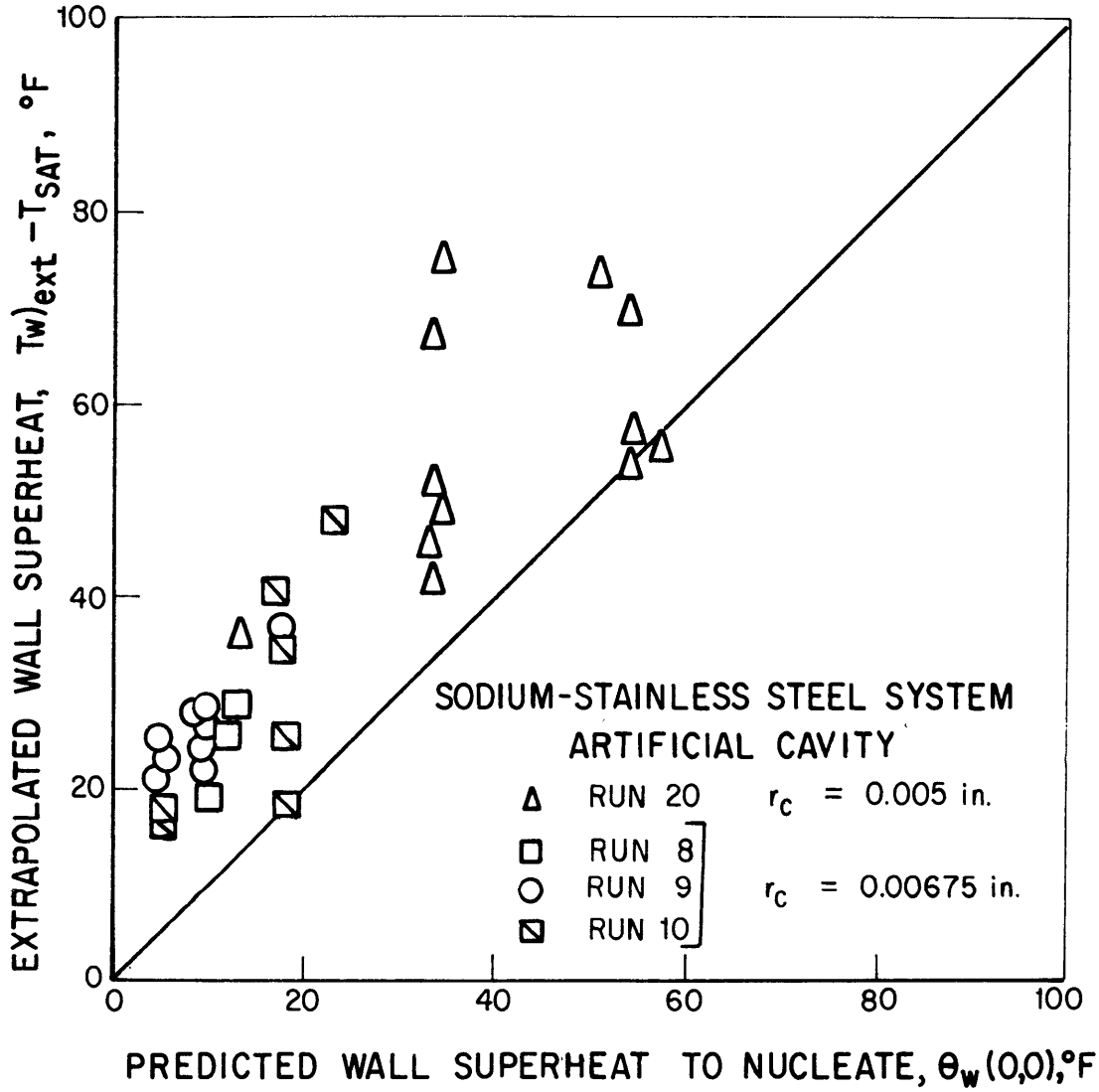

Fig. 35 Prediction of Wall Superheat for Nucleation from Artificial Cavities in Stainless Steel Surface

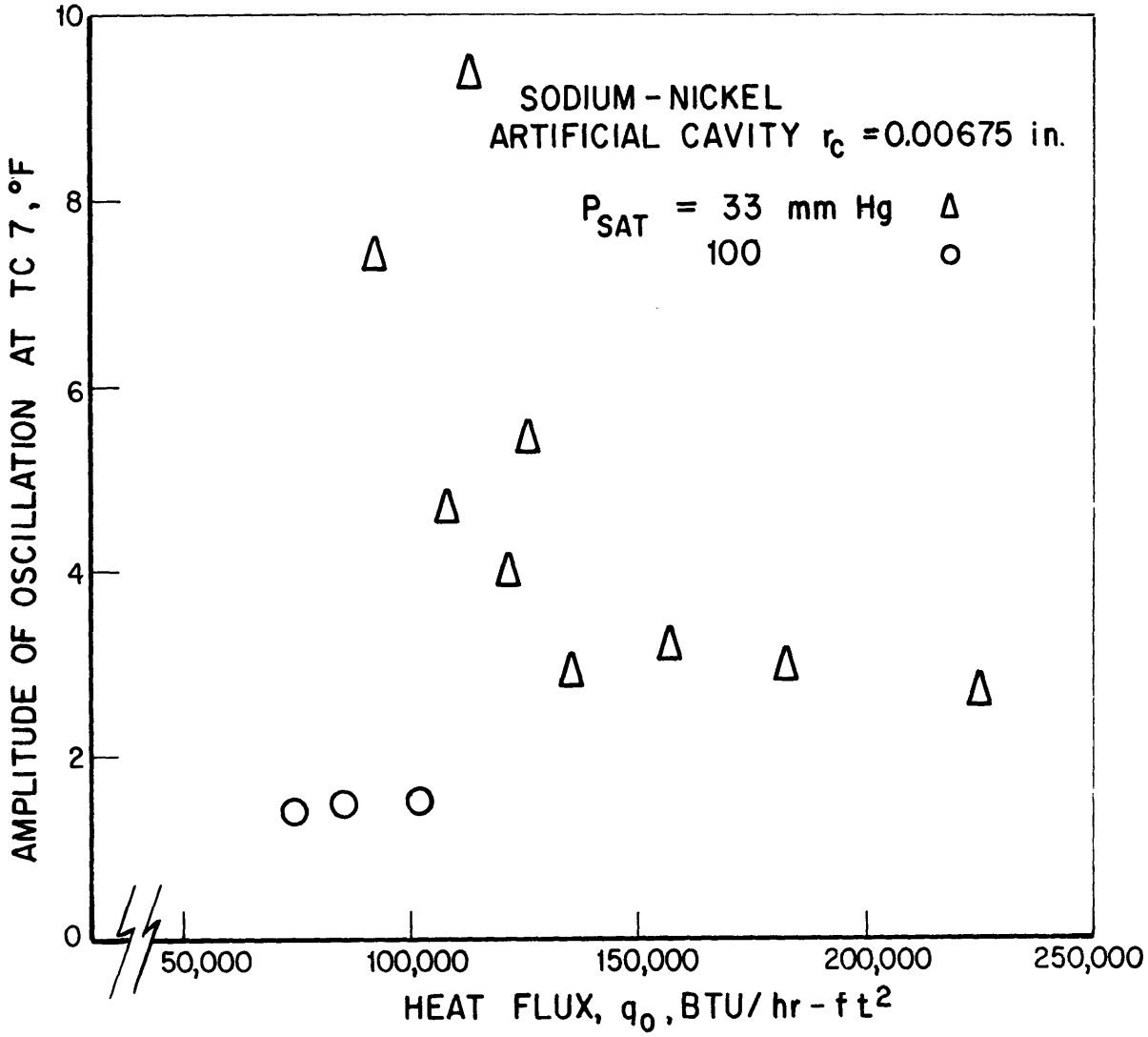

Fig. 36 Amplitude of Temperature Oscillation at Thermocouple 7 (TC 7) for Stable Boiling of Sodium From an Artificial Cavity in Nickel Surface

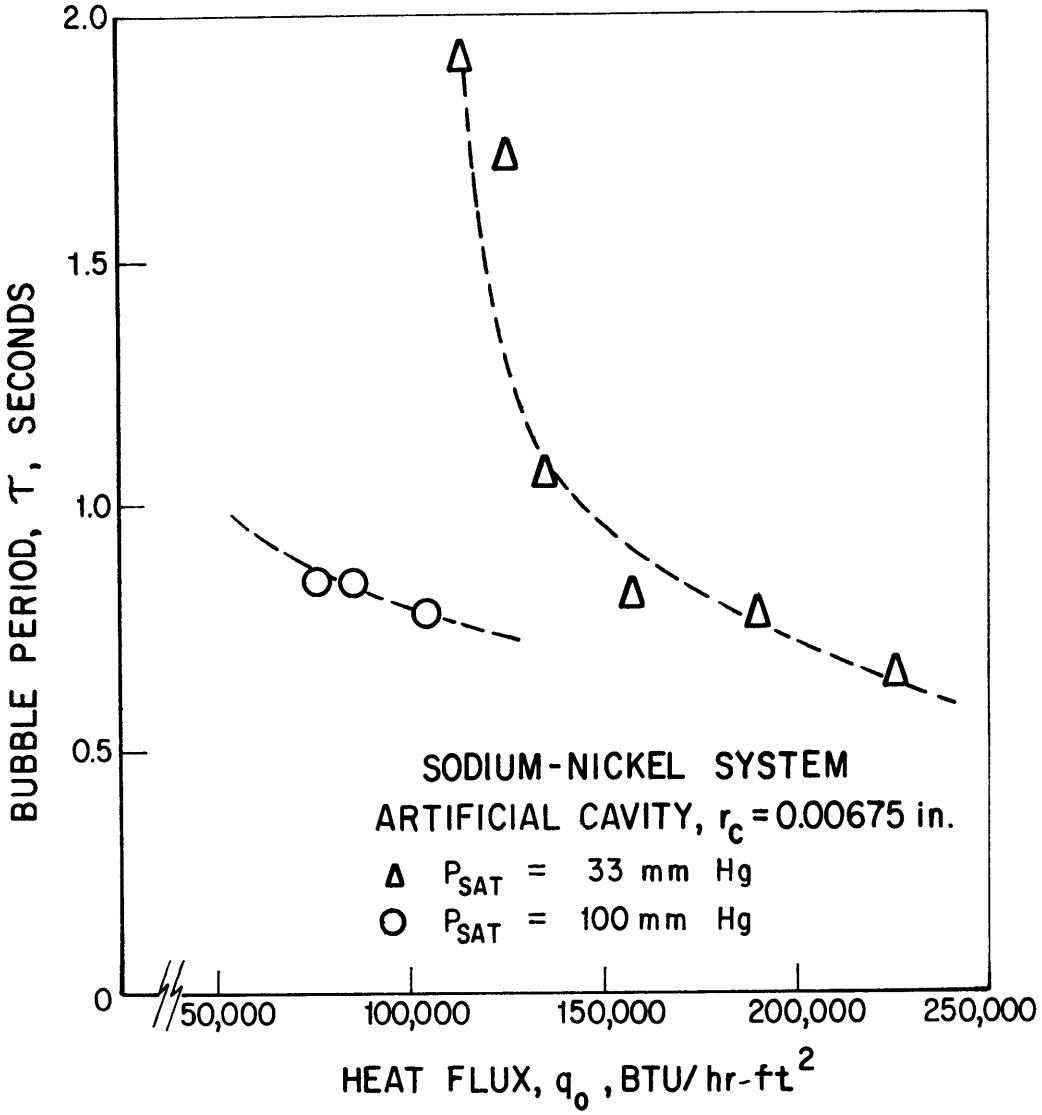

Fig. 37 Bubble Period for Nucleate Boiling of Sodium from an Artificial Cavity in Nickel Surface

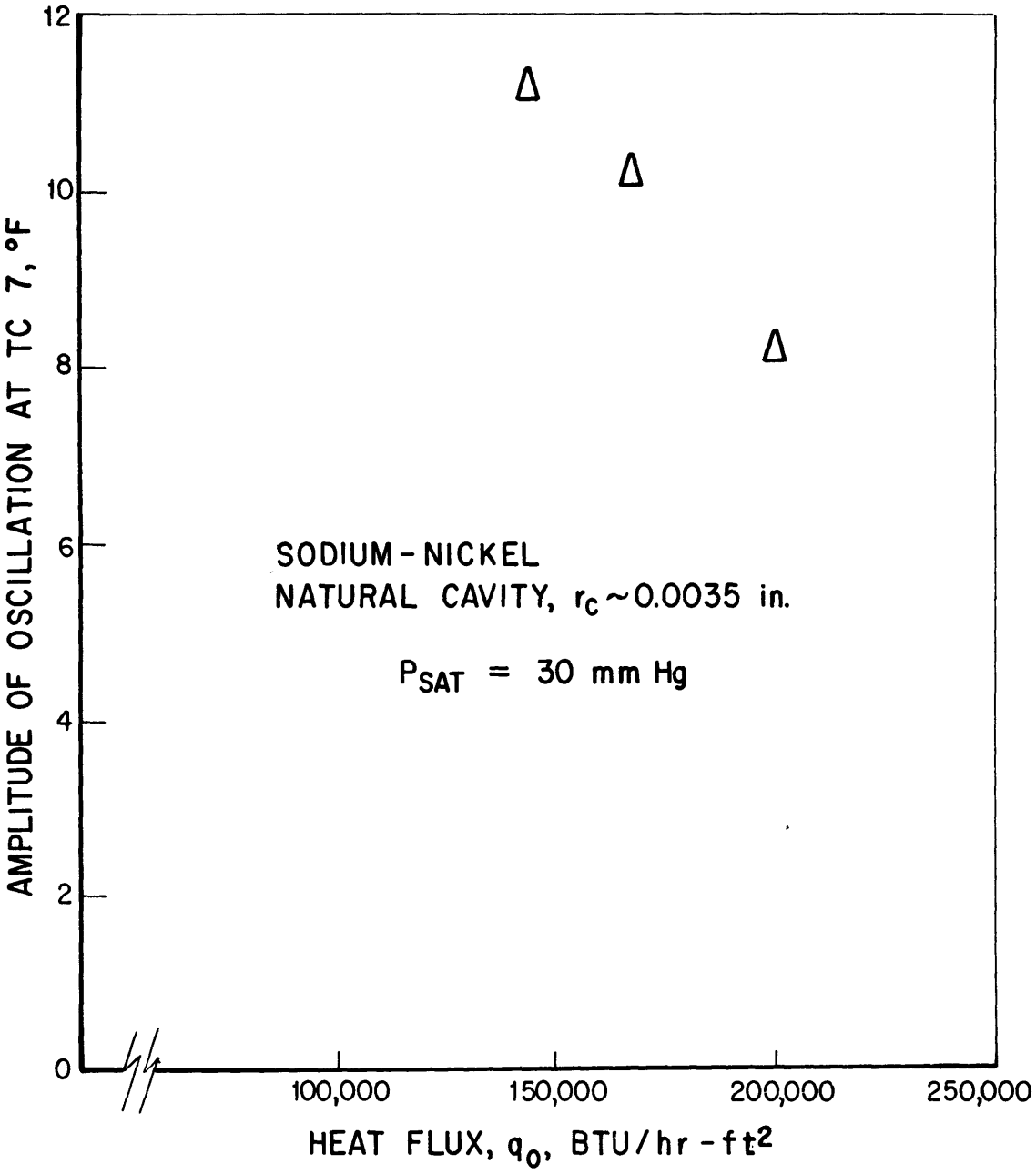

Fig. 38 Amplitude of Temperature Oscillation at Thermocouple 7 (TC 7) for Stable Boiling of Sodium from a Natural Cavity in Nickel Surface

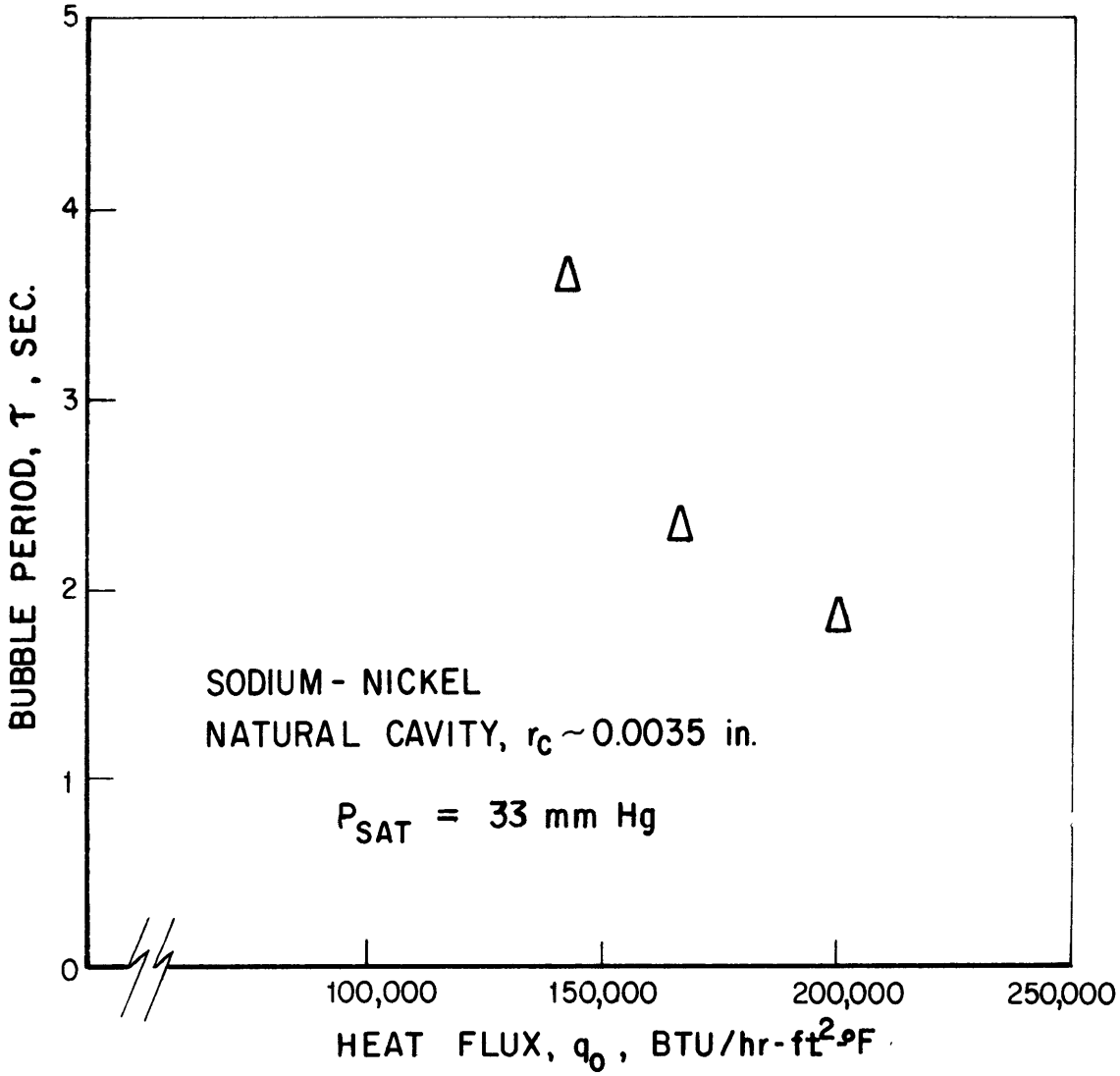

Fig. 39 Bubble Period for Stable Boiling of Sodium from a Natural Cavity in a Nickel Surface

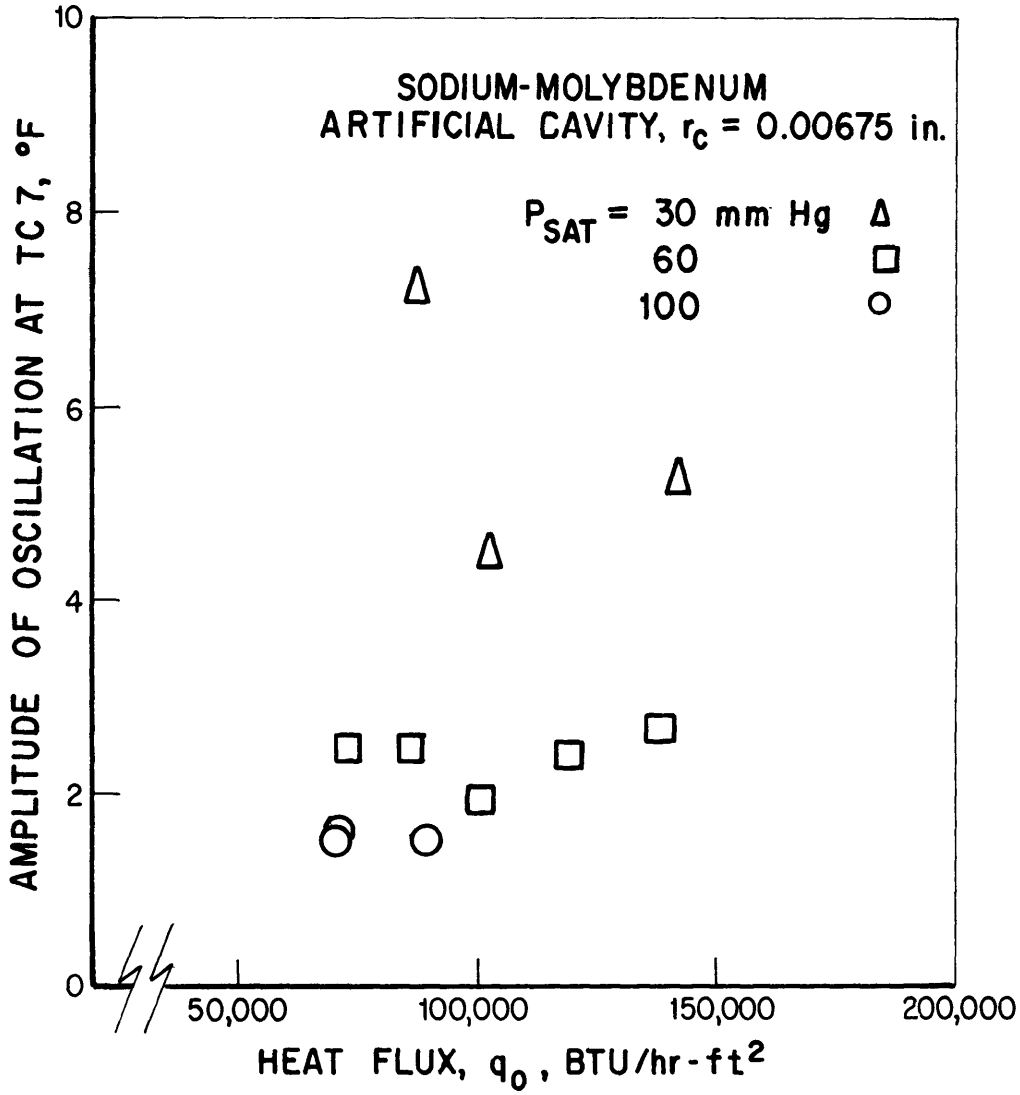

Fig. 40 Amplitude of Temperature Oscillation at Thermocouple 7 (TC 7) for Stable Boiling From an Artificial Cavity in a Molybdenum Surface

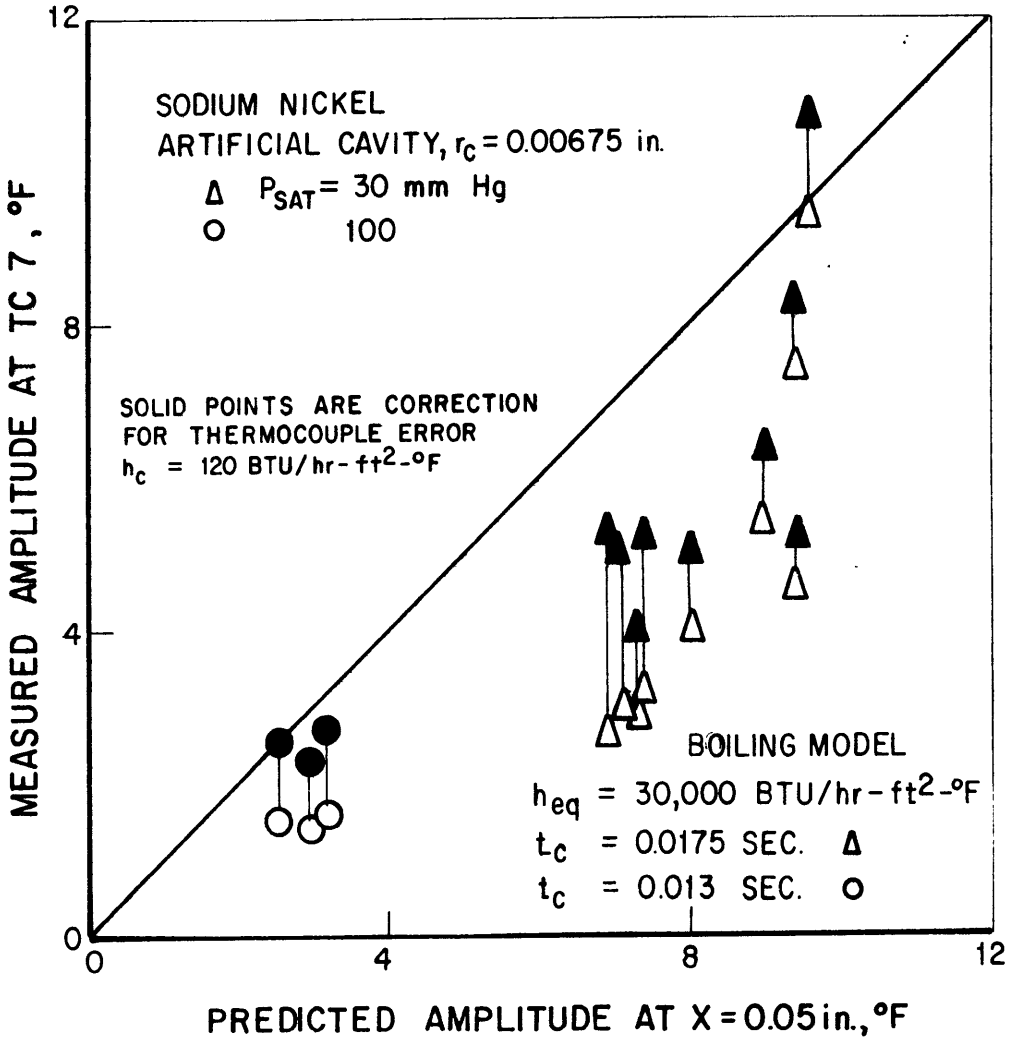

Fig. 41 Comparison of Predicted and Measured Amplitudes of Temperature Oscillation at TC 7 for Stable Boiling of Sodium from an Artificial Cavity in Nickel Surface

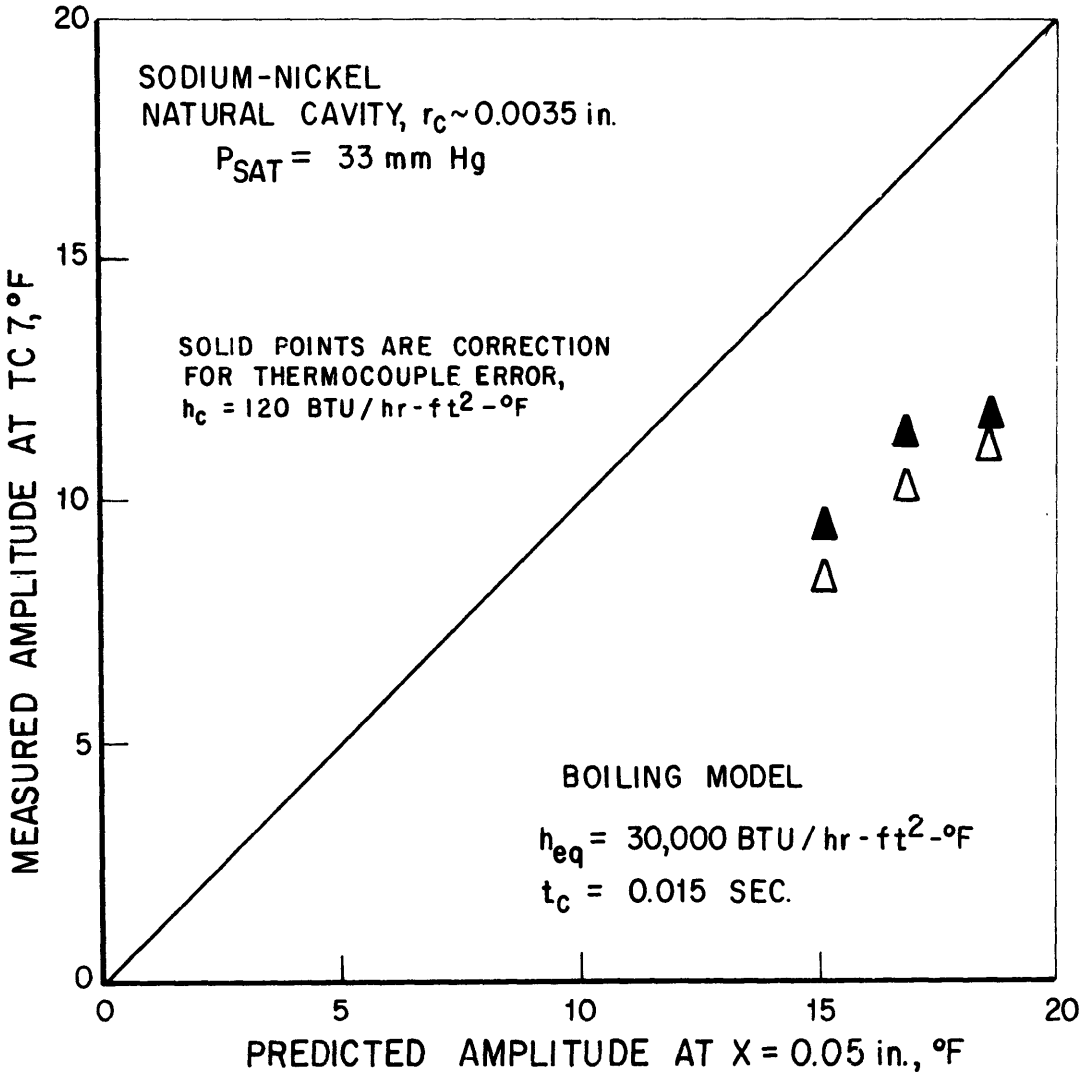

Fig. 42 Comparison of Predicted and Measured Amplitudes of Temperature Oscillation at TC 7 for Stable Boiling of Sodium from a Natural Cavity in Nickel Surface

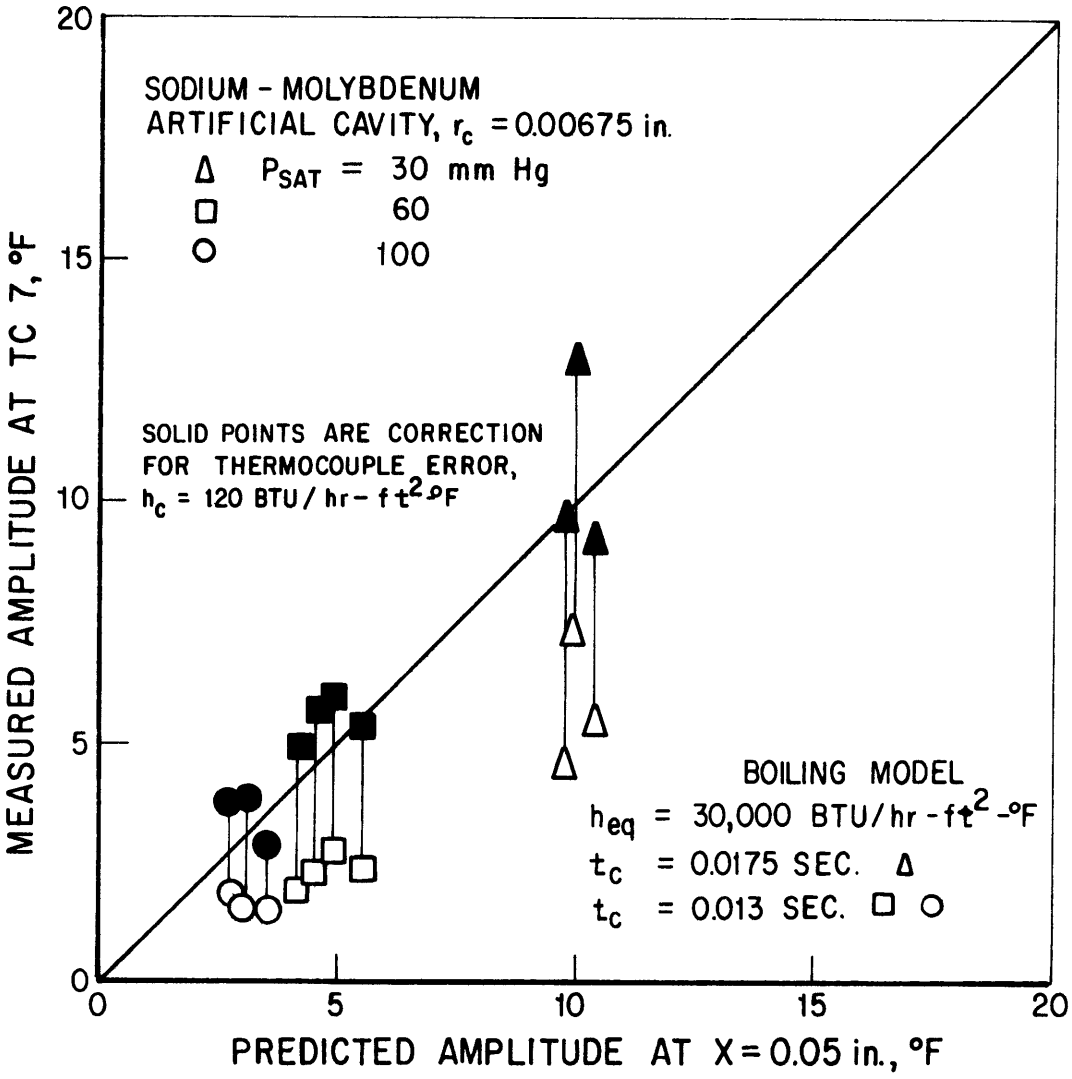

Fig. 43 Comparison of Predicted and Measured Amplitudes of Temperature Oscillation at TC 7 for Stable Boiling of Sodium From an Artificial Cavity in Molybdenum Surface

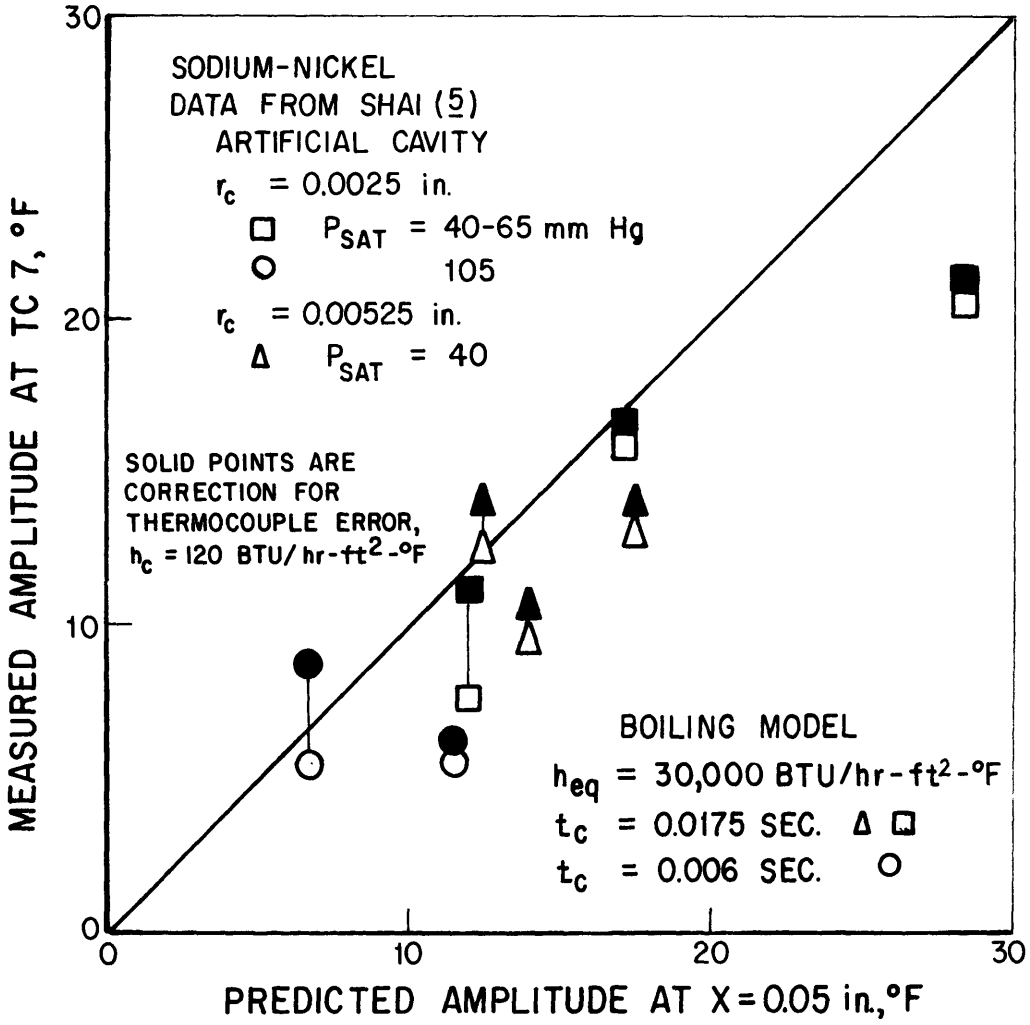

Fig. 44 Comparison of Predicted and Measured Amplitudes of Temperature Oscillation at TC 7 for Stable Boiling of Sodium From an Artificial Cavity in Nickel Surfaces (Data from Shai (5))

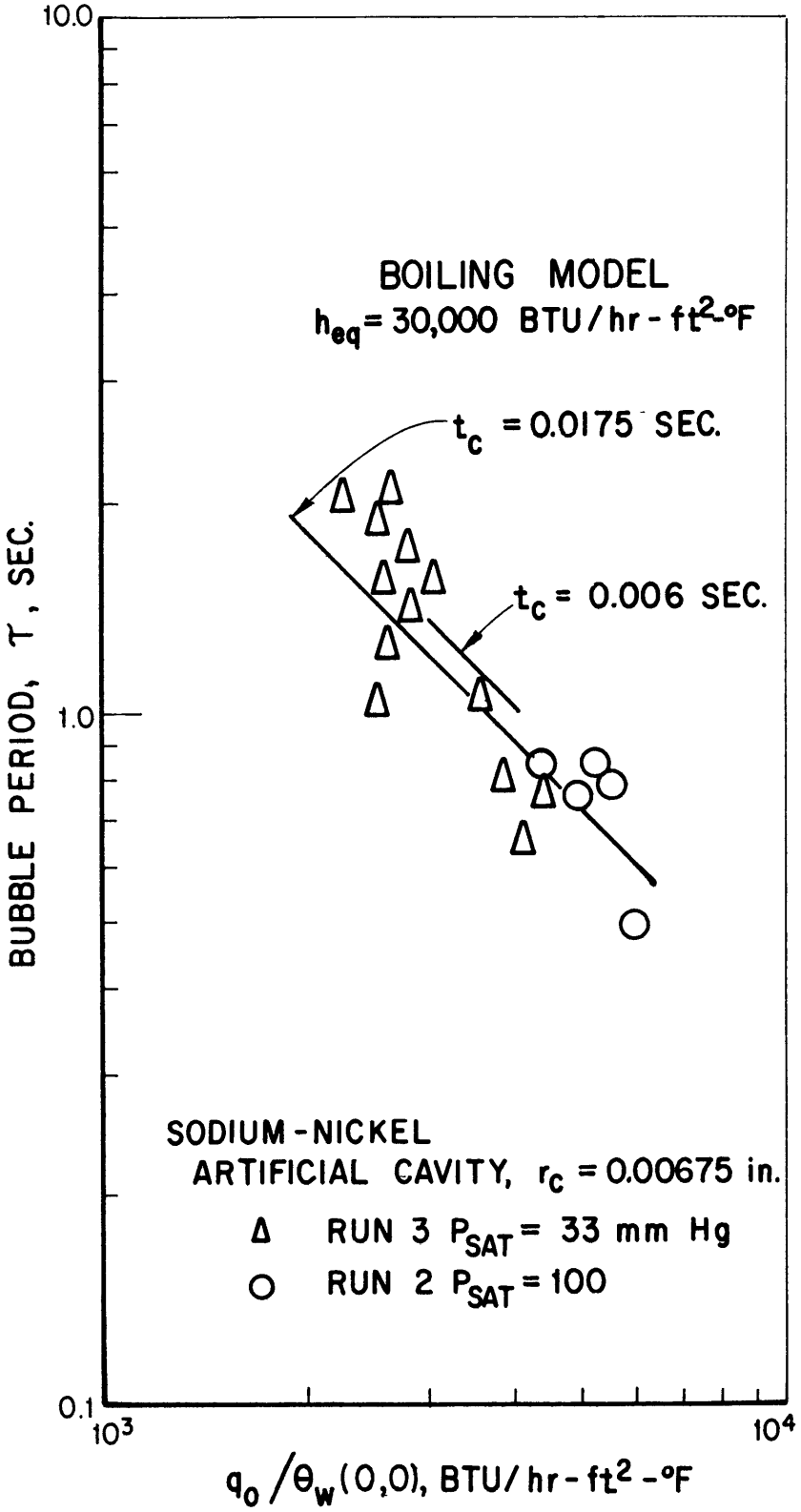

Fig. 45 Comparison of Bubble Period Data with Prediction for Sodium Boiling From an Artificial Cavity in Nickel Surface

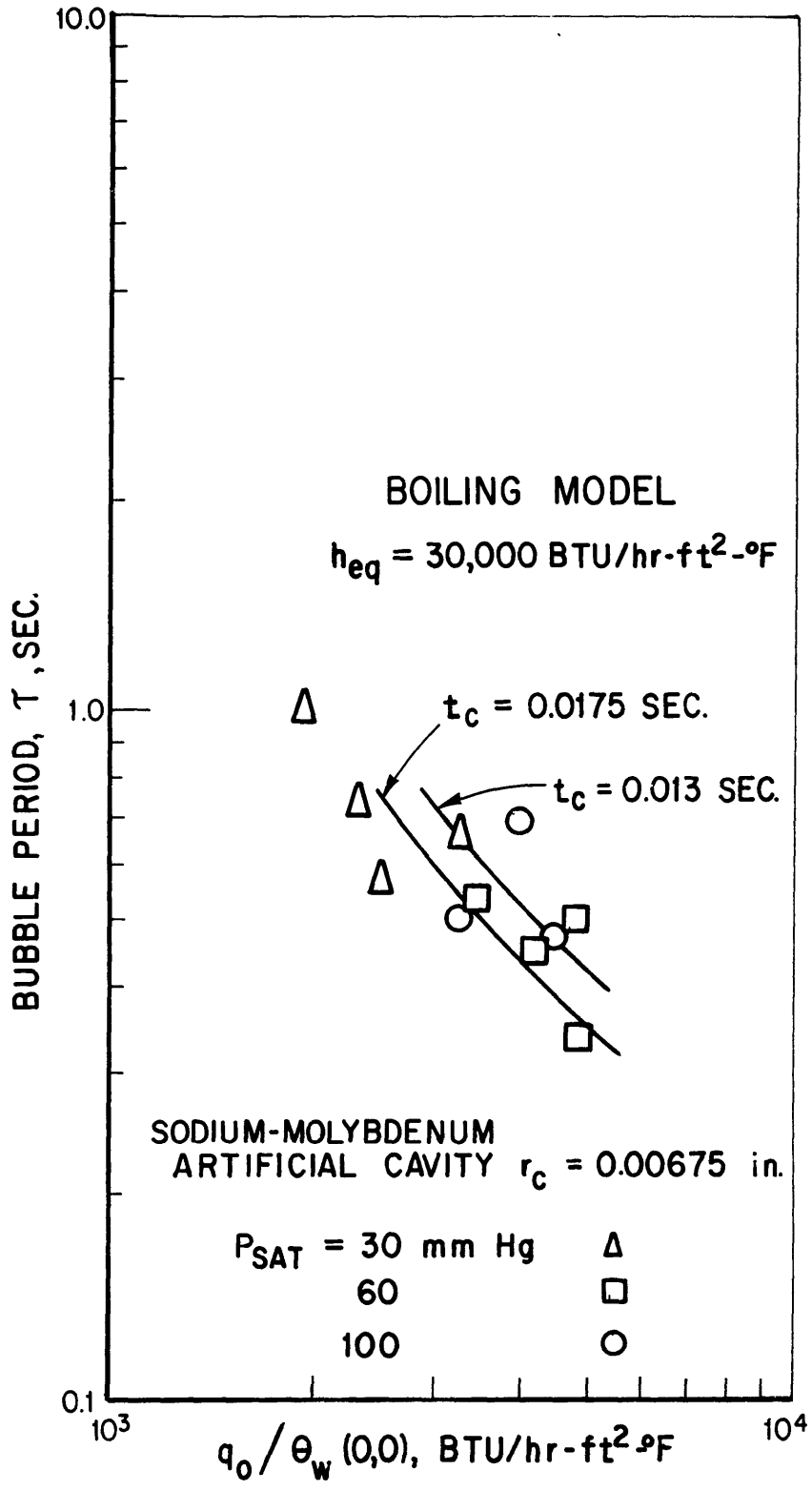

Fig. 46 Comparison of Bubble Period Data With Prediction for Sodium Boiling From an Artificial Cavity in Molybdenum Surface

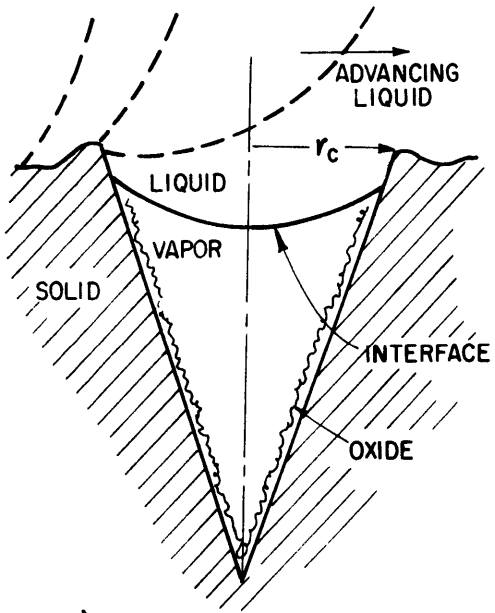

a.) AT INITIAL FILLING

Filling Procedure Bridges Cavity and Traps Non-Condensible Gas

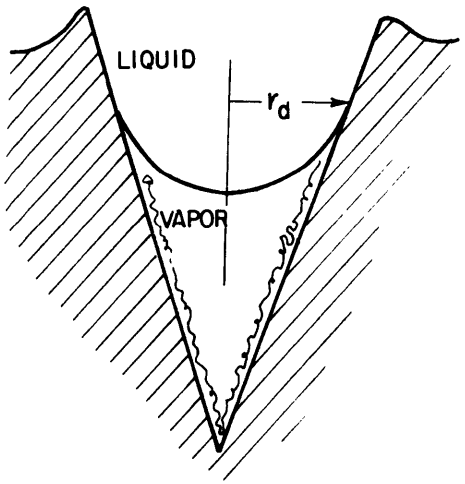

b.) AT DEACTIVATION

Vapor-Liquid Interface Recedes into Cavity at Radius r_d during Pressurization P_l' and Subcooling T_l'

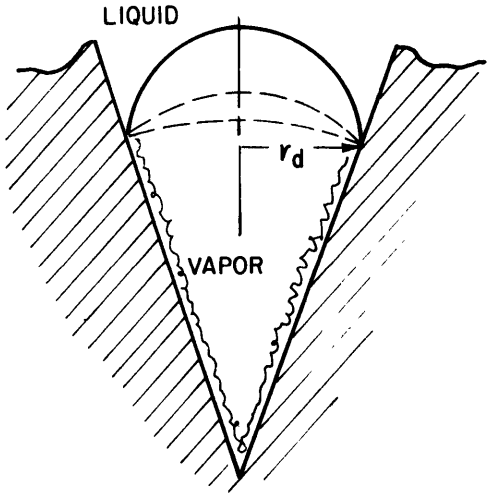

c.) AT INCIPIENT VAPORIZATION

Contact Angle Flips from Non-wetting Condition and Cavity Nucleates at Radius r_d when Sufficient Superheat is Available

Fig. 47 Model of Chen (8) for Incipient Nucleation Subsequent to Pressure-Temperature History

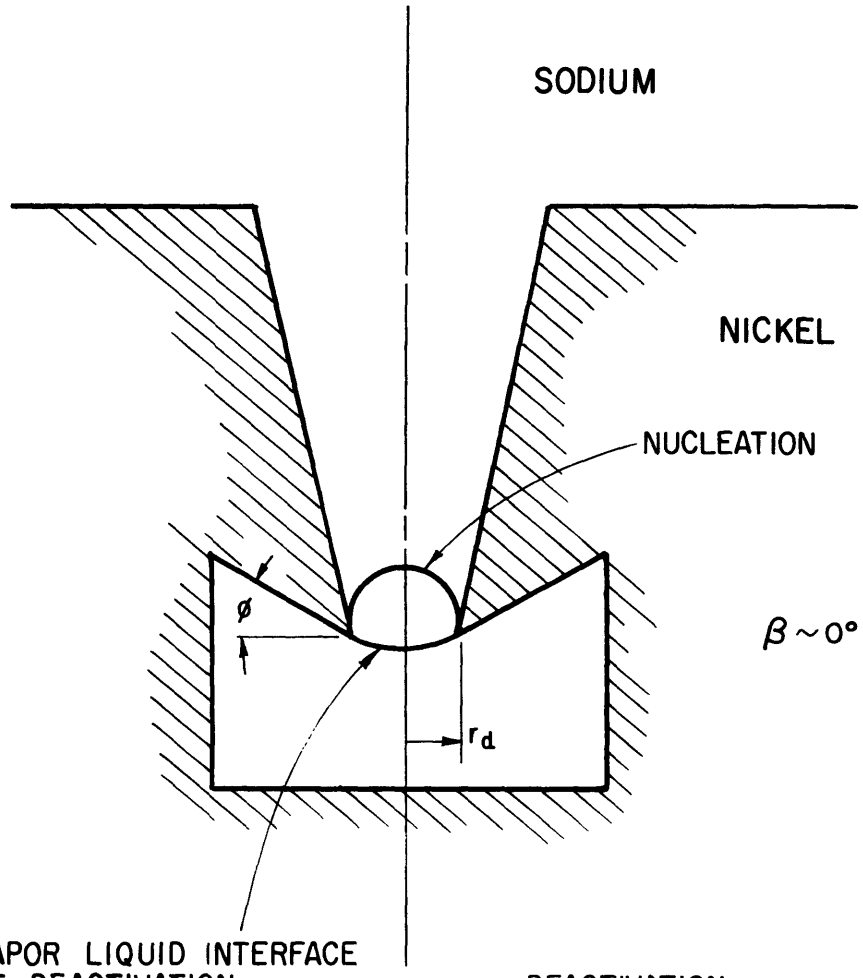

DEACTIVATION

$$P_\ell' - P_V' - P_g'(t) = \frac{2\sigma' \sin \phi}{r_d}$$

NUCLEATION

$$P_V + P_g(t) - P_\ell = \frac{2\sigma}{r_d}$$

Fig. 48 Incipient-Boiling Model for Re-entrant Cavity, Subsequent to Deactivation Pressure P_ℓ' and Subcooling T_ℓ'

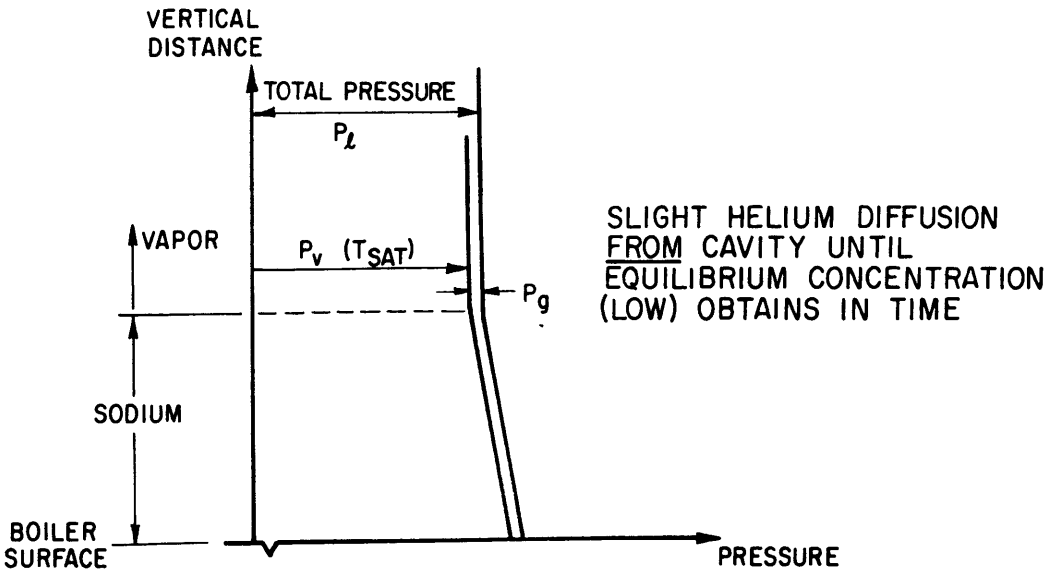

A. HELIUM TRANSFER WHEN SYSTEM IS AT TEMPERATURE

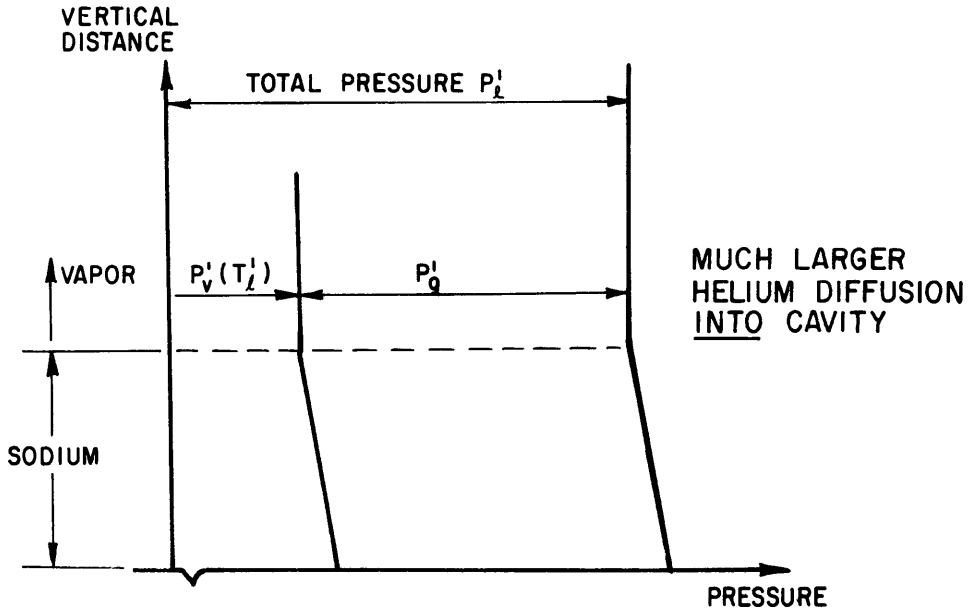

B. HELIUM TRANSFER DURING DEACTIVATION

Fig. 49 Inverse-Time Effect on Sodium Deactivation Due to Diffusion of Inert Gas

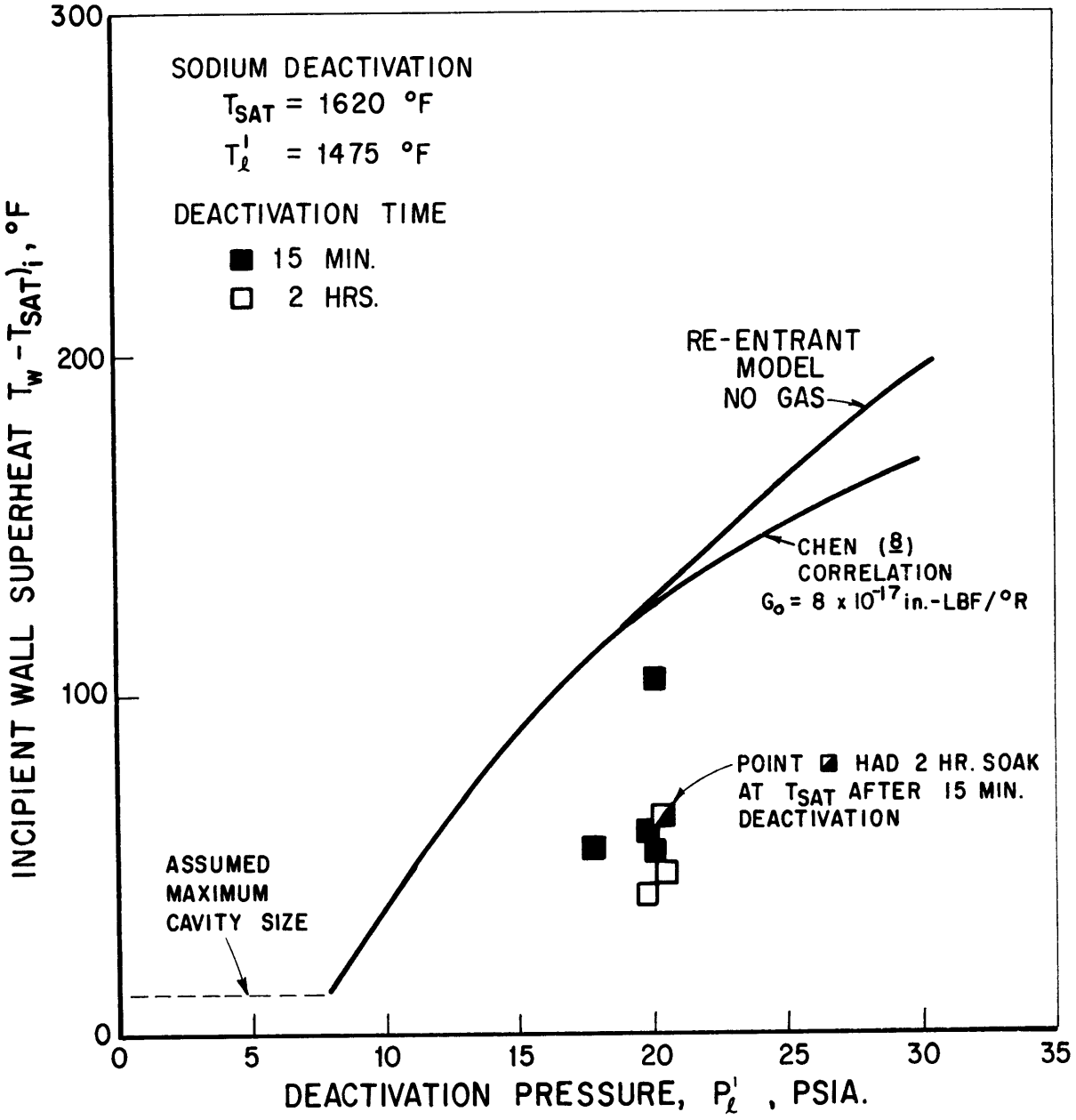

Fig. 50 Incipient Wall Superheat Data for Boiling Subsequent to Deactivation Conditions.

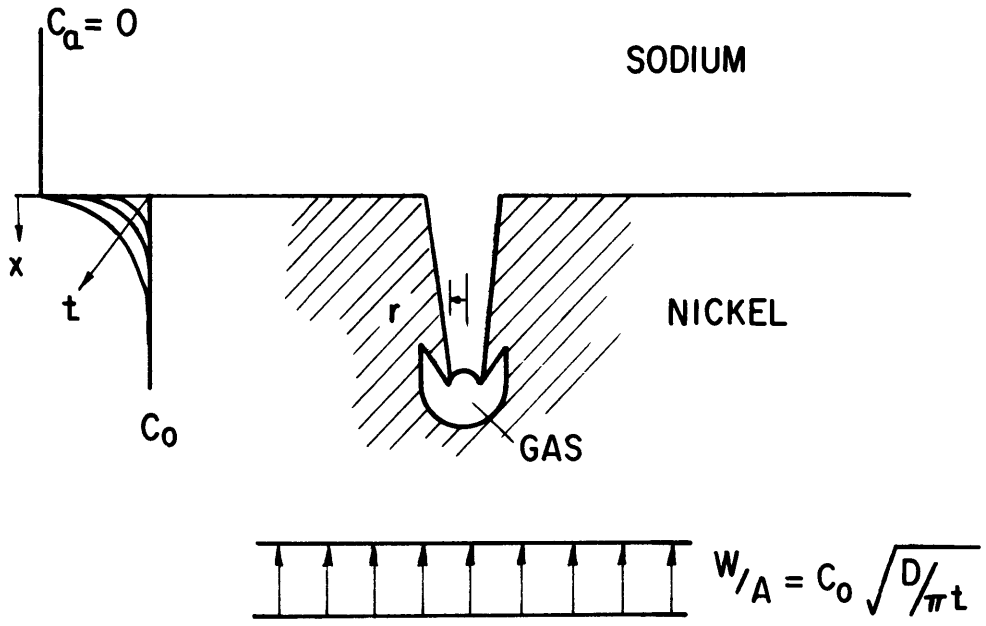

W/A = MASS FLUX

C_o = INITIAL CONCENTRATION (UNIFORM)~0.10 cm^3 gas (STP)/cm^3 NICKEL

D = DIFFUSION COEFFICIENT ~ 3.1 x 10^{-12} cm^2/sec

Fig. 51 Boiler Surface Outgassing Into Natural Re-entrant Cavity and Triggering Nucleation If Sufficient Superheat is Available

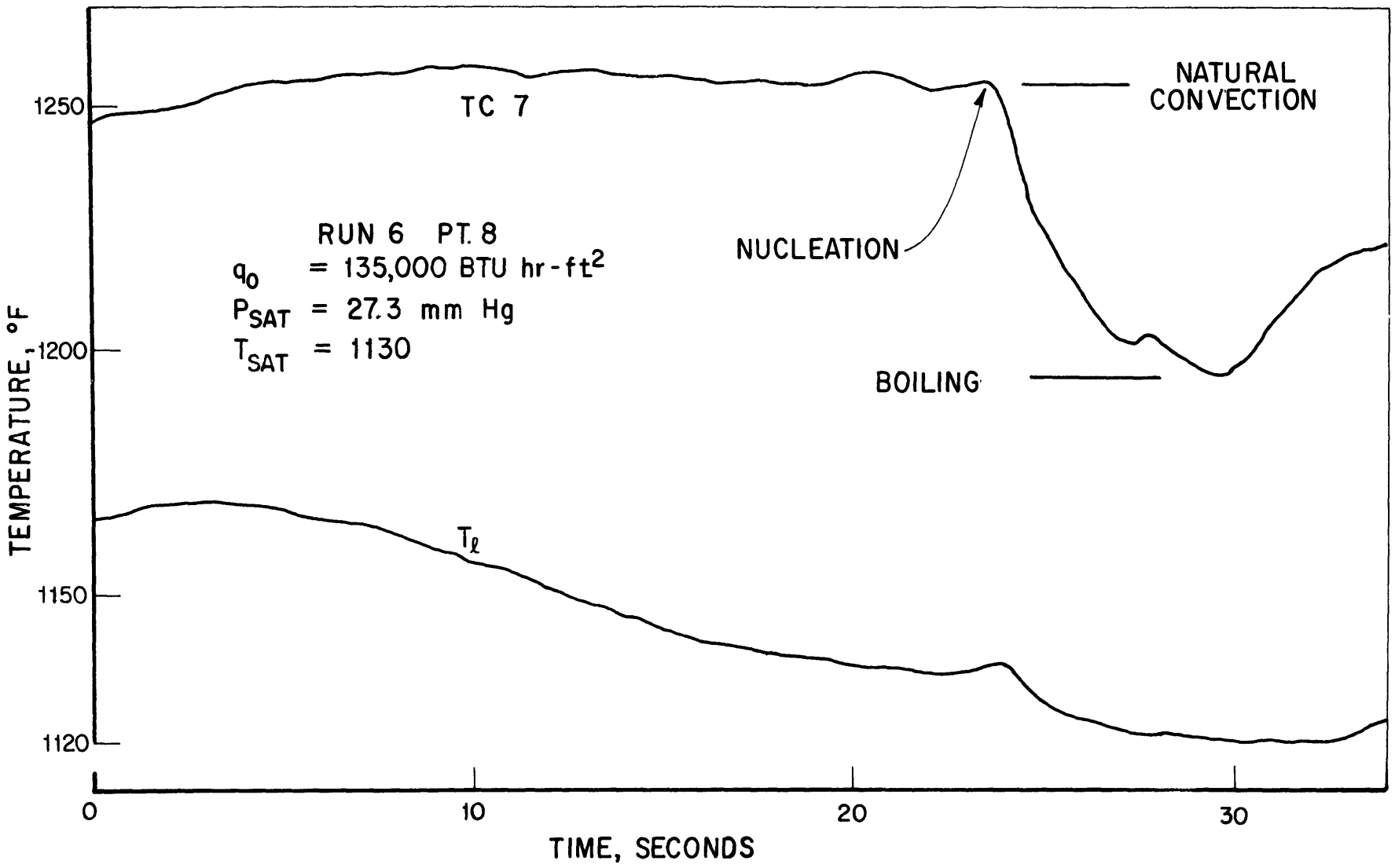

Fig. 52 Unstable Boiling at Low Pressure on Stainless Steel Surface

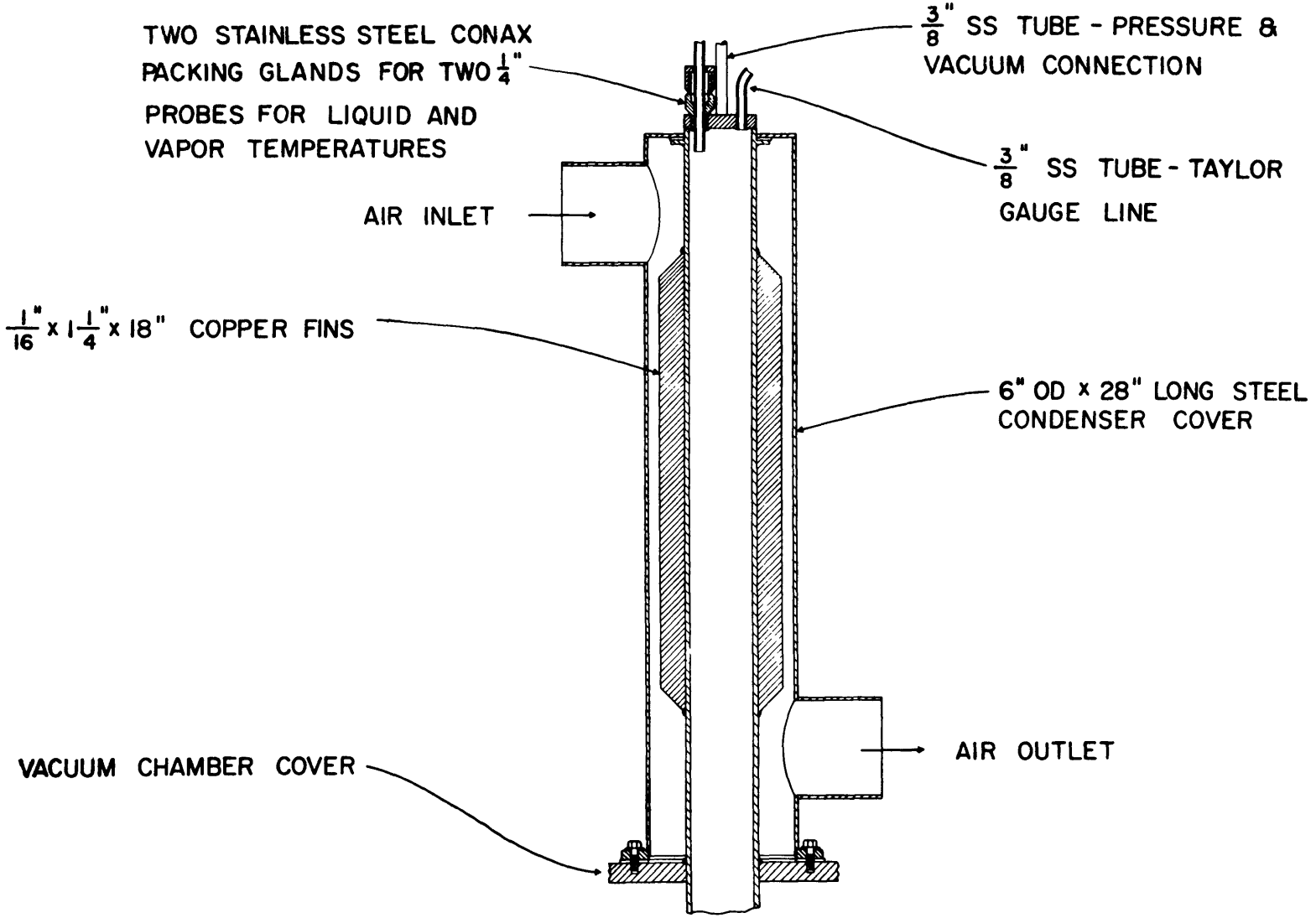

Fig. 53 Sectional Drawing of Condenser

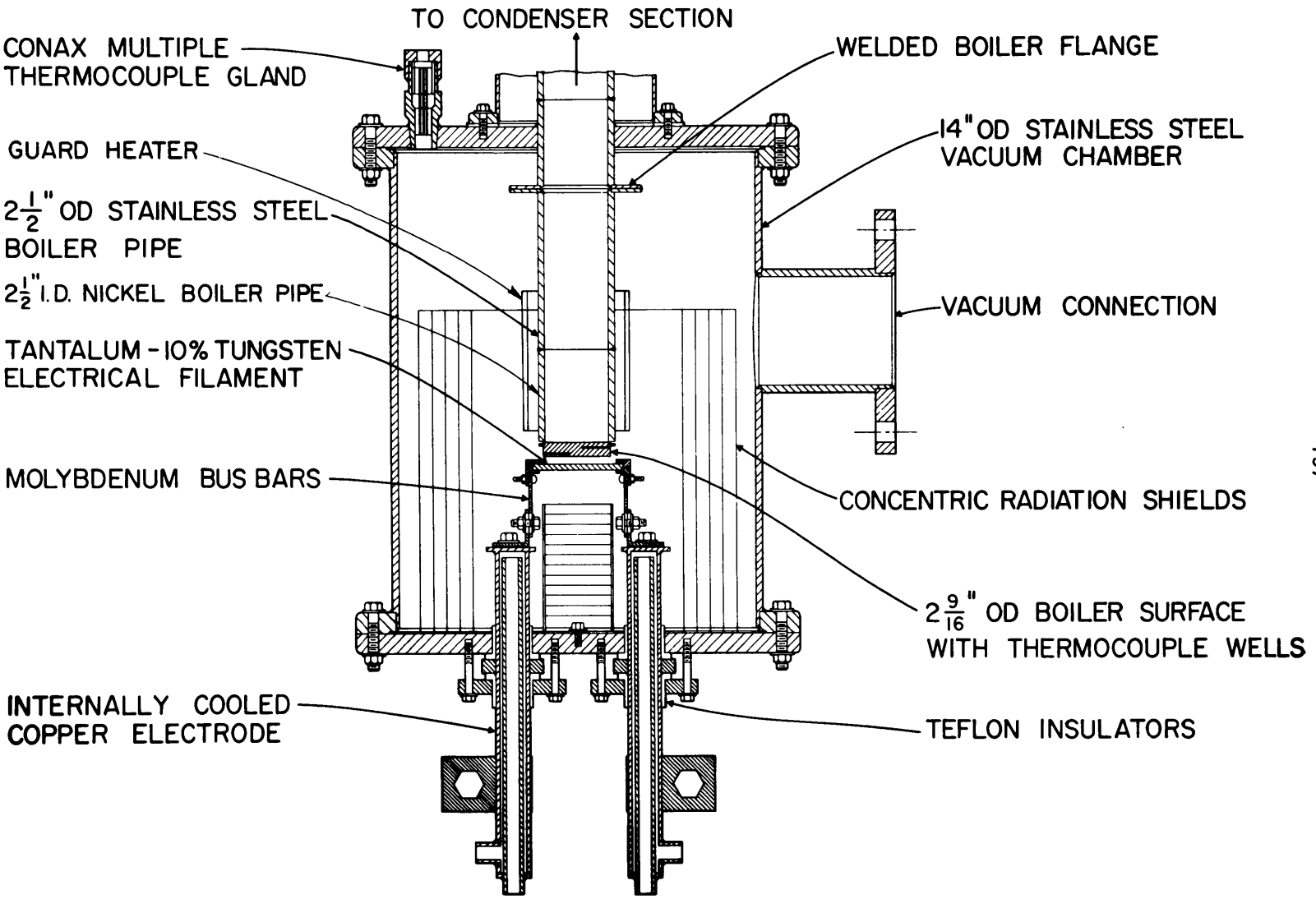

Fig. 54 Sectional Drawing of Heater and Boiler

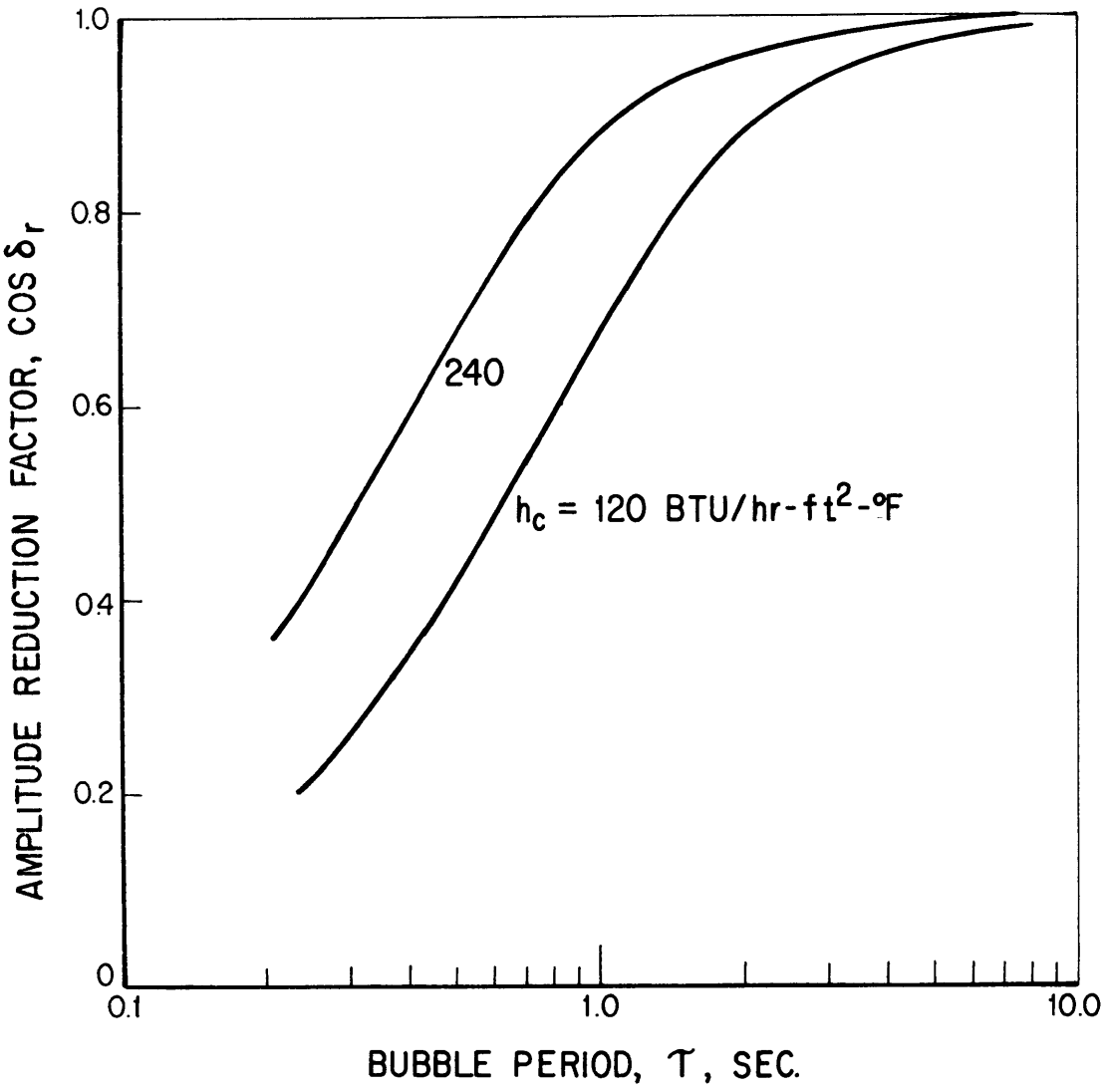

Fig. 55 Amplitude Reduction Factor

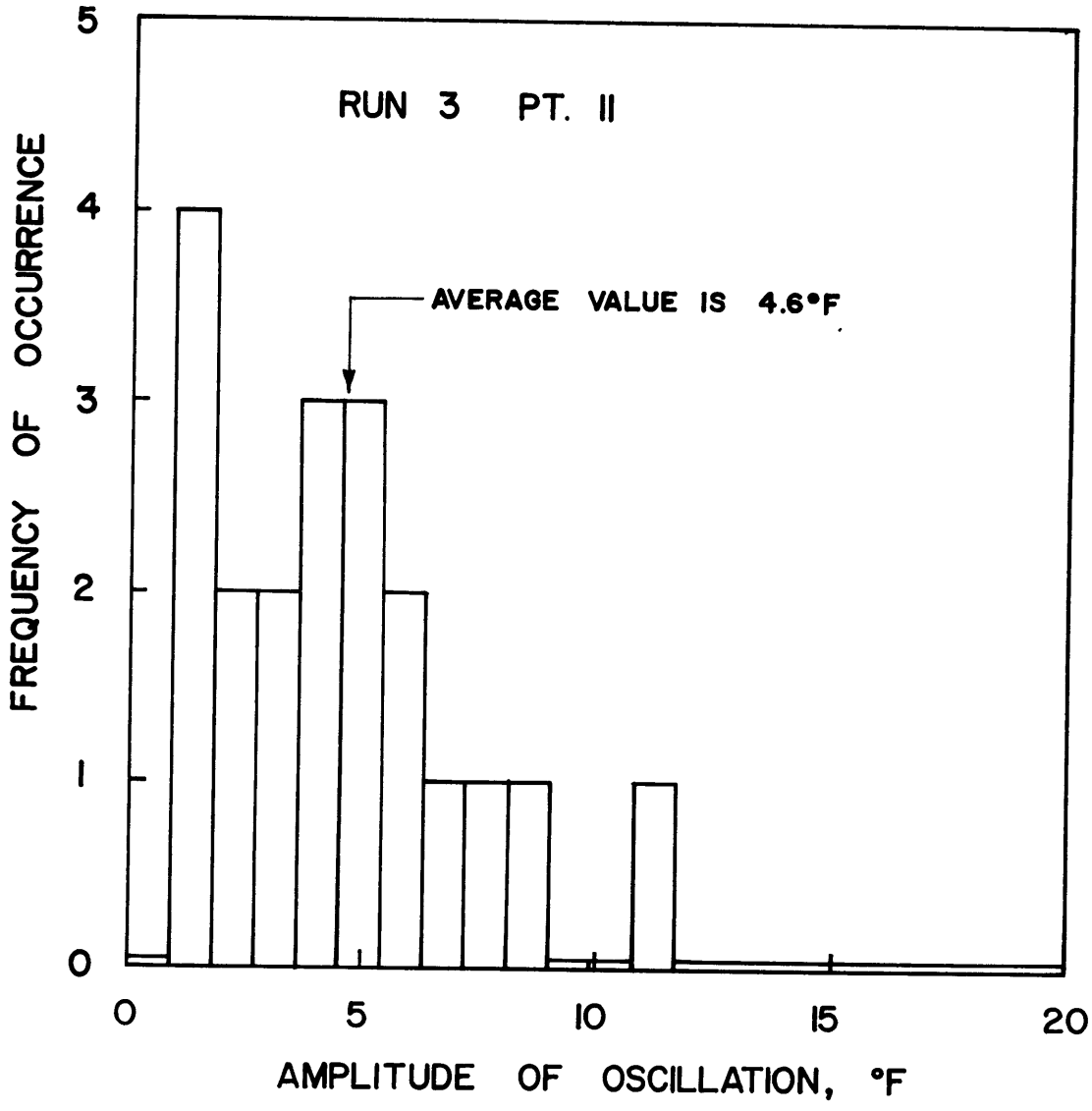

Fig. 56 Sample of Data at One Operating Condition for Amplitude of Temperature Oscillation at TC 7

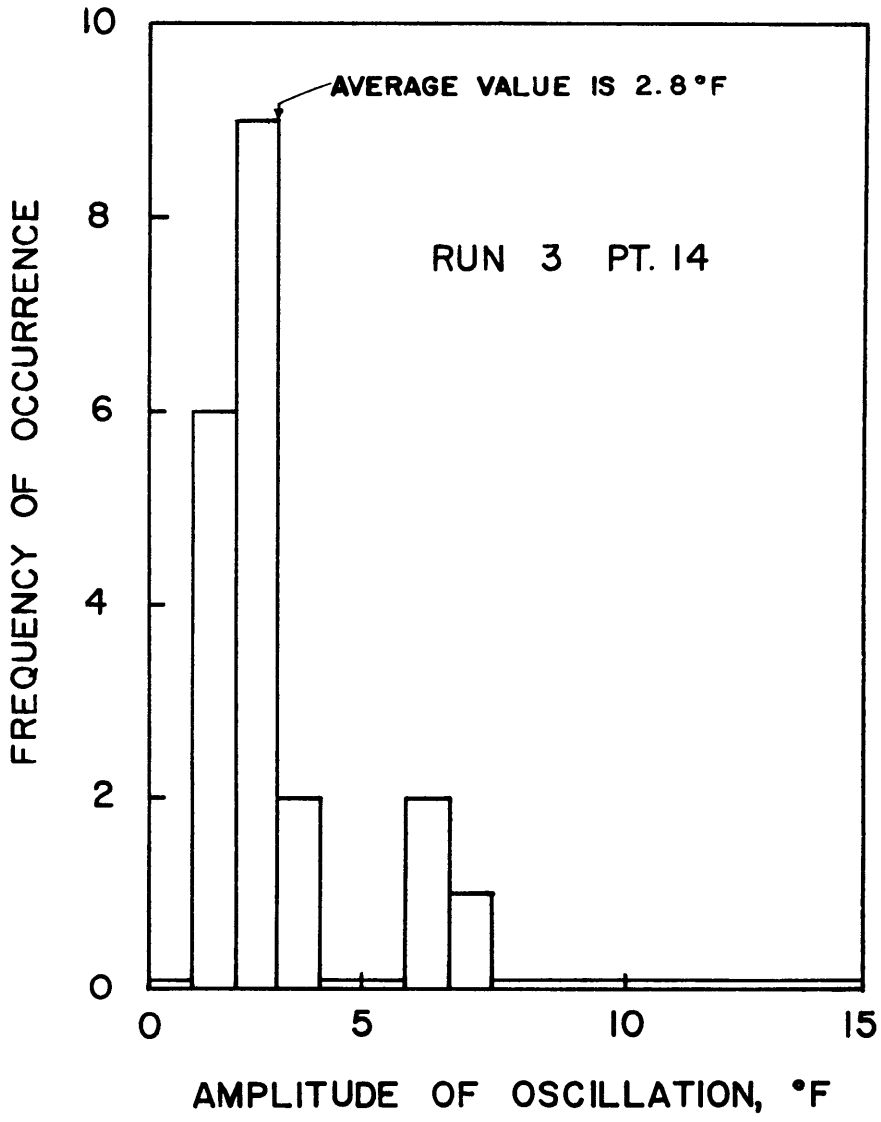

Fig. 57 Sample of Data at One Operating Condition for Amplitude of Temperature Oscillation at TC 7

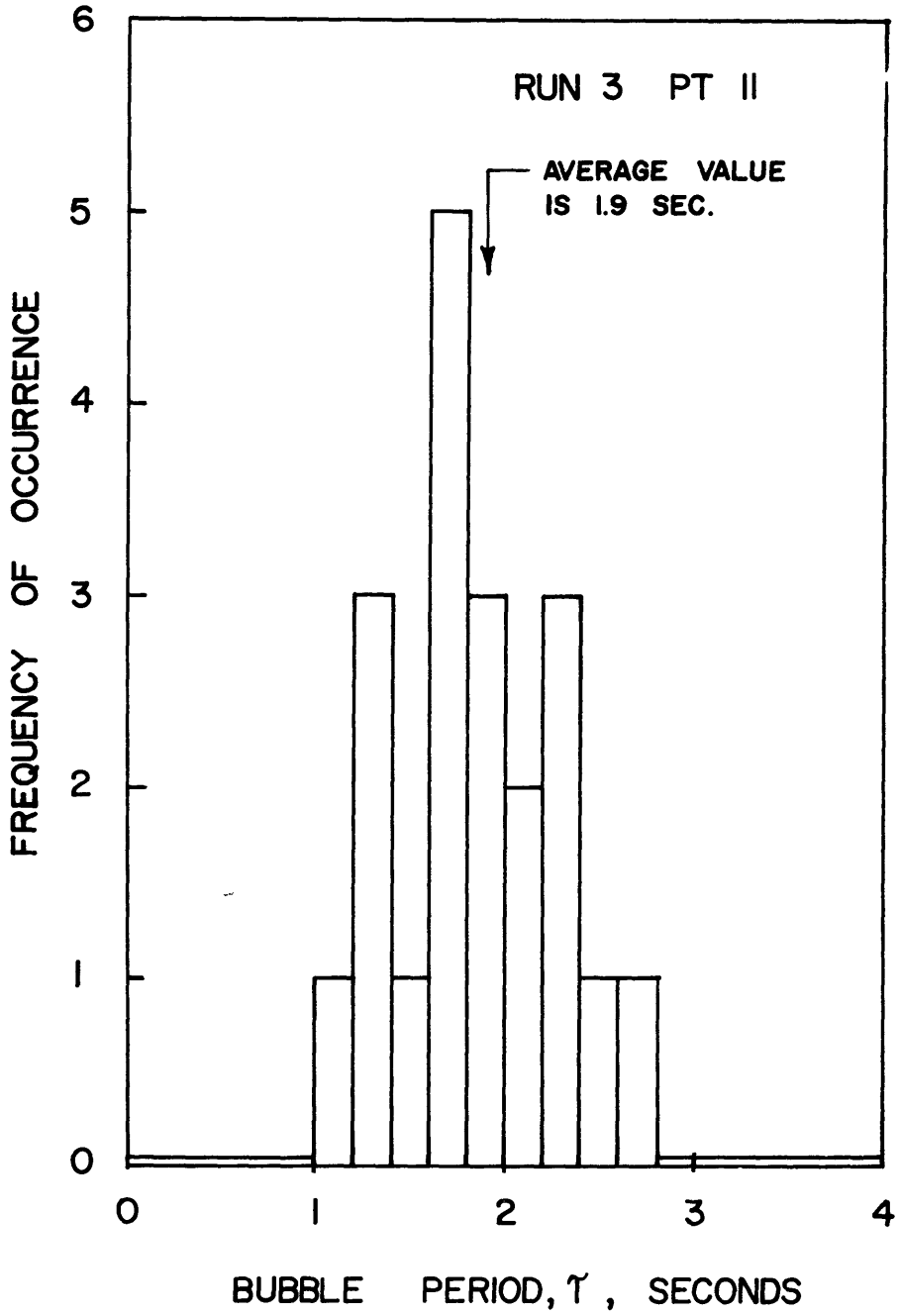

Fig. 58 Sample of Data at One Operating Condition for Bubble Period

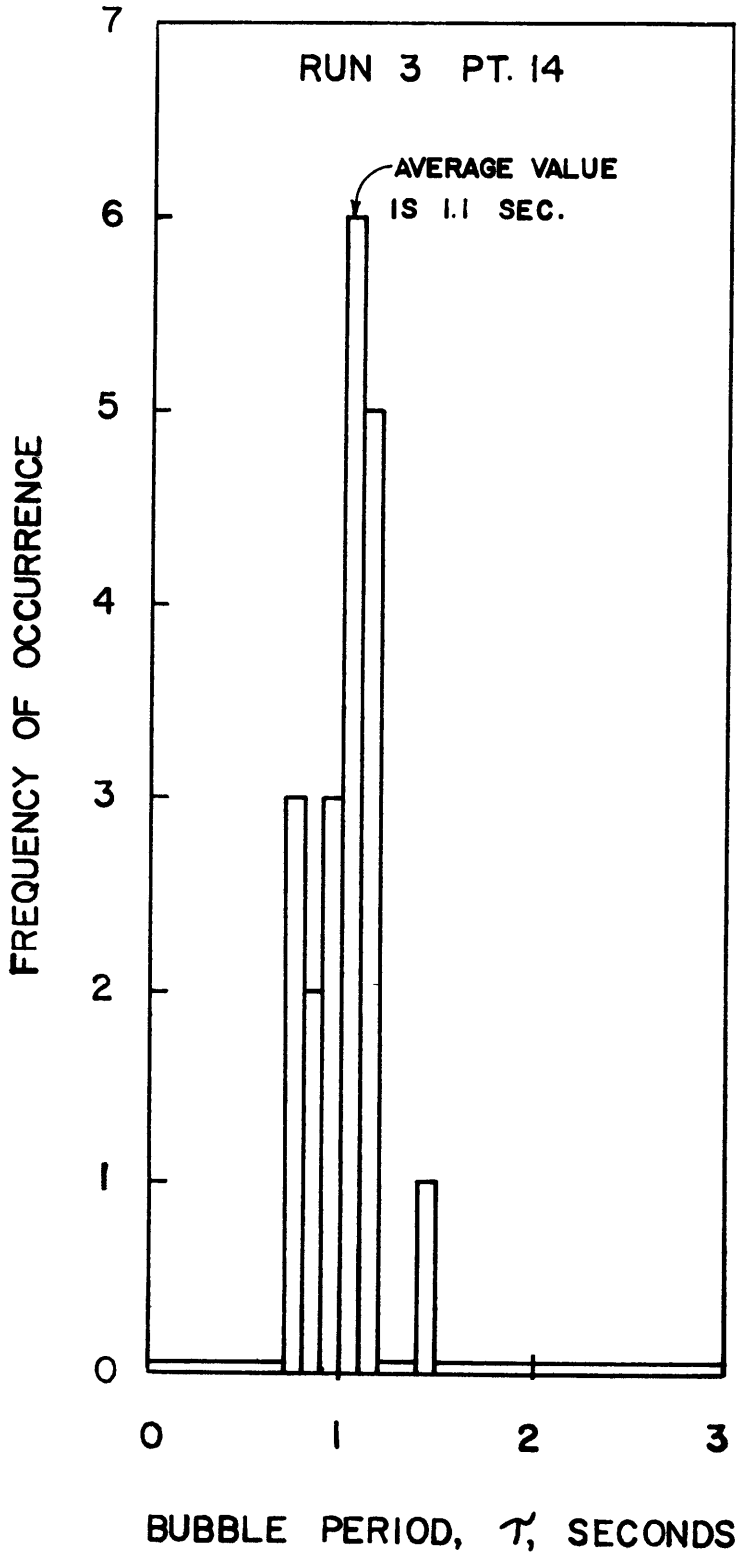

Fig. 59 Sample of Data at One Operating Condition for Bubble Period

BIOGRAPHICAL NOTE

Charles W. Deane, IV, was born July 19, 1943, in Summit, Ner Jersey, the eldest son of Charles W. Deane, III, and the former Elizabeth Felt. He was graduated in June 1961, from Scarsdale High School in Scarsdale, New York, where he played the French horn in the Concert Band.

He entered the Massachusetts Institute of Technology as a freshman in September, 1961. He received the Bachelor of Science degree in the Department of Mechanical Engineering in June, 1965.

In September, 1965, he entered Graduate School at M.I.T., and received an appointment as a Research Assistant under Professor S. William Gouse, Jr. The research resulted in a thesis for the degree of Master of Science in September, 1966; the work was extended during the following year, and was subsequently presented at and published* by the Symposium on Two-Phase Flow and Dynamics in Eindhoven, Netherlands, in September, 1967.

Work on the present investigation of boiling heat transfer to the alkali liquid metals under Prof. W.M. Rohsenow was formally begun in September, 1967.

He is a member of Sigma Xi.

He has accepted a position with the Heat Transfer Section of the Nuclear Systems Programs division of the General Electric Company, which is investigating forced-convection heat transfer to potassium.

---

*Crowley, J.D., Deane, C. and Gouse, S.W., "Two-Phase Flow Oscillations in Vertical, Parallel, Heated Channels," Proceedings of the Symposium on Two-Phase Flow and Dynamics, Eindhoven, Netherlands, September, 1967.